JNES-SS-0602

Investigation Report on the Integrity of Thermally-Embrittled Cast Stainless Steel Pipe

JNES-SS Report

April 2006

Safety Standard Division, Japan Nuclear Energy Safety Organization

About JNES-SS Reports

JNES-SS Reports are reports published from time to time by the Safety Standard Division (SS) of the Japan Nuclear Energy Safety Organization (JNES) on the activities of the Division not covered by the regularly published JNES reports on the studies, tests, and research that the organization conducts. Specifically, they include timely interim reports on the activities of the Safety Standard Division, materials for seminars and other events, studies related to the standards used in JNES inspections, results of studies by field-based task teams, reports on the results of voluntary investigative researches, and recommendations regarding regulations.

The activities of the Safety Standard Division extend beyond the mere implementation of programs and projects to multifarious [TN: or “diverse”] independent activities as an organization providing regulatory support to the Nuclear and Industrial Safety Agency. Since the purpose of the activities is to ensure nuclear safety, we felt that it was essential in terms of conducting ourselves with transparency as well as gaining broad public understanding on nuclear safety that we provide information proactively once results with a certain degree of coherence are achieved. Accordingly, we have decided to release the information to the public as JNES-SS Reports.

Further, because JNES-SS Reports pertain to a wide range of matters as mentioned above and the basic intent is to provide prompt reporting, the contents vary greatly from report to report. Opinions of the general public presented through questions or comments on the reports are always welcome, as they will help improve the quality of our activities. Therefore, please direct any inquiry you might have to the following group.

Planning Group, Safety Standard Division,
Japan Nuclear Energy Safety Organization
Tokyu Reit Toranomon Building
3-17-1, Toranomon, Minato-Ku, Tokyo 105-0001 Japan
Tel: +81-3-4511-1702
Fax: +81-3-4511-1898
E-mail: SSD@jnes.go.jp

ABSTRACT

In the 1990's, it was confirmed that cast stainless steel used in the primary coolant pipes, etc. of pressurized water type nuclear power plants suffered thermal aging and that operating a light water reactor at a temperature of even about 300°C may result in a significant reduction of fracture toughness (thermal embrittlement) in some cases. A light water reactor equipment having a structural design premised on the ductile behavior of materials is required to have appropriate fracture toughness even after embrittlement. The thermal embrittlement of cast stainless steel, like the irradiation embrittlement of materials, is a deterioration phenomenon relating to equipment materials that is critical in terms of light water reactor safety. In a technical evaluation of the integrity of highly aged plants, it is necessary to take thermal embrittlement into consideration in conducting an evaluation of the primary coolant pipe and other components made of cast stainless steel; thus, relevant evaluation guidelines are required.

Stainless cast steel is a two-phase stainless steel having a ferrite phase inside an austenite base. Since thermal aging causes embrittlement of the ferrite phase, cast stainless steel having a higher ferrite content is more prone to embrittlement. While there is no non-ductile fracture due to the presence of the austenite base, progress in thermal embrittlement will result in loads smaller than the plastic collapse load causing crack growth and lead to unstable ductile fracture. It is necessary for a thermally embrittled primary coolant pipe to have adequate fracture toughness so that even if there are cracks of a size that is not detectable by inspection, the ductile cracks undergo minimal development under operating loads and unstable ductile fracture does not occur even when subjected to the maximum load in an accident or other unexpected situations.

Although such fracture behavior of pipes is expected to take place in accordance with elastoplastic fracture mechanics, there were a number of problems in carrying out analysis and evaluation. It had not been experimentally verified whether a small crack in a non-homogeneous low-toughness material comprising an extremely brittle phase grew as predicted in accordance with elastoplastic fracture mechanics. While it is necessary to predict and use the stress–strain characteristics following thermal aging in evaluating the crack driving force, a prediction equation that can be applied for a markedly thermally-embrittled material had not been proposed. There is no data from actual equipment either in the absence of monitoring tests. Because the pipes are of special materials with uneven thickness, there is no data related to defect detection by ultrasonic crack scanning inspection. Further, pipes having medium wall thickness are used between thick plates and pipes having thin walls, there is no method

available for easily evaluating the crack driving force. In consideration of the fact it is necessary to give thought to thermal shock stress in the evaluation of crack growth in embrittled materials as well as strength of seismic stress, it is necessary to stipulate integrity evaluation guidelines.

This investigative research was conducted with respect to primary coolant pipes, which are subjected to severe usage conditions, in order to consider ways of addressing various issues and establish integrity evaluation guidelines therefor. First, in order to understand the fracture behavior of thermally-embrittled pipes, cracks were made on the surface of a reduced-scale simulated primary coolant pipe that has been thermally aged to achieve a condition equivalent to 60 years of operation. It was then subjected to a 4-point bending test. The test was carried out in a quasi-static manner, since it had already been confirmed that the dynamic fracture toughness of thermally-embrittled cast stainless steel it higher than its static value. The results of the test were analyzed using the stress–strain characteristics that were actually measured using the test materials, and it was confirmed that the fracture behavior of the pipes were being controlled by the J-integral value at the crack tip obtained by an appropriate analysis method. Using the analysis method verified by experiments, the crack driving force that occurs in a crack imagined to be present in a primary coolant pipe with the actual cross-sectional dimensions was analyzed, and the crack driving data was acquired. It was made possible to obtain, using the crack driving force evaluation diagram, the crack driving force of a long-time thermally aged material according to the size of the crack, the stress–strain characteristics corresponding to the amount of ferrite, and the level of the stress. Here, the assumed range of the size of the cracks was about 10 to 25% of the typical plate thickness, considering the results of the detectability of fatigue cracks carried out in parallel with this study research. The predicted stress–strain characteristics used in the analysis were determined using a private-sector prediction equation proposed in 2005 in consideration of the plentiful private-sector data. In using this prediction equation, its appropriateness was confirmed by comparing in advance the stress–strain characteristics of a thermally aged material obtained by this research. Further, the lower limit of the fracture toughness during thermal embrittlement that should be compared with the crack driving force was evaluated under typical conditions using a prediction model created separately so as to grasp it easily from the aging temperature and the amount of ferrite, and a relevant figure is shown in the appendix of this report.

This report is a compilation of the above contents and provides technical data to be used in examining the appropriateness of documents prepared by business operation on the technical evaluation of highly aged equipment, such as primary coolant pipes, with regard to thermal embrittlement. Until appropriate standards are established, this report shall be used to

ensure the explainability and transparency of an appropriateness evaluation using this report. The significance of conducting a technical evaluation of highly aged equipment lies in keeping track of the materials used in the plants concerned as well as the embrittlement of the materials at the operating temperature of the corresponding plant, gaining a quantitative understanding of the size of the cracks permissible under the load conditions of the plants, and reflecting the information in future inspection and repair plans. It is believed that this report, which has been compiled to facilitate the quantitative understanding of the foregoing, will be useful to business operators in the evaluation of structural soundness as well as in the consideration of measures to be implemented.

When using the drawings and tables for the evaluation in this report, note the fact that they take into consideration the wide variations in test data and the specific conditions applied in preparing them. In the future, it is hoped that embrittlement will be monitored as necessary by, for example, non-destructive methods and that integrity evaluation will be conducted in a manner suitable for the actual equipment being evaluated.

CONTENTS

APPENDIX

ABBREVIATIONS AND SYMBOLS

a	crack depth
Δa	magnitude of ductile crack growth
FN	ferrite content
J	integral value of J
J_{app}	J-applied crack propagation force
Jc	J-integral value in cases where fracture occurred under maximum load
J_{Ic}	J-integral value in cases where a ductile crack begins to grow under conditions of surface strain
J_{mat}	fracture resistance J-integral value of materials before and after ductile crack growth
JQ	J-integral value at which ductile crack growth begins
USE	upper shelf energy absorption

1. Preface

1.1 Introduction

In Japan, it is expected that light water reactors will be mainstream in the field of nuclear power generation for the foreseeable future, and light water reactor equipment will therefore continue to age. Outlining measures for coping with light water reactors that are aging, in 1996, the Ministry of International Trade and Industry summarized its "Basic Thoughts on Aging." As requisite steps for ensuring safety in the case where a light water reactor is to remain in operation for a long period of time, this report indicated a need to establish standards that took aging into account, as well as, from a technical standpoint, a need to establish inspection and monitoring technologies, preventive maintenance and repair technologies, and aging-related change evaluation technologies. And in the aging technological evaluations for individual plants to be executed up to thirty years following the start of operations initiated in that same period, it was deemed necessary to improve precision in the evaluation of aging-related change.

Among technical issues pertaining to aging-related change in light water reactor equipment, the following three items were identified and subsequently researched in regards to monitoring technologies and aging-related change evaluation technologies for embrittlement phenomena in the structural materials of safety-critical devices.

① A method for measuring reductions in the fracture toughness of reactor pressure vessel materials in the upper shelf temperature region

② Technologies pertaining to the reproduction of reactor pressure vessel monitoring test pieces

③ An integrity assessment method for cast stainless steel primary cooling pipes subject to thermal embrittlement

Of the above three items, the present report summarizes outcomes pertaining to item ③ in such a way as to contribute to aging-related change evaluation technologies for thermal embrittlement.

1.2 Background and Objectives

Some of the primary cooling pipes that form the primary system pressure boundary of the nuclear power plant are made up of cast stainless steel. It has been known for quite some time that under higher temperatures, cast stainless steel undergoes thermal aging and becomes brittle (in other words, it undergoes thermal embrittlement). However, between the

1980s and 1990s, it was confirmed that at times, toughness may even be drastically reduced due to thermal aging at approx. 300°C, which is the operating temperature of a light water reactor.[1) 2)] In Japan, based on experiments conducted by operators as well as plant longevity technological developments implemented by the Japan Power Engineering and Inspection Corporation (Foundation), thermal embrittlement data has been accumulated for cast stainless steel. In addition, recently, by collecting both domestic and overseas research data, a predictive assessment method for fracture toughness and tensile properties of cast stainless steel has been developed and published.[3)] Cast stainless steel is a duplex (or "two-phase") stainless steel having a ferrite phase in an austenitic fabric. Its thermal embrittlement is a phenomenon produced because the ferrite phase becomes brittle. And because it has an austenitic fabric, even if it undergoes thermal embrittlement, above ambient temperatures, it will not exhibit non-ductile fracture behavior, but if the ferrite content is high, then fracture toughness is greatly reduced. The ferrite content of the primary cooling pipes that are used in Japan is 23.5% or less. The solid lines of Figure 1.2-1 assess the predicted fracture toughness JR-Δa in the case where cast stainless steel has undergone thermal aging over a long period of time at 325°C based on a thermal embrittlement prediction formula[3)] employing the ferrite content in the material as a parameter. The rupture line in the figure is the line of the predicted fracture toughness.

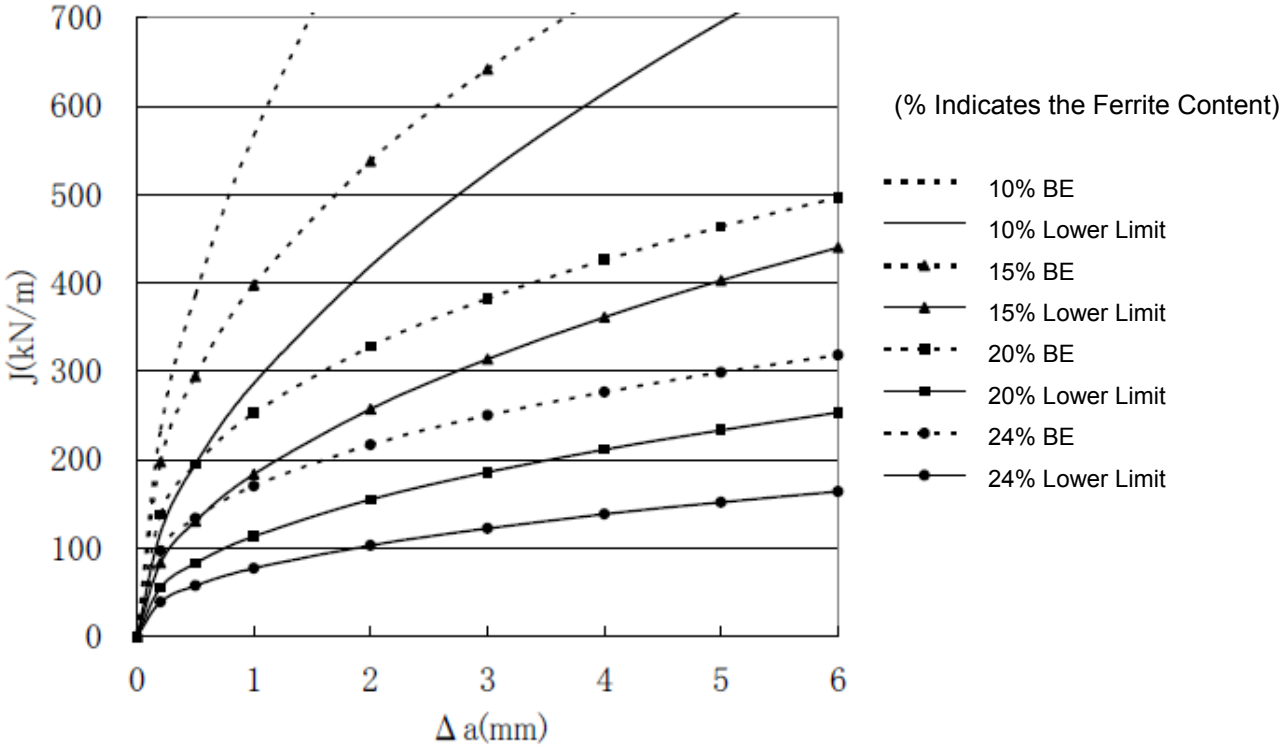

Figure 1.2-1 Examples of Predicted Fracture Toughness for Thermally Embrittled Materials[3)]

As an embrittlement phenomenon in light water reactor materials, neutron irradiation embrittlement of reactor pressure vessel materials is well known. In electronic technology regulation JEAC-4206[4)] of the Japan Electric Association, in cases where the upper shelf energy absorption (USE) falls under 69J, it is mandatory to confirm structural integrity. The predicted fracture toughness in cases where the USE of a reactor pressure vessel material is 69J is of the same order as in the case in Figure 1.2-1 where the ferrite content is great. In cases where cast stainless steel has undergone thermal embrittlement, it will have approximately the same fracture toughness as reactor pressure vessels that have been determined to have undergone irradiation embrittlement. If cast stainless steel having a high ferrite content becomes thermally embrittled and cracks are present, the cracks will grow under comparatively little stress, and the steel will undergo ductile unstable fracture under loads that are smaller than the plastic collapse load. Because such materials are ductile materials but have low fracture toughness, their fracture behavior is evaluated using elasto-plastic fracture mechanics. As such, there is a need to establish procedures governing the use of elasto-plastic fracture mechanics to evaluate the structural integrity of primary cooling pipes that have undergone thermal embrittlement induced by long-term operation.

Elasto-plastic fracture mechanics evaluates the crack propagation force produced by a load on cracks in a material as well as the behavior of the cracks based on the size relationship of the fracture toughness of the material. Because the fracture toughness value obtained based on a prediction formula proposed in previous research[1)2)3)] is a small value, the crack propagation force targeted for comparison must be precisely evaluated. In actuality, there have been a number of issues surrounding attempts to apply elasto-plastic fracture mechanics to integrity assessments of actual equipment that has undergone marked thermal embrittlement. A first point of concern is that there has yet to be experimental confirmation as to whether the propagation behavior of small cracks in non-homogeneous materials can be precisely evaluated at the microstructure level, as in the case of cast stainless steel that has been subjected to thermal embrittlement. Secondly, Document 2) proposes stress-strain characteristics following thermal embrittlement for use in the analysis of crack propagation forces, but long-term thermal aging conditions as found in 60 years of operation are outside the scope of applicability. Because observation tests have not been conducted, tensile test data is also nonexistent. Thirdly, a method for easily evaluating the crack propagation forces of surface cracks has yet to be proposed. Furthermore, the detectability of defects in cast stainless steel when using ultrasonic defect inspection methods is known to be inferior to cases when applied to single-phase materials.

The fact that there has been insufficient data to serve as a foundation for determining the size of the cracks that must be assumed to occur in integrity assessments is due to the fact that—other than in fatigue evaluations taking highly ductile materials as a precondition and taking the temperature distribution in the plate thickness direction as something that does not affect behavior for pipe girders—such cracks are beyond the scope of consideration with regards to loads that must be considered in evaluation in the design construction standards of the Japan Society of Mechanical engineers[5]. In integrity assessments of embrittled pipes, however, shock loads also influence the behavior of cracks. Taking such points into consideration, this project was undertaken with the aim of creating procedures for conducting integrity assessments of primary cooling pipes that have undergone thermal embrittlement.

Regions that have become embrittled have a lowered margin against fracture. It is necessary to confirm whether integrity has been ensured with an appropriate margin taking into consideration the characteristics of maintenance and inspection as well as the loads on these regions. In the case of reactor pressure vessels, using the standards adopted at the time of design,[5] it is required that fracture not take place even if one assumes a semi-elliptical surface defect having a depth relative to the plate thickness of 1/4 (approx. 50 mm) and a length 1.5 times the plate thickness (approx. 300 mm). However, for pressurized thermal shock events on a reactor pressure vessel that has been subject to irradiation embrittlement, the standards[4] are prescribed assuming that defects have a depth of 10mm. The defect assumed to have a depth of 10 mm is set as a value for applying a margin for detection precision at the time of manufacture, taking into consideration the characteristic that pressurized thermal shock loads become larger in the vicinity of the inner surface and the special characteristic that the cyclic loading applied to the belt line region of the reactor pressure vessel is small and the extent of fatigue crack propagation is also small. In the evaluation of primary cooling pipes that have become thermally embrittled, there is a need for evaluation periods that can assess their structural integrity in line with the actual conditions while taking into consideration the usage conditions of the region under evaluation. With regards to the magnitude of the assumed cracks, we sought to establish data of an appropriate range so that it might be possible to make prescriptions while taking into consideration test results on actual devices together with defect detection test results[6] on life-sized primary cooling pipes undertaken separately by the Japan Nuclear Energy Safety Organization. As for measurements of the stress-strain characteristics, we considered a prediction formula formulated in the private sector based on material test

results originating from within Japan and abroad along with material test results undertaken as part of this project. We undertook a detailed analysis of the crack propagation forces produced on an assumed crack while taking into consideration the predicted stress-strain characteristics set in accordance with the amount of ferrite present, and summarized our analytical results in a graph for easy evaluation. Doing this has made it possible to conduct integrity assessments simply and easily. In addition, it has become easier to confirm the validity of detailed analytical results. It is now possible to seek to improve the descriptions of integrity assessments.

Here, for the method used for crack propagation force analysis, we employ a method that we verified using the fracture test results for thermally embrittled pipes. For the purposes of high-aging technical evaluations, there is a need to obtain a margin for fracture and growth behavior in accordance with the service conditions of cracks that run only part way through. An experiment was conducted overseas where the maximum load was obtained by applying cracks running part way through to thermally embrittled pipes.[8)] However, as the thermal aging conditions were relatively gentle, data on the growth of cracks running part way through was not obtained. As part of a study on the feasibility of leak before break (LBB) conducted in Japan, testing and analysis of thermally embrittled pipes having through-crack defects were conducted. These formed the basis for standards[7)] pertaining to pipe rupture protection design by the Japan Society of Mechanical Engineers. In LBB, target defects are limited to through-crack defects that produce leakage, and the data does not touch on the growth behavior of partial cracks. In this study, we manufactured cast stainless steel simulation pipes where the ferrite content was up to the maximum of materials actually used in Japan. We subjected them to accelerated thermal aging equivalent to 60 years of real-life operation, and determined the fracture behavior of cracks running part way through by conducting pipe rupture experiments. By analyzing and evaluating the fracture behavior of pipes, we established a method of evaluation. Because we did not have large-capacity testing equipment that would be suitable for conducting destructive testing of life-size primarily cooling pipes, the experiments were conducted using small-scale test specimens. The crack propagation forces produced assumed cracks in actual equipment were analyzed using a life-size model constructed using an analytical method verified through testing. Using the actual-equipment-size model, we performed our analysis taking the load levels, crack sizes, and amounts of ferrite in the actual equipment into consideration, and developed a crack propagation force evaluation diagram.

Now, in the maintenance standards[9] of the Japan Society of Mechanical Engineers, a two-parameter method that evaluates defects in austenite cast stainless steel pipes discovered through in-service inspections has been prescribed. It is the sole standard that can be adopted to cast stainless steel having high levels of ferrite that has been subjected to marked thermal embrittlement. A general-purpose fracture evaluation plot diagram has been determined based on this two-parameter method. We will also discuss its applicability to general-purpose fracture evaluation plot diagrams in light of the test results of thermally embrittled materials obtained as part of this study.

1.3 Overall Plan

1.3.1 Outline

An overall flowchart of this study is shown in Figure 1.3-1, and the cross-section specifications of the primary cooling pipes of a Japanese plant and the ferrite content employed are shown in Figure 1.3-2. As the typical outer diameter D of the hot leg, which is the part of the primary cooling pipe that becomes hottest, is 882 mm, and its thickness t is 72.7 mm, Rm/t will be approximately 5.6 in most plants. The maximum value for the ferrite content is 23.5%. Once reduced-dimension pipe test specimens manufactured taking into consideration the ferrite content and the cross-section specifications of actual pipes had been subjected to thermal embrittlement under conditions that were equivalent to 60 years of operation, we conducted material tests and pipe fracture behavior tests. Using the stress-strain characteristics used in the material tests, we analyzed the fracture behavior of the pipe test specimens. By comparison with the fracture toughness obtained in material tests, we verified our analytical technique. We verified the suitability of a predictive evaluation method by comparing the fracture toughness and stress-strain characteristics obtained in the material tests against the respective values predicted based on existing predictive evaluation techniques. On that basis, we obtained the crack propagation forces produced on actual equipment using an analytical model for life-size pipes having the predicted stress-strain characteristics.

1.3.2 Test Plan

(1) Basic Policy

We imparted a monotonically increasing load to thermally embrittled pipes to which partial through cracks had been applied, and measured the crack growth behavior and load/displacement characteristics. The results were employed in the verification of

analytical modeling techniques in combination with the material test results for the materials.

① Test Specimen Material

The toughness of cast stainless steel that has been thermally aged under the same temperature time conditions decreases as the ferrite content in the steel increases. In addition, based on previous research,[3] it has been found that the fracture toughness values following long-term aging, such as 60 years of operation, can essentially be determined solely based on the ferrite content. For that reason, the material quality of the test specimens was determined taking into consideration the maximum ferrite content of material found in equipment actually used in Japan. The ferrite content of cast stainless steel can be estimated based on its chemical composition. Various estimation methods have been proposed, but here the base material was estimated using the method prescribed in the Appendix of ASTM A800,[10] and in the case of welding materials, estimated based on a Delong diagram. Taking into consideration the maximum value of ferrite content in actual materials used in Japan, we assumed the ferrite content for the base material test specimen representing an initial plant where the ferrite content was high to be 23.5%. We adopted two types of test specimen for the base material: the one just mentioned, and a material with a ferrite content of approximately 10%. This latter material simulated the kind of material that would be found in a comparatively new plant.

As for welding materials, all of the actual welding section normally has a ferrite content of 10% or less, and so thermal embrittlement is not significant. For this reason, we set the ferrite content as being of one type, and tested the change in material characteristics due to thermal aging. Moreover, for the welding method when manufacturing the welded metal test pieces, we applied a shielded metal arc welding method that—among submerged arc welding and shielded arc welding— tends to exhibit the lowest fracture toughness.

② Thermal Embrittlement of the Test Specimen

The test specimen was subjected to thermal aging under conditions that were equivalent to the operation period (60 years) assumed in the high-aging technical evaluation. We set the thermal aging temperature to 450°C, taking into consideration a temperature range over which it has been confirmed that a reduction in fracture toughness equivalent to that of actual equipment could be simulated in an accelerated manner. And because it is known, based on prior research, that the activation energy is

within a range of 100 - 180 kJ/(mol • K), when setting the thermal aging temperature, we employed the lower limit value of 100 kJ/(mol • K). We evaluated the thermal aging time at 450°C corresponding to the aging time—equivalent to 60 years at actual operating temperatures—based on the embrittlement prediction model of Eq. 1.3-1, and performed 13,300 hours of thermal aging.

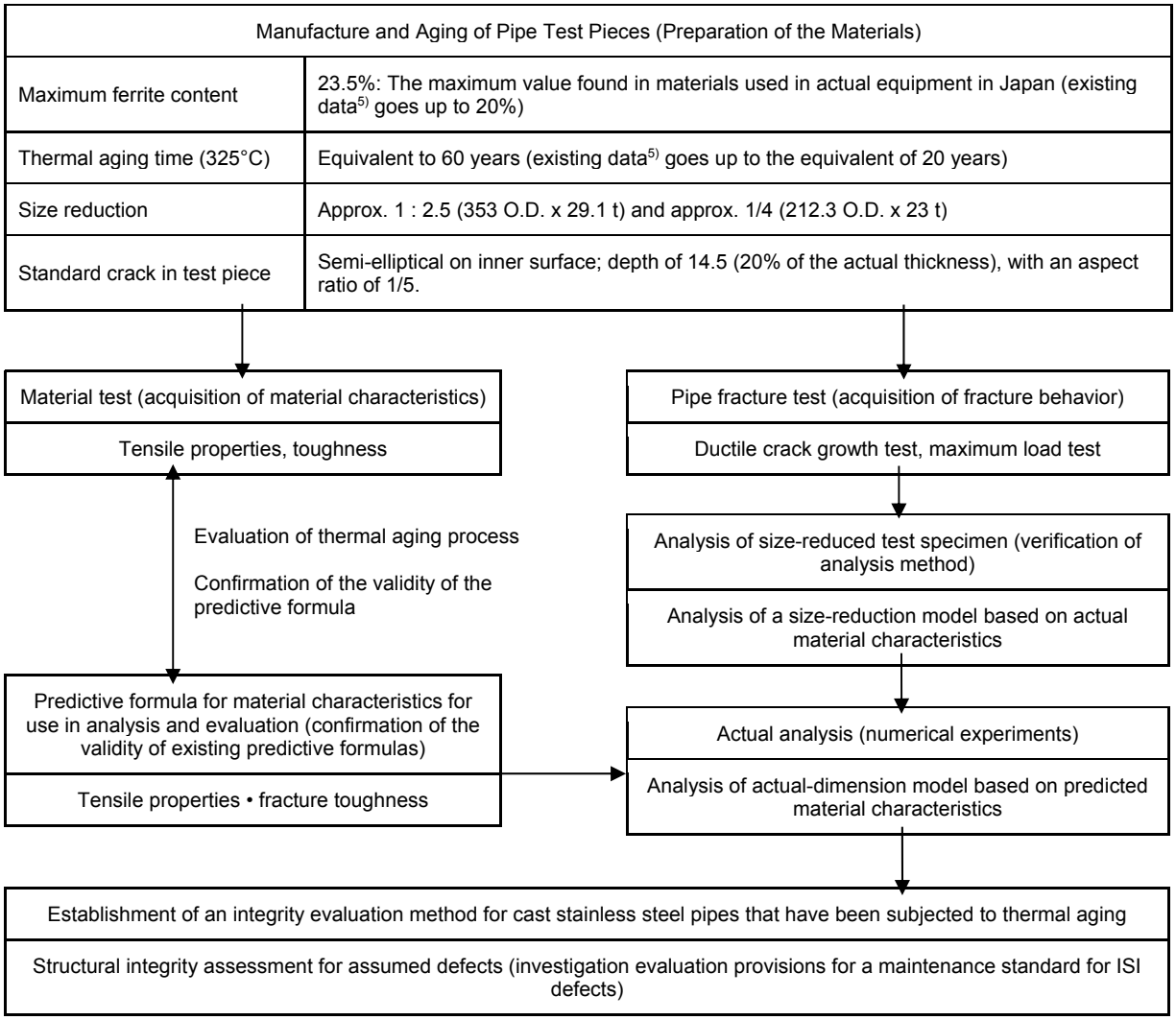

Figure 1.3-1 Research Flowchart

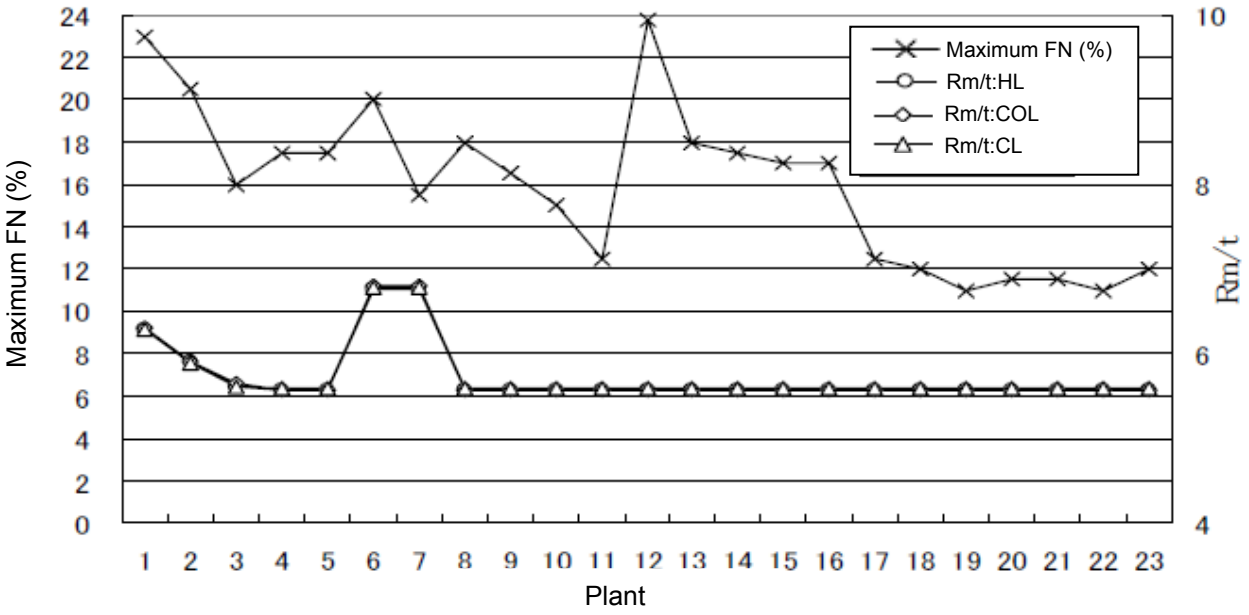

Figure 1.3-2 Average Diameter/Thickness and Ferrite Content of Primary Cooling Pipes

$$P(t,T) = \log_{10} t + 0.4343 \frac{Q}{R}\left(\frac{1}{673.2} - \frac{1}{T}\right) \quad \cdots\cdots\cdots\cdots \quad (1.3\text{-}1)$$

Where:

P(t, T): parameters

t: aging time (hr)

T: aging temperature (K)

Q: activation energy (= 100 kJ/mol)

R: gas constant 8.39×10^{-3} kJ/(mol • K)

③ Types of Experiments

We performed pipe tests and material characteristics tests. The loads that are applied to pipes consist of static loads and dynamic loads. With thermally embrittled cast stainless steel, it is known that, compared to static characteristics, dynamic tensile characteristics exhibit greater yield points and growth, and that the fracture toughness increases with dynamic tests.[12] For this reason, all of our tests were implemented quasi-statically.

a. Pipe Fracture Tests

When the fracture toughness of a material decreases due to thermal embrittlement, there is a possibility that the pipe will fracture under a load that is smaller than the plastic collapse load of the pipe. When the load is small, a ductile crack grows stably, but

subsequently, the crack grows suddenly, and unstable ductile fracture is produced. Unstable ductile fracture is a phenomenon whereby, even if outside forces do not increase, simply by means of the strain energy stored by the cracked pipe, the ductile crack propagates and reaches the fracture point. A thermally embrittled pipe containing a high ferrite content is predicted to exhibit this kind of fracture behavior. In order to prevent pipe rupture, it is necessary to ensure that ductile crack growth is stable and restricted under the load conditions found in service states A - C, and that unstable ductile fracture is not produced under service condition D. In order to grasp the rupture behavior of such pipes, we performed pipe rupture tests. The temperature of the test specimen was fixed. The normal operating temperature of actual equipment was approx. 290°C (the low temperature side) - approx. 320°C (the high temperature side). In this temperature region, fracture toughness was nearly constant. Moreover, although the tensile characteristics (the yield point and tensile strength) tended to decrease slightly on the high temperature side, the change was minimal. Taking into consideration transient changes in the high temperature side operating temperatures of actual equipment, the test temperature was set to 325°C.

Because the weld metal had a low ferrite content and no significant embrittlement, a pipe test was not performed on it. In the rupture behavior of welded regions, since the base material of high ferrite content had a higher yield point than the welded regions, there was a possibility that localized strain concentrations might arise under loads greatly exceeding the yield point of the weld metal. However, in experiments on thermally aged weld materials to which through-crack defects have been applied, special signs in the pipe fracture behavior have not been observed.[13)]

b. Material Tests

For the experiments, we cut out a tensile test piece, CT test piece, and Charpy impact test piece from the pipe test specimen prior to and after thermal embrittlement. The tensile test results were used as input properties for the test specimen analysis. The CT test results were compared against the J-integral value obtained from test specimen analysis. For this reason, the test temperature was set to 325°C, the same as for the pipe specimen. Moreover, between room temperature and 290°C, the change in fracture toughness of a thermally aged material is small.[1)] All of the material test results were compared against predicted material characteristics for thermally embrittled materials that have been published so as to test the applicability and validity of the predictive formula.

④ Loading System and Crack Monitoring

The loading system for the pipe tests employed four-point bending for displacement control. Actual primary cooling pipes are subjected to internal pressure, thermal load, external load, and thermal shock load, but the dominant stress is pipe bending stress due to external loads. It was felt that among thermal loads and axial loads due to internal pressure, the plate bending stress due to the temperature distribution in the plate thickness direction—something that could not be handled as an external load—was relatively small. Thus, in the tests, we applied only a bending load to pipes to which circumferential cracks had been induced. Because Document 12) reports that there is a tendency for fracture toughness and break elongation of thermally embrittled cast stainless steel to increase due to dynamic effects, in this experiment we sought to understand the static behavior of pipes.

In an experiment designed to understand the growth behavior of ductile cracks in the pipe tests, one must perform unloading prior to reaching the maximum load. Data based on the electric potential method was employed as information on the growth of ductile cracks during the experiments. In the electrical potential method, an electric field is formed between constant current output terminals mounted at positions sandwiching but sufficiently distant from a crack on a test specimen, and changes in the electric potential due to crack growth are detected. Due to constraints on electrode construction, the detection terminal for an inner surface defect is mounted on the pipe's outer surface, the changes in electric potential when crack growth begins are small, and it is not possible to perform a quantitative analysis of crack growth magnitudes based on those changes. Electrical potential output was used for displacement control at the time of the tests and for monitoring crack growth semi-quantitatively. In the ductile crack growth behavior test, we determined the start of crack growth based on the electric potential output, and determined the maximum load of the experiment. The magnitude of crack growth during the maximum load was actually measured by causing the test specimen to undergo fatigue or brittle fracture following unloading, and opening up the cracked surface.

⑤ Size Reduction of the Test Specimen

For the testing device, out of the existing devices available in Japan, we chose to employ a large-scale testing device from JNES having a maximum load capacity of approximately 6 MN • m. As a representative cross-sectional dimension for a primary cooling pipe, we selected the hot leg (the pipe situated between the nuclear reactor and the steam generator) which is subjected to the most extreme thermal embrittlement

conditions for setting representative values, and settled on an outer diameter of 882 mm and a thickness of 72.7 mm. Because this was an extremely large pipe, even if we applied a maximum load of existing devices to the pipe test specimen having the representative size, we could only have produced a stress of approximately 0.2% the yield strength. For this reason, we adopted size-reduced test specimens. We employed two levels of size reduction, with the outer diameters being approx. 1/2.5 and approx. 1/4 of the actual size.

	Outer Diameter (mm)	Plate Thickness (mm)	Average Radius/Plate Thickness
Representative Size of Actual Equipment	882.0	72.7	5.566
Large-Sized Pipe Test Specimen	353.0	29.1	5.565
Medium-Sized Pipe Test Specimen	212.3	23.0	4.115

The plate thickness of the large-sized pipe test specimen, which was reduced by a ratio of approx. 1:2.5, was set so that the ratio of the pipe's outer diameter to the plate thickness was the same as would be found in actual equipment. The medium-sized pipe test specimen, which was dimensionally reduced by a ratio of approx. 1:4, was manufactured so as to ascertain the effect of the size reduction. The plate thickness of the medium-sized pipe test specimen was comparatively thicker than the outer diameter when taking into account the initial crack size. We verified our analytical method using the test results for the two kinds of pipes having different extents of size reduction along with the fracture toughness test results. Moreover, in order to investigate the precision of the analytical results employing a life-size model, we also assessed the differences in the plastic constraint of the crack tip due to size reduction; we also evaluated the degree of plastic constraint in the fracture toughness test piece as well as in a mid-sized pipe, large-sized pipe, and life-sized pipe.

⑥ Introduction of Cracks into the Test Pieces

As the purpose of a pipe test is to verify the analysis method for thermally embrittled pipes, it is desirable to provide cracks having the same size as the maximum hypothetical crack assumed in actual equipment evaluation.

The assumed crack size when assessing actual equipment is determined by taking into consideration the fatigue crack propagation in crack dimensions that can be detected during in-service inspections and at the time of actual manufacture. With regards to the detectability of inner surface fatigue cracks using a longitudinal wave

oblique angle ultrasonic wave detection method applied from the outer surface during in-service inspections, experiments have been conducted by JNES.[6] As a result, as shown in Appendix 3, the smallest detectable crack dimension is smaller than approx. 1/5 of the pipe plate thickness, and it was reported that even comparatively shallow fatigue cracks were detectable.

We thought that the cracks applied to test specimens in the present test were sharp inner surface circumferential semi-elliptical cracks having1/5 of the actual representative thickness and 1/5 the aspect ratio. We called these cracks having a depth of 14.5 mm and an inner surface length of 72.7 "standard cracks." We tested mainly standard cracks in both the mid-sized and large-sized pipe test specimens. For the standard cracks, because we grew and applied fatigue cracks at the leading end of electro-discharge machining processing slits that were slightly smaller than the standard crack dimension, the actual initial crack size was identified by opening the crack-applied cross section following the test.

Moreover, in order to change the plasticity restraint using the same size-reduced test specimen, we tested cracks other than standard cracks.

(2) Test Materials and Test Matrix

Based on the above approach, we manufactured the service test materials. The chemical composition and ferrite content of the service test materials was as shown in Table 1.3-1. In the large-sized pipe material, the ferrite content was 23.7%. In the mid-sized pipe material, it was 22.7%, and in the weld metal, it was 9%. The pipe test matrix is shown in Table 1.3-2. The shape of the large-sized pipe test specimen is shown in Figure 1.3-3. The moment arm of the four-point bending test was 2,575 mm. We tested the mid-sized pipe test using a smaller testing apparatus. The moment arm in that case was 750 mm.

Table 1.3-2 Pipe Test Matrix

Supplied Test Pipe	Ferrite Content	Thermal Aging	Fracture Prediction	Test Specimen Name	Crack Size	Test Objectives
Mid-Sized Pipe OD: 212.3 mm Plate Thickness: 23 mm	10.9%	None	Plastic Rupture	M1	Standard	Measurement of Maximum Load
		Yes(Note)	Plastic Rupture	M2	Standard	
	22.7%	None	Plastic Rupture	M3	Standard	
		Yes(Note)	Elasto-Plastic	M4	Standard	
				M5	Standard	Determination of Crack Growth Behavior
Large-Sized Pipe OD: 353.mm Plate Thickness: 29.1 mm	11.4%	Yes(Note)	Elasto-Plastic	L1	Standard	
	23.7%			L2	Standard	
				L3	Standard	

Note: Thermal aging was conducted at 320°C under conditions equivalent to 60 years of operation (48EFPY).

1.3.3 Analysis Plan

(1) Analysis of the Test Specimen

We analyzed the fracture behavior of the dimensionally reduced pipe test specimens, and verified our modeling method. In a three-dimensional finite element test specimen model having stress-strain characteristics that were actually measured using pipe test specimen material and crack shapes (initial crack + the magnitude of crack growth Δa) actually measured by opening the ruptured surface following the ductile crack growth test, we evaluated the crack propagation force J_{app} at the time loads were applied up to the test's maximum load using the path integral method. We compared J_{app} values against the J_{mat} - Δa property of the pipe test specimen material. If both are the same, then one may conclude that the rupture of thermally embrittled primary cooling pipes is governed by the J-integral value evaluated using the analysis method that was adopted. Here, the validity of the analysis method was confirmed by analysis of the test specimen in addition to the analysis by the test practitioner who implemented the test without knowing the fracture toughness of the material. We decided to apply this modeling method to the analysis of life-sized equipment.

In order to investigate the precision of our analysis on life-sized scale equipment, we also evaluated the extent of plastic restraint. For a ductile crack, the greater the extent of plastic restraint of the crack tip, as expressed by Eq. 1.3-2, the easier it is for the crack to grow.

$$q = \sigma_h / \sigma_{eq} \qquad (1.3\text{-}2)$$

Here, σ_h is the hydrostatic stress in the vicinity of the crack tip. It is the sum of three orthogonal stress components. σ_{eq} is the von Mises equivalent stress. Because the magnitude of plastic restraint of the crack tip region in the pipe test specimen was less than the magnitude of plastic restraint at the crack tip region on a fracture toughness test specimen, a relationship of J_{app} (Δa) > J_{mat} (Δa) was established. We then evaluated the extent of plastic constraint of the CT test piece, actual equipment model, and pipe test specimen.

Table 1.3-1 Chemical Composition of the Test Material

		Chemical Composition (wt%)								(ppm)		Ferrite Content (%)
		C	Si	Mn	P	S	Ni	Cr	Mo	N	O	
Standard	JIS G 5121 SCS14A	≤ 0.08	≤ 1.50	≤ 1.50	≤ 0.040	≤ 0.040	9.00 - 12.0	18.00 - 21.00	2.00 - 3.00	—	—	—
Target Value	High Ferrite Content	0.02 - 0.08	0.50 - 1.30	0.40 - 1.20	≤ 0.040	≤ 0.040	9.00 - 10.5	19.00 - 21.00	2.00 - 2.70	Report	Report	21 - 25
Large-Sized Pipe	Weld Metal Analysis	0.046	1.27	0.86	0.027	0.007	9.54	20.72	2.30	310	203	23.9
	Product Analysis	0.046	1.26	0.88	0.024	0.007	9.26	20.47	2.22	324	106	23.7
Medium-Sized Pipe	Weld Metal Analysis	0.046	1.30	0.79	0.024	0.007	9.47	20.78	2.29	419	167	23.1
	Product Analysis	0.046	1.30	0.78	0.024	0.007	9.57	20.88	2.28	431	98	22.7
Target Value	Low Ferrite Content	0.02 - 0.08	0.50 - 1.30	0.40 - 1.20	≤ 0.040	≤ 0.040	9.50 - 11.0	18.00 - 20.50	2.00 - 2.70	Report	Report	8 - 12
Large-Sized Pipe	Weld Metal Analysis	0.050	0.84	0.90	0.026	0.005	9.94	19.70	2.23	570	110	11.5
	Product Analysis	0.050	0.90	0.82	0.025	0.005	9.96	19.58	2.23	583	57	11.4
Medium-Sized Pipe	Weld Metal Analysis	0.055	0.79	0.87	0.027	0.006	9.89	19.23	2.29	531	135	10.3
	Product Analysis	0.050	0.79	0.84	0.025	0.005	9.86	19.29	2.29	557	54	10.9
Standard	JIS Z 3221 D316L	≤ 0.040	≤ 0.90	≤ 2.50	≤ 0.040	≤ 0.030	11.0 - 16.0	17.0 - 20.0	2.00 - 2.75	—	—	—
Target Value	Weld Metal	≤ 0.040	≤ 0.90	≤ 2.50	≤ 0.040	≤ 0.030	11.0 - 16.0	17.0 - 20.0	2.00 - 2.75	Report	Report	6 - 12
Actual Value	Weld Metal	0.04	0.37	1.26	0.014	0.006	11.6	19.6	2.27	0.03	0.06	9.0

Ferrite Content: Computed based on the value of $\frac{Cre}{Nie} = \frac{Cr(\%)+1.5Si(\%)+1.4Mo(\%)+Nb(\%)-4.99}{Ni(\%)+30C(\%)+0.5Mn(\%)+26(N-0.02\%)+2.77}$ and using the graphs in ASTM A800.

Now, in the case of weld metals, the ferrite content is based on a Delong curve (ASME Sec. III Subsection NB).

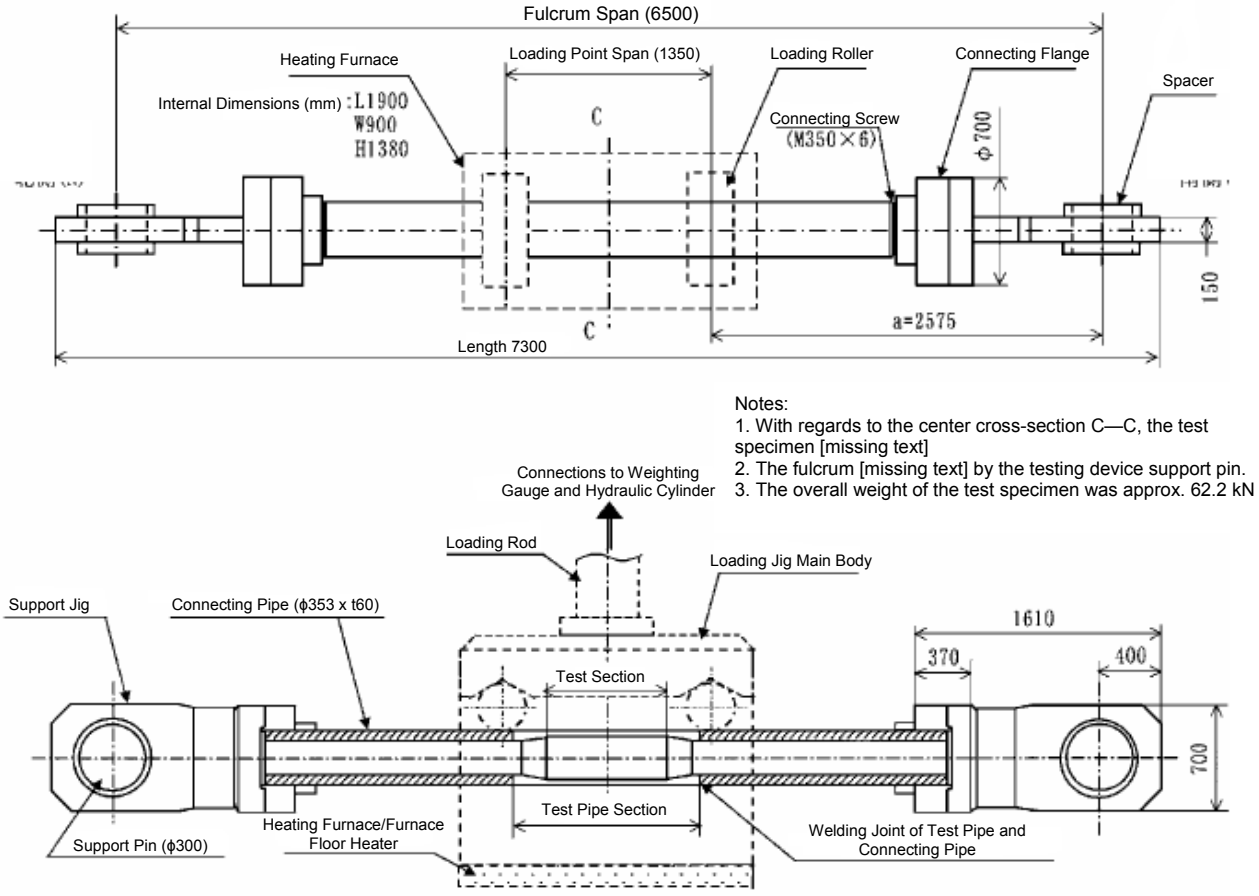

Figure 1.3.2-3 Schematic of Large-Sized Pipe Test Specimen

(2) Investigation of General Purpose Fracture Evaluation Curve

A general purpose fracture evaluation curve for austenitic stainless steel is given in Appendix E10 of the Maintenance Standards of the Japan Society of Mechanical Engineers. It consists of a regulation that can be applied to the evaluation of defects in cast stainless steel that have been discovered during in-service inspections. This curve is the same as that prescribed in ASME Sec. XI. When introducing this curve to the maintenance standard in a form that can be applied to cast stainless steel, its conservative nature can be appreciated by comparing the stress-strain characteristics of thermally embrittled materials obtained in the private sector to the curve created based on R6 Option 2. Here, more directly applying the pipe rupture test results for thermally embrittled materials obtained by this study, we evaluated the suitability of the general purpose fracture evaluation curve.

(3) Scale Analysis of Actual Equipment

① Analytical Model

We created an analytical model for the scale of life-sized equipment using the modeling method that was verified using test specimen analysis. The stress-strain characteristics used in the analysis of the actual equipment scale analytical model are the predicted characteristics when thermal embrittlement has been induced through 60 years of operation. A predictive formula for the stress-strain characteristics of thermally-embrittled materials needed for fracture mechanics analysis has been proposed in Reference Document 3). In this study, we investigated the validity of this predicted stress-strain characteristic by comparing it to material test data, and applied it in such a way as to obtain a conservative result for our analysis.

② Analysis Target

The primary cooling pipes made of cast stainless steel are found in the form of elbows, straight pipes, and—in some parts of a plant—branched pipe nozzles. We analyzed straight pipes, elbows, and branched pipe nozzles (only the straight pipe region thereof) at the scale of actual equipment.

1.3.4 Preparation of a Simple Evaluation Diagram

In the high-aging technical evaluation, we assumed an initial crack size taking into consideration crack detectability and fatigue crack propagation, and evaluated the safety margin for fracturing of the assumed crack in accordance with the load for each of the service conditions. To that end, we prepared a data set for representative conditions in such a way that it was possible to directly compare the crack propagation force from the expected

result and the fracture toughness. In cases where one is making evaluations as to whether continued service is possible when small cracks that are felt to have a wide safety margin are detected, utility is high if one settles on a permissible load table or fracture evaluation plot adding this data. That said, in a high-aging technical evaluation, it is important to assess integrity under the assumption that large cracks are present, and to investigate such matters as the size of cracks that must be reliably detected or the need for a reduction in stress levels. In order to permit use in such a study, we prepared crack propagation forces that changed in accordance with the degree of brittleness at the time that the crack size and stress were changed and fracture toughness of the material that changed in accordance with the aging temperature and ferrite content in such a way that they could be compared directly.

A simple evaluation method for crack propagation forces that are produced in typical thin-walled pipes with a ratio of average radius to plate thickness of 10 is given in EPRI NP-6301.[14] The ratio of the average radius to the wall thickness in primary cooling pipes is about half. The thinner the pipe, the flatter it becomes due to the bending load, and the greater the crack propagation forces exerted on the crack become. When applying a simple evaluation method for use on thin-walled pipes functioning as primary cooling pipes, there are times when the crack propagation forces will become several times the value obtained by performing a detailed analysis. Applying existing simple evaluation methods is conservative, but such an approach clearly does not result in a realistic evaluation. For this reason, we prepared crack propagation force data that was highly precise and that could be applied to the cross-section contour of primary cooling pipes. Using a detailed analysis method that was verified by pipe tests on the cross section of actual pipes used in Japan, we evaluated the crack propagation forces produced on circumferential semi-elliptical cracks residing on the inner surface, and created a plot for simple evaluation use.

1.4 Method of Pursuing the Research

This research study was conducted by the Material Evaluation Group of the Standards Evaluation Section of the Japan Nuclear Energy Safety Organization under a grant from the Ministry of Economy, Trade and Industry's Nuclear and Industrial Safety Agency. The design and manufacture of materials simulating those of an initial plant, as well as the thermal aging, pipe tests, and evaluation conditions for actual equipment were conducted by Mitsubishi Heavy Industries (Corp.). Mitsubishi has design and manufacture performance results for primary cooling pipes that are unequaled in Japan. It also has the largest pipe

fracture testing apparatus in Japan installed on its premises, together with the expertise to run it. Analysis of crack propagation and the like was performed by CRC Solutions (Corp.)

As shown in Figure 1.3.3-1, the study was conducted over a span of seven years, from 1999 - 2005. Up until the first half of 2003, it was conducted by the Japan Power Engineering and Inspection Corporation, and starting in the second half of 2003, it was conducted by the Japan Nuclear Energy Safety Organization.

Table 1.3.3-1 Overall Process

Year	1999	2000	2001	2002	2003	2004	2005
(1) Preparation of Test Material				Thermal Aging			
(2) Material and Pipe Tests							
(3) Analysis of Test Specimens and Actual Equipment							
(4) Conclusion							

1.5 Application to High-Aging Technical Evaluations

The Japan Nuclear Safety Energy has prepared a technical assessment manual for evaluating the validity for high-aging technical evaluations performed by practitioners. The technical assessment manual clarifies the public data and regulation standards utilized in the evaluation, and prescribes concrete applicable regulations, as needed. Unfortunately, specifications and standards that can be directly applied to the thermal embrittlement of cast stainless steel do not exist. This report was written with the objective of preparing technical data for use in evaluations prescribed by the technical assessment manual.

Until private standards and the like are upgraded, the descriptive property and transparence of validity evaluation will be ensured using this report to evaluate the validity of high-aging technical evaluation reports. Utilization of the data and information obtained by the present research undertaking is expected to promote private standardization.

2. Main Discussion

2.1 Material Tests

We measured the characteristics of materials used for the pipe specimens before and after thermal aging.

(1) Tensile Test

Table 2.1-1 shows comparisons before and after thermal aging for the 0.2% yield strength, tensile strength, elongation, reduction in area, and true-stress - true-strain characteristic. The 0.2% yield strength changed little before and after thermal aging, but the tensile strength increased due to thermal aging. This increase in tensile strength was more significant the greater the ferrite content. Elongation was lowered by thermal aging. The magnitude of the reduction in elongation was also greater the higher the ferrite content, and in materials having the greatest ferrite content, the drop in elongation from before to after thermal aging was on the order of 45%. Figure 2.1-1 shows the true-stress - true-strain characteristic at 325°C before and after thermal aging.

Predictive equations for the true-stress - true-strain characteristics of cast stainless steel that has been thermally embrittled are proposed in Reference Documents 2 and 3. The applicable range for the predictive equation of Reference Document 2 is limited, and cannot be employed for predictions following highly extended aging periods, as would be the case following 60 years of operation. Here, we compared the true-stress - true-strain characteristic obtained in this test against the prediction values based on Reference Document 3. The predictive equation of Reference Document 3 is a statistical regression equation for Ramberg-Osgood parameters from the tensile test data at 325°C. Its parameters are the function for thermal aging parameter P(t, T) shown in Eq. 1.3-1 as well as the ferrite content and chemical composition of the material. Table 2.1-2 shows the relationship between the optimal predicted value for true-stress - true-strain based on the predictive value and the tensile test results obtained in this study.

The test data for materials having a high ferrite content closely matched the predicted characteristics in the low strain region. In addition, the increase in tensile strength tended to be lower compared to the test data. The 0.2% yield strength was nearly the same, meaning that when the tensile strength was low, the plastic strain produced by the same load increased, such that the crack propagation force also increased. Consequently, the crack propagation force J_{app} for high-ferrite materials as assessed based on the predictive equation was on the high or conservative (safe) side. In pipes in actual equipment, the sum of the axial bending stress and membrane stress is typically on the order of Sm, and even if

one adds the thermal shock stress, typically, with the hypothetical elastic stress, it is predicted to not reach 3Sm (at 325°C and 350 MPa). When the ferrite content is high, the true strain at the crack tip when the stress is 3Sm is on the order of 5%, and in that range, there is no major discrepancy between the predictive equation and the test data. An appropriate value of J_{app} is obtained.

On the other hand, in the case of materials having a low ferrite content, in the low strain region, the predictive equations yields higher stress values than the test data, and in the high strain region, the reverse is true. This means that when the strain is high, applying the predictive equation is conservative (safe), but whenever the loads are small, the assessed crack propagation forces are too small, and caution must be exercised.

Table 2.1-1 Tensile Test Results

Section	Material		Test Temperature	0.2% Proof Stress	Tensile Strength	Elongation	Twisting	Ramberg-Osgood Parameters			
	Ferrite Content	Aging Process		(Mpa)	(Mpa)	(%)	(%)	σo	εo	α	n
Large-Sized Pipes	23.70%	Aged	Ambient	300	764	17.3	26.9	300	0.00154	0.895	4.320
				300	759	22.7	29.1	300	0.00154	10.001	4.268
			325°C	210	585	13.7	24.3	210	0.00121	1.541	3.597
				226	600	13.3	25.1	226	0.00130	1.333	3.794
		Unaged	Ambient	311	615	32.5	76.1	311	0.00159	2.871	4.283
				312	619	39.8	76.2	312	0.00160	3.484	4.133
			325°C	220	496	28.9	62.7	220	0.00126	6.131	3.222
				221	507	31.0	64.9	221	0.00127	6.662	3.069
	11.40%	Aged	Ambient	256	651	34.8	52.6	256	0.00131	3.997	3.259
				258	652	36.9	58.8	258	0.00132	3.783	3.326
			325°C	160	494	23.5	36.0	160	0.00092	6.036	2.630
				162	507	25.4	44.7	162	0.00093	6.031	2.675
		Unaged	Ambient	245	522	40.0	76.3	245	0.00126	6.775	3.360
				248	526	50.9	78.0	248	0.00127	10.228	3.043
			325°C	145	394	37.8	68.1	145	0.00083	13.751	2.421
				149	407	39.9	77.6	149	0.00086	15.305	2.444
Medium-Sized Pipes	22.70%	Aged	Ambient	303	778	25.3	26.4	303	0.00155	1.189	4.060
				312	782	27.1	30.6	312	0.00160	1.273	4.107
			325°C	207	604	15.7	24.3	207	0.00119	1.249	3.707
				212	609	15.9	27.2	212	0.00122	1.579	3.518
		Unaged	Ambient	308	630	38.1	67.4	308	0.00158	3.517	3.964
				311	631	10.2	73.2	311	0.00159	3.619	3.964
			325°C	200	496	39.9	61.2	200	0.00115	6.008	3.018
				202	401	30.1	64.9	202	0.00116	7.252	2.925
	10.90%	Aged	Ambient	228	601	45.8	61.1	228	0.00117	6.544	2.886
				232	609	48.6	66.6	232	0.00119	6.258	2.951
			325°C	144	460	31.7	54.8	144	0.00083	8.895	2.451
				146	462	31.9	55.3	147	0.00084	8.811	2.464
		Unaged	Ambient	238	507	49.9	80.7	238	0.00122	11.955	2.913
				239	514	52.5	81.1	239	0.00123	12.325	2.863
			325°C	141	392	38.2	64.1	141	0.00081	16.529	2.345
				142	405	39.8	69.9	142	0.00082	17.447	2.251

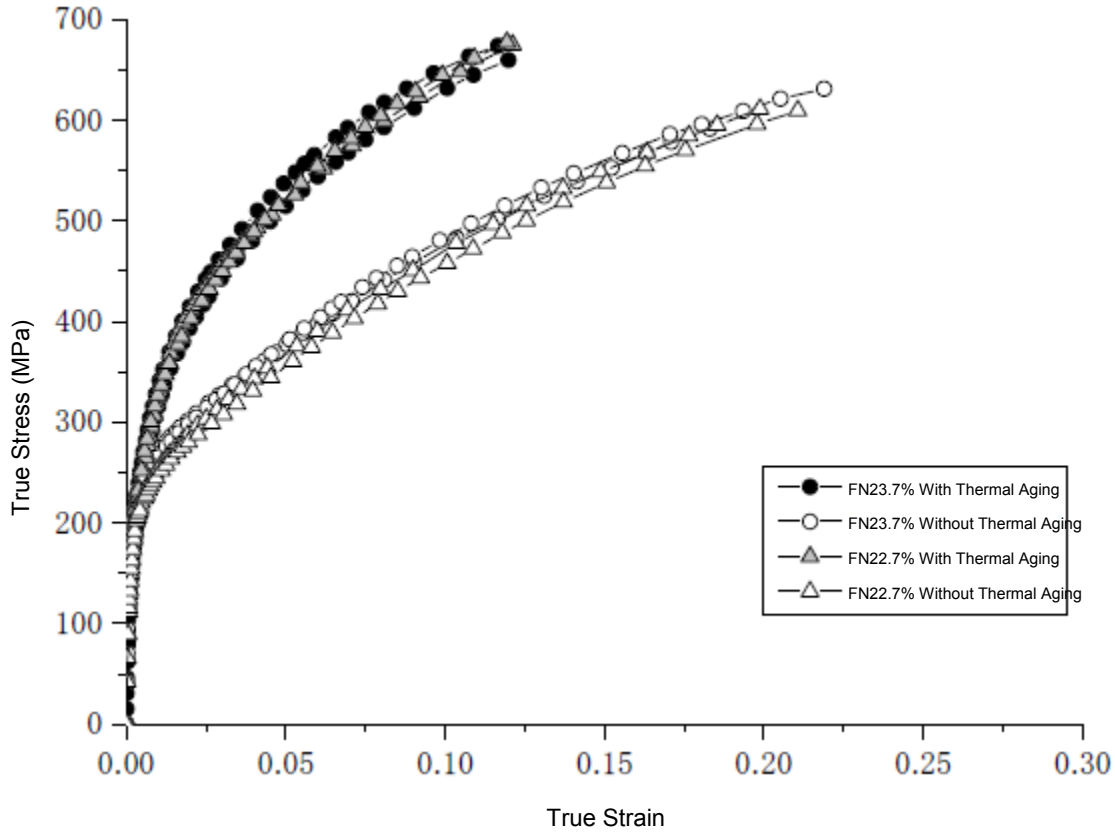

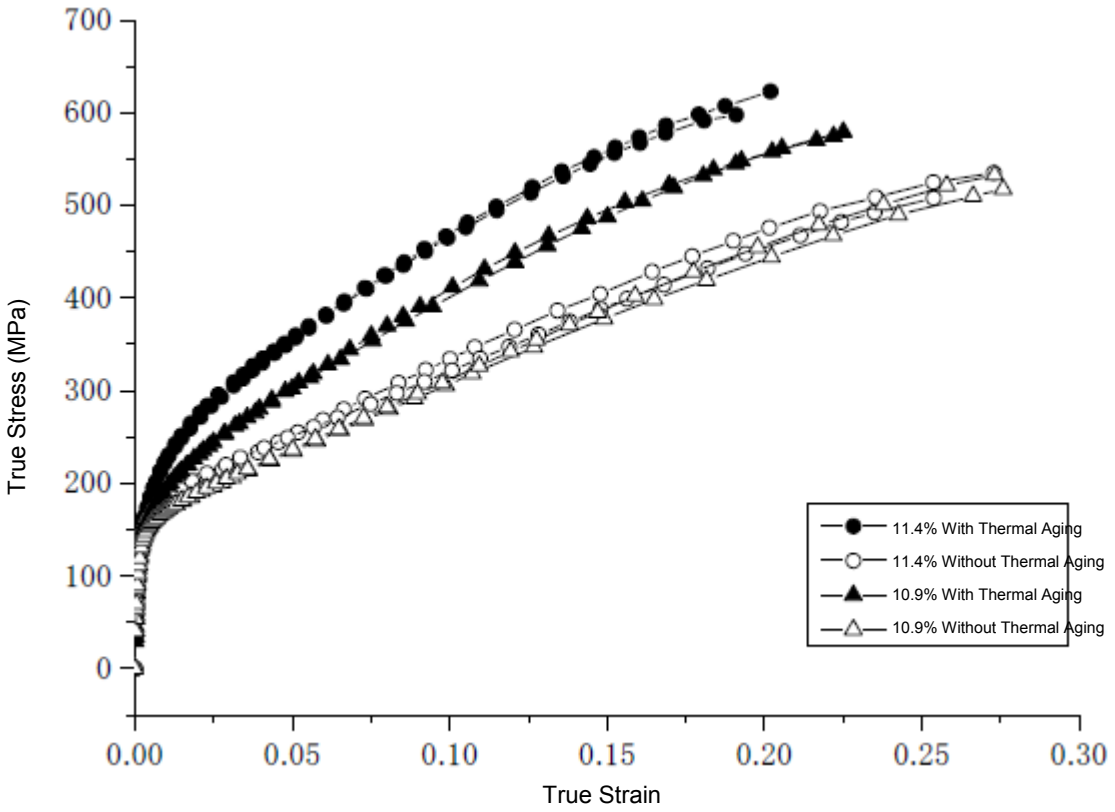

Figure 2.1-1 True Stress - True Strain Before and After Thermal Aging (325°C)

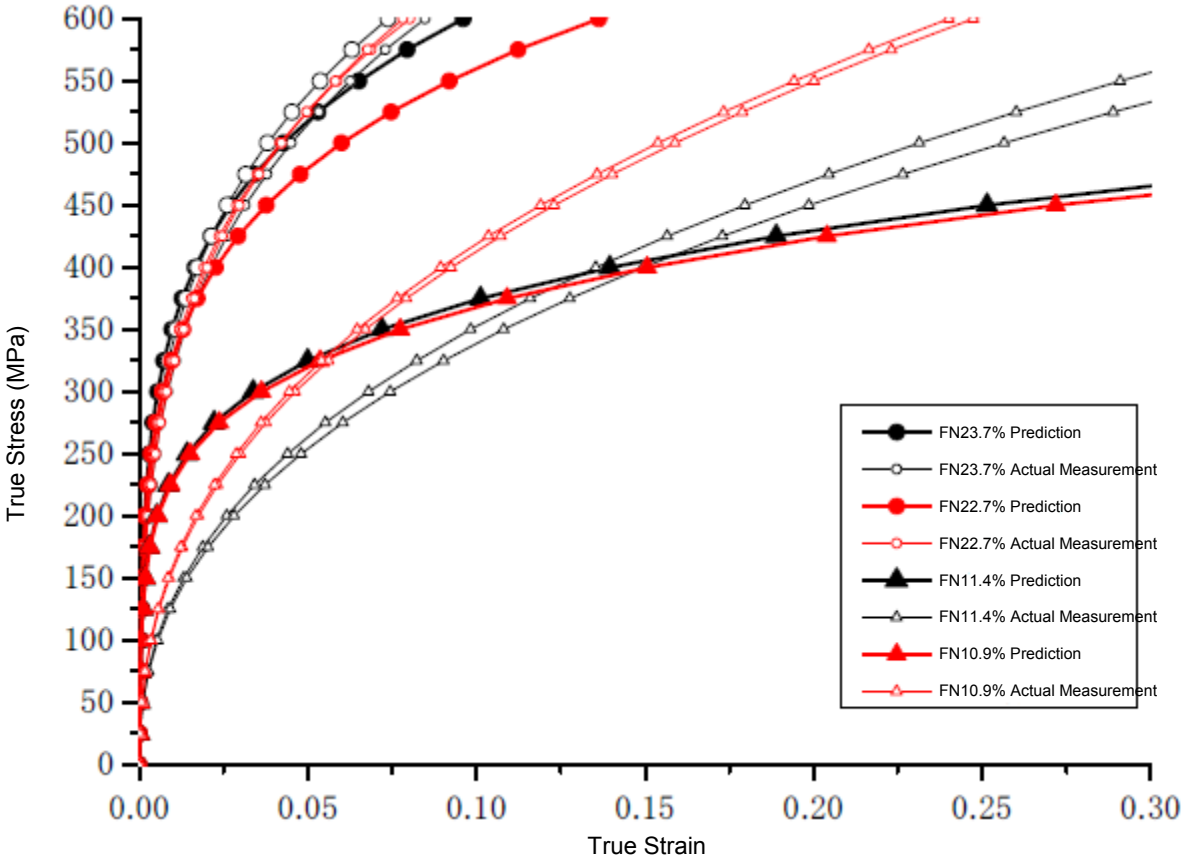

Figure 2.1-2 Comparison of Prediction Line and Actual Values for True-Stress - True-Strain

(2) Charpy Shock Test

Table 2.1-2 shows the results for the Charpy shock test. The Charpy absorbed energy decreased the greater the ferrite content of the material became. With materials having a high-ferrite content, there were cases where the absorbed energy fell as low 40J even at high temperatures. The Charpy absorbed energy value following thermal aging fell within the range predicted by Reference Document 3. The predictive equation from Reference Document 3 is a model where the Charpy absorbed energy and the fracture toughness taken after the elapse of time t when embrittlement has begun are expressed in the form of Eq. 2.1-1.

$$M = A + \frac{B}{t + C} \qquad (2.1\text{-}1)$$

M: Toughness value following thermal aging conducted for time t (USE value, $J1_c$, J_6)

A: Toughness value when the thermal aging time is infinitely large

B: Constant relating to the thermal aging temperature

t: Thermal aging time

C: Time constant

A, B, and C are obtained by means of a multiple regression analysis of test data serving as a function of the chemical composition of the material. A is the low value of toughness arrived at with long-term aging. A is expressed solely in terms of the ferrite content of the

Table 2.1-2 Charpy Shock Characteristic (325°C)

Section	Ferrite Content FN(%)	Orientation of Test Piece	Absorbed Energy (J)					
			Non-Aged Material	Aged Material			Post-Aging Predicted Value[3]	
							Average	Range
Large-Sized Pipe	23.7	LT	246-298	40	44	47	27	13-58
		LS	248-267	47	49	51		
	11.4	LT	275-298	113	116	116	146	69-311
		LS	287-298	105	116	122		
Medium-Sized Pipe	22.7	LT	213-250	62	62	67	31	15-67
	10.9	LT	270-285	127	130	159	157	74-333
	Weld Metal 9.0	LT	---	80	83	88	---	---

Note: The ductile fracture rate was 100% for aged material and non-aged material.

material, its temperature-dependence is slight, and so can be ignored. The value of A for the upper shelf Charpy absorbed energy of the base material is expressed by Eq. 2.1-2.

$$\log_{10}[A(J)] = 2.8357 - 0.0592 \times FN \qquad (2.1\text{-}2)$$

FN: ferrite content (%) computed in accordance with ASTM A800

Standard deviation = 0.1638

Term 2 on the left-hand side depends on the temperature and time, but in cases of long-term thermal aging as is found with 60 years of operation, it will be such a small value compared to M that it can be ignored. The column showing the predictions in Table 2.1-2 shows results computed based on Eq. 2.1-2.

(3) Fracture Toughness Test

Table 2.1-3 shows the results of the fracture toughness test. The lowered magnitude of $J_Q(J_{Ic})$ is as large as that for materials having a high ferrite content. The numerical values in the column for predicted values in Table 2.1-3 are predicted values for the low value of J_{Ic} (kJ/m^2). The predictive equation for fracture toughness is laid out in the same format as in the case of the Charpy shock test piece, and Eq. 2.1-3 shows the low value of fracture toughness after long-term thermal aging. The predictive equation has been

defined for J_{Ic} and for the J-integral value J_6 in cases where the ductile crack has grown 6 mm.

$$\log_{10}[J_{I_c}(kJ/m^2)] = 3.2961 - 0.0530 \times FN \quad \text{Standard Deviation} = 0.2518 \qquad (2.1\text{-}3)$$

$$\log_{10}[J_6(kJ/m^2)] = 3.6699 - 0.0490 \times FN \quad \text{Standard Deviation} = 0.1490$$

It can be seen that $J_Q(J_{Ic})$ for a thermally aged base material falls within the range of predicted values obtained using Eq. 2.1-3. J_{mat}-Δa following long-term thermal embrittlement is obtained by substituting the predicted values of $J_Q(J_{Ic})$ and J_6 into the equation $J = C1(\Delta a)^{C2}$.

$J_Q(J_{Ic})$ for weld metals was smaller than that for the base material, and this is because the fracture toughness prior to aging was lower than that of the base material. Because the ferrite content of the weld metal was low, the extent of thermal embrittlement was low. Table 2.1-3 shows an example of the Jmat-Δa characteristic before and after thermal aging. A representative example of the Jmat-Δa characteristic, which depends on the ferrite content of the material and the thermal aging temperature, is shown in Appendix 1.

Table 2.1-3 Fracture Toughness (325°C)

Section	Ferrite Content FN(%)	Orientation of Test Piece	Test Piece Size	$J_Q(J_{Ic})$ kJ/m^2						
				Non-Aged Material		Aged Material			Predicted Value for Aged Material	
				Min.	Max.	1	2	3	Minimum	Average
Large-Sized Pipe	23.7	LT	1TCT	661	874	103	120	121	35	110
		LT	1TCT*	53	631	99	100	100		
		LS	1TCT*	463	488	90	97	115		
	11.4	LT	1TCT	792	1298	266	297	331	156	497
		LT	1TCT*	764	1266	211	251	269		
		LS	1TCT*	802	932	276	298	318		
Medium-Sized Pipe	22.7	LT	1TCT*	546	600	134	147	163	39	125
	10.9	LT	1TCT*	718	1125	526	553	680	166	528
	Weld Metal 9.0	LT	1TCT			160	175	246		

Note: The numerical values shown are all J_Q values. 1TCT* indicates a test piece whose thickness is 1/2 T.

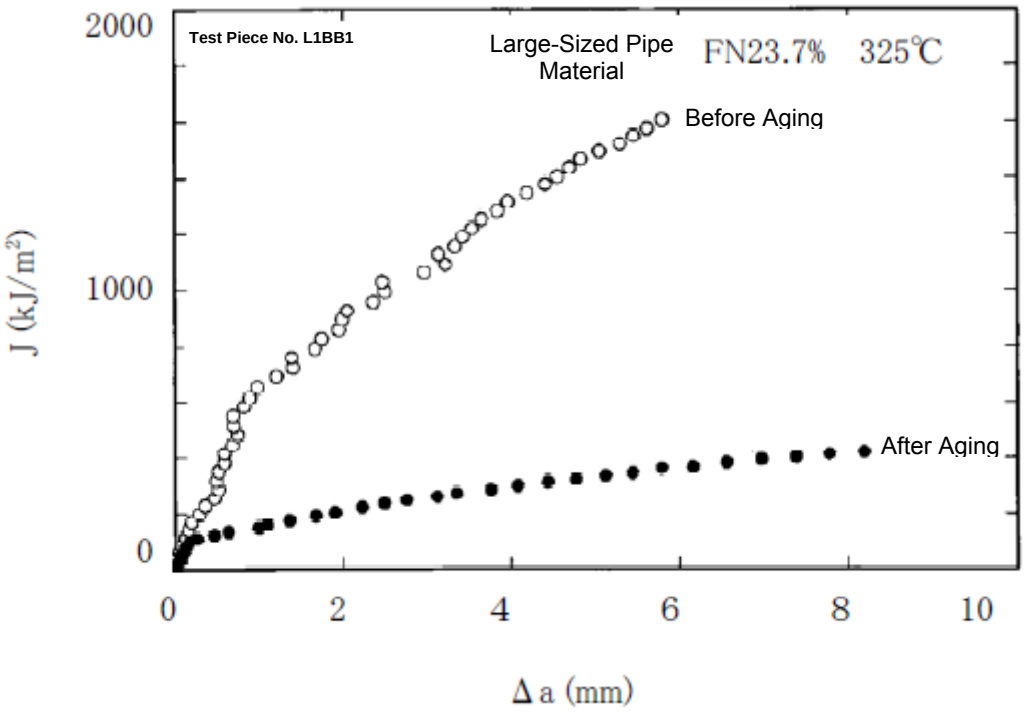

Figure 2.1-3 Example of Change in Fracture Toughness Before and After Thermal Aging (Part 1)

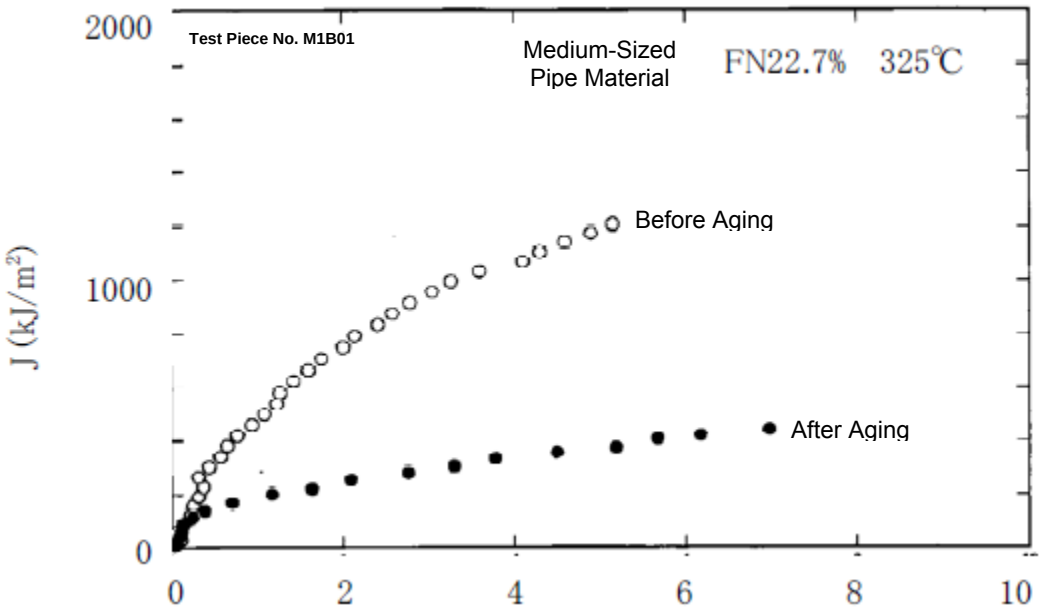

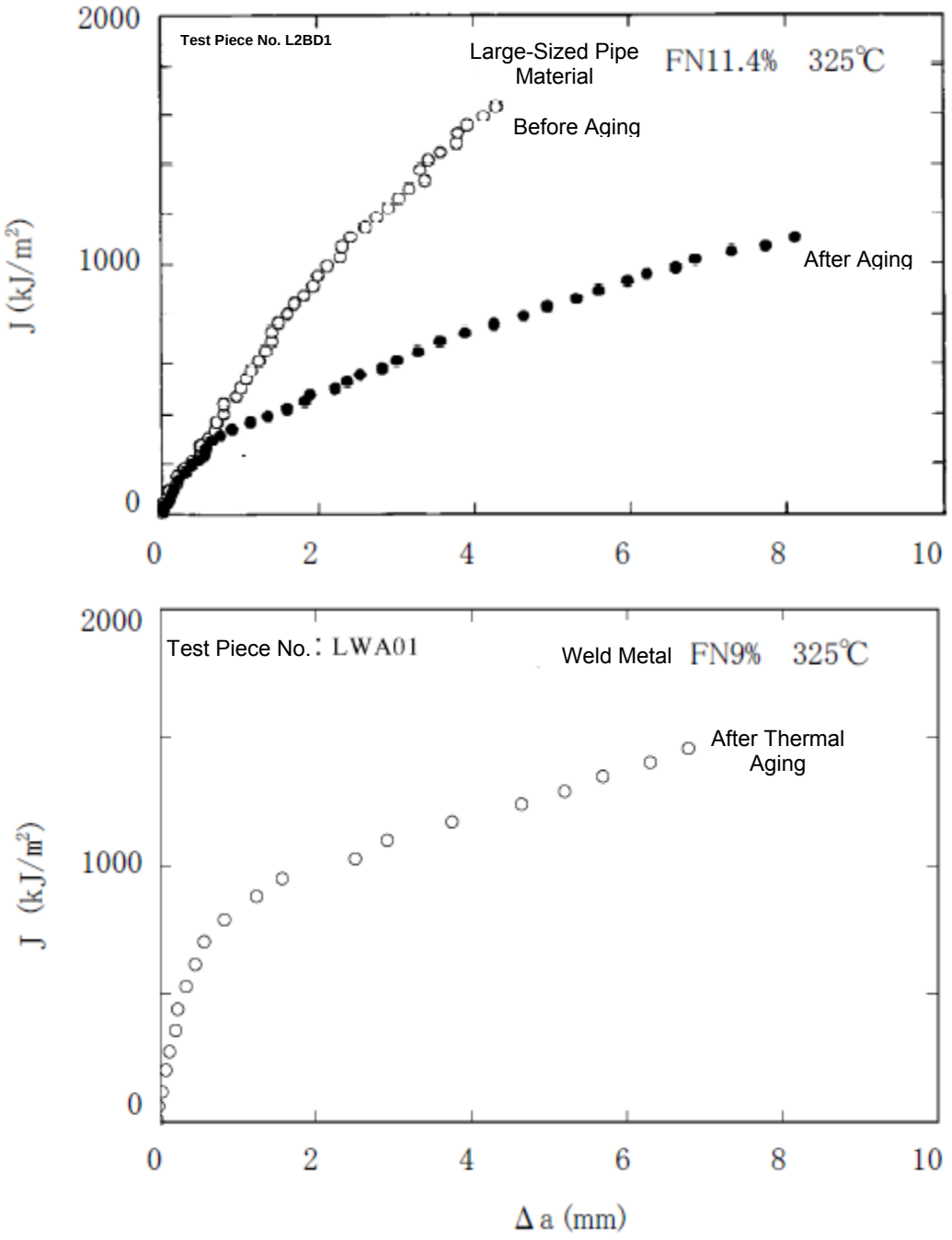

Figure 2.1-3 Examples of Change in Fracture Toughness Before and After Thermal Aging (Part 2)

(4) Structure Observation

Microphotographs of material having a ferrite content of 23.7% and 11.4% before and after thermal aging are shown in Figures 2.1-4 and 2.1-5. In addition, although thermal aging was performed this time at 450°C, they exhibit the same kind of two-phase

structure comprising austenite and ferrite as that obtained during longevity-oriented technological development for plants aged at temperatures of 290°-400°C. The ferrite phase is darker and etched; this is felt to be due to the precipitation of a G phase.

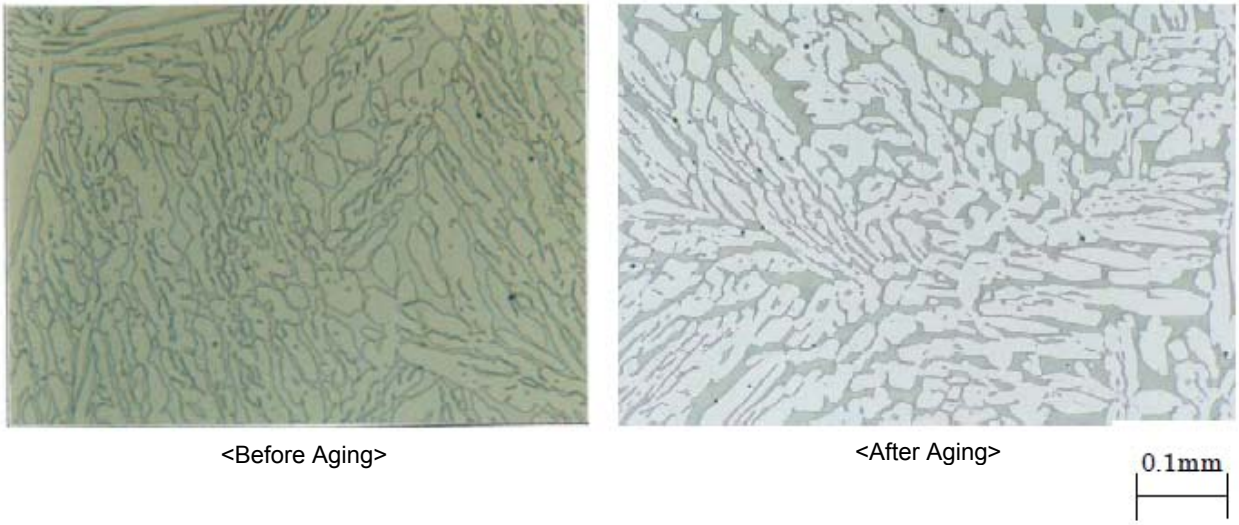

Figure 2.1-4 Microstructure of Material with a Ferrite Content of 23.7%

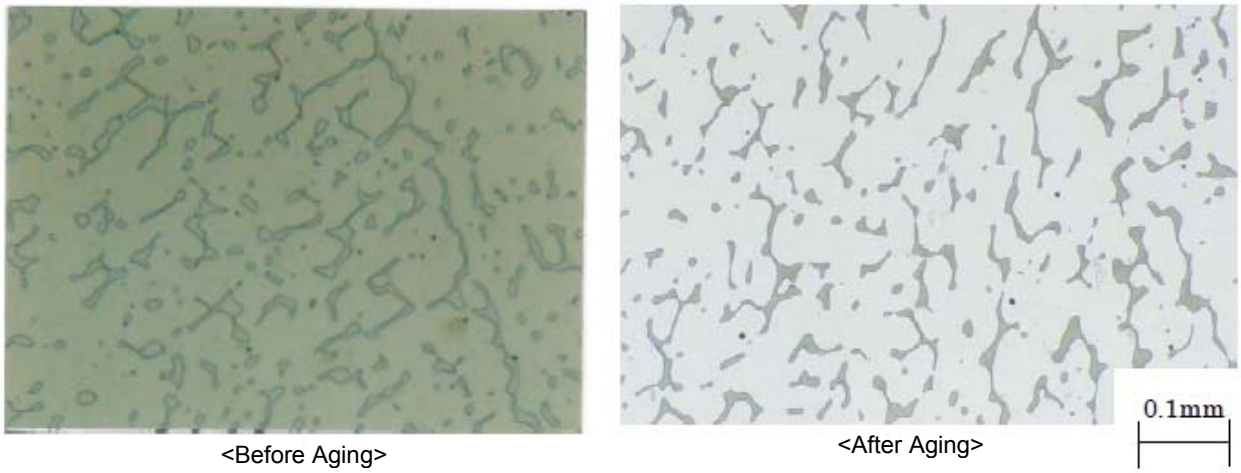

Figure 2.1-5 Microstructure of Material with a Ferrite Content of 11.4%

2.2 Pipe Tests

We performed a four-point bending fracture test on a large-sized pipe and medium-sized pipe that had been provided with semi-elliptical initial cracks in the circumferential direction on their inner surfaces. We measured the load-displacement and the growth of the cracks so as to ascertain their fracture behavior. We also performed before and after aging tests for

the mid-sized pipe test specimen. In addition to ascertaining the plastic collapse prior to thermal aging, we also determined the growth of a ductile crack due to thermal embrittlement and the behavior up to ductile instability. Upon obtaining that result, using the large-sized pipe test specimen, we turned our attention to the growth behavior of ductile cracks in a thermally aged test specimen.

(1) Mid-Sized Pipe Test

We tested a total of five test pieces M1 - M5 to which standard cracks had been applied. We increased the four-point bending load in small increments using displacement control on a test piece that was maintained at a test temperature of 325° ± 10°C using a heater installed inside the test piece.

① Test Results for Test Pieces M1 - M3

Test pieces M1 - M3 were test specimens consisting of non-aged materials and aged materials having a low ferrite content. Using these test pieces, and using the plastic collapse load that corresponded to the plastic flow stress obtained through the material tests for these materials, it was not possible to confirm the growth of cracks based on changes in electric potential output. As a representative example of the test results, the test results for non-aged material having a low ferrite content (M1) shown in Table 2.2-1 are described.

The plastic collapse load for test specimen M1 was obtained based on the plastic collapse moment Mo of a cylinder having a circumferential inner surface crack given by Eq. 2.2-1.

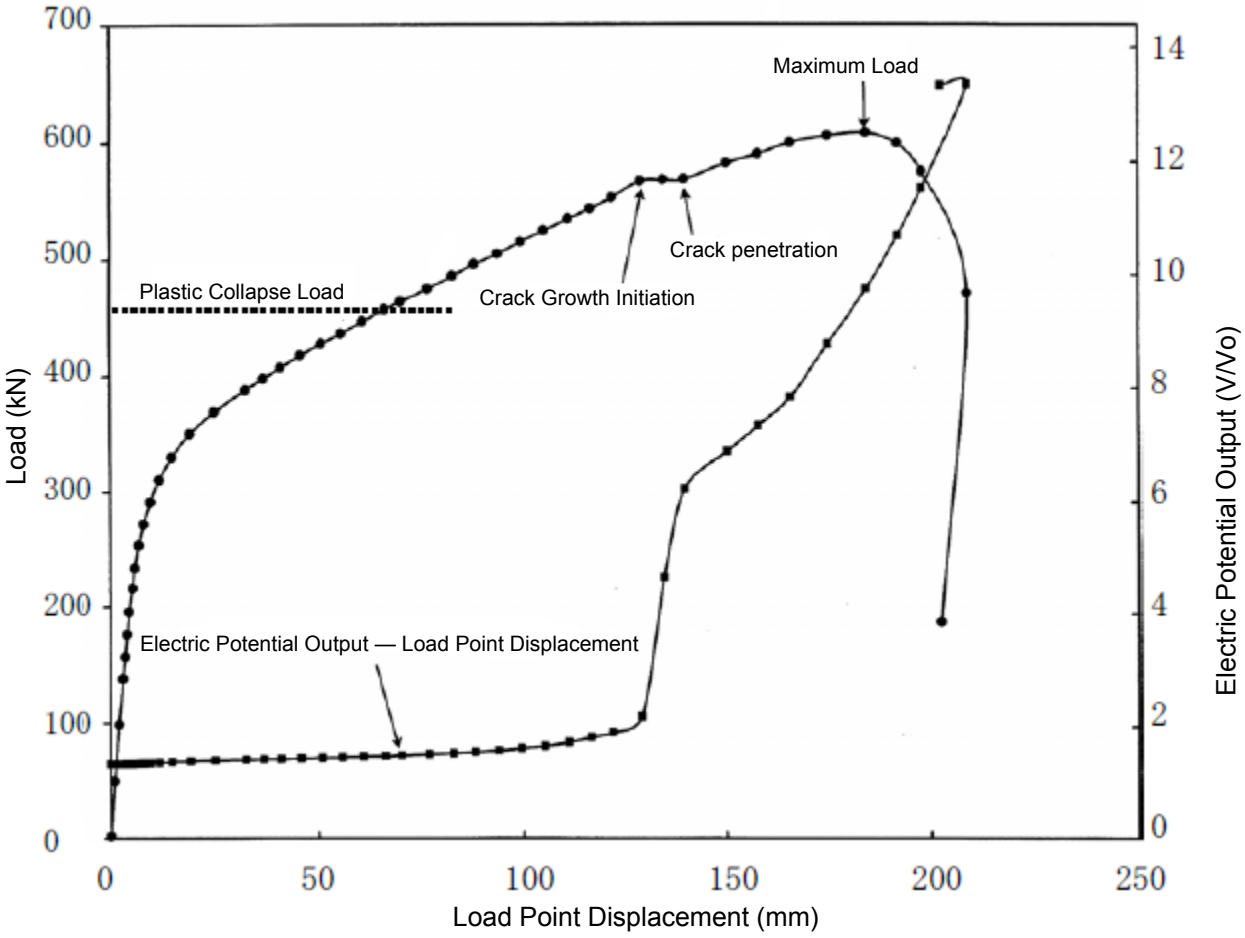

Figure 2.2-1 Electric Potential Output and Load Displacement of Test Piece M1

Denoting the distance between the load-bearing point and the support point at the time of the test as ℓ, the plastic collapse load L that imparts a plastic collapse moment is given by L = 2Mo/ℓ.

$$Mo = \frac{2Z\sigma_f}{\pi}\left(2\sin\beta - \frac{a}{t}\sin\theta\right) \qquad (2.2\text{-}1)$$

$$\beta = \frac{1}{2}\left(\pi - \frac{a}{t}\theta\right)$$

Z: Cross-section coefficient $\left(= \frac{\pi}{32}\left(\frac{D_o^4 - D_i^4}{D_o}\right)\right)$

σ_f: Plastic flow stress (the average value of the 0.2% yield strength and the tensile strength)

a: Crack depth t: Plate thickness D_i: Inner diameter

θ: Crack half angle D_o: Outer diameter

Based on the fracture cross section following the test, the initial crack dimension provided by propagating the fatigue crack at the front of the EDM notch became a semi-elliptical surface crack having a depth of 14.0 mm and a length of 72.0 mm. Due to the four-point bending load, the ductile crack grew in the plate thickness direction and passed through. When the tests were completed, the length of the through crack was approx. 130mm on the inner circumference. The shape of test specimen M1 was Do = 212.3 mm, Di = 166.3 mm, t = 23.0 mm, ℓ = 750 mm, a = 14.0 mm, and θ = 0.433 rad. Based on the 0.2% yield strength and tensile strength of Table 2.1-1, the plastic flow stress σ_o reached a maximum of 274 MPa. When using these figures, the plastic collapse load of test specimen M1 became 470 kN.

On the other hand, from the test results, and based on changes in the electric potential output of Figure 2.2-1, it appears the ductile crack began to grow at approx. 570 kN. Consequently, under conditions where the computed plastic collapse load was applied, cracks did not grow in test specimen M1.

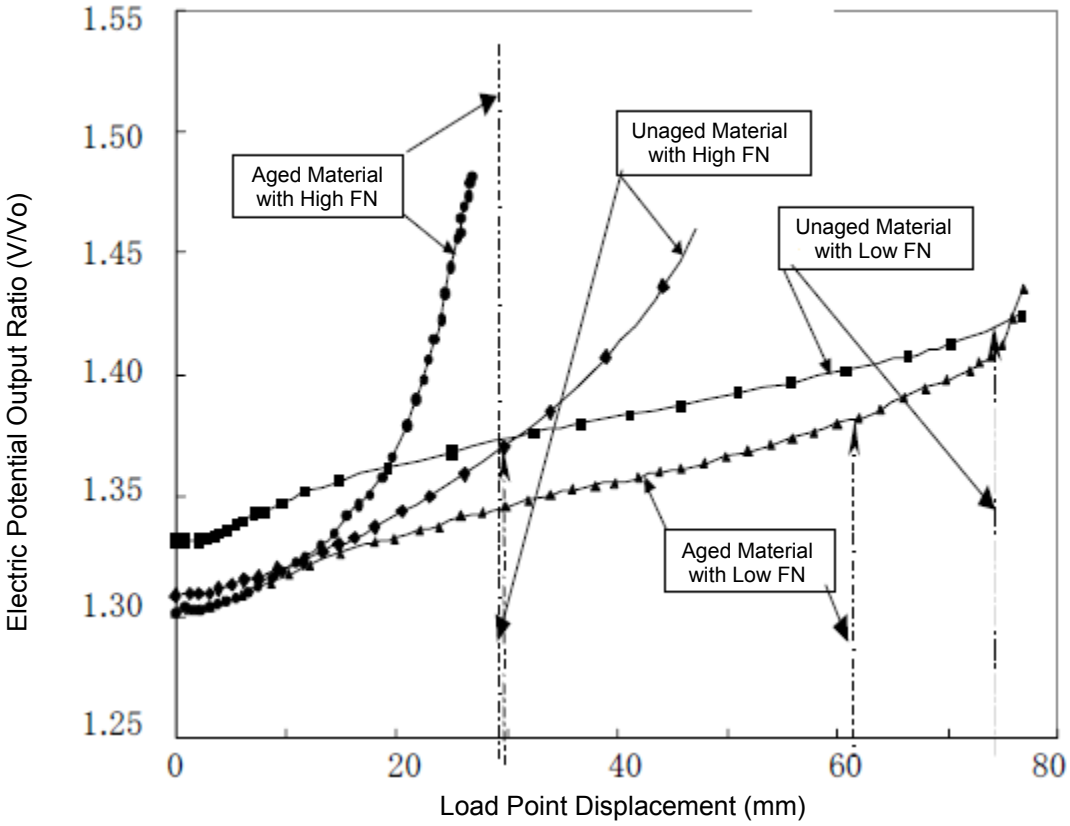

Figure 2.2-2 Electric Potential Output and Load Point Displacement

(↑ is the displacement corresponding to the plastic flow stress)

Figure 2.2-2 shows the measurement results of the load point displacement and the electric potential output of test specimens M1 - M3 and M5. The vertical lines in the figure show the load point displacements where the test specimens reached their plastic collapse load. In the figure, for the test specimen M5, a small amount of ductile crack growth on the order of 1.7 mm (to be described later) was confirmed with a maximum load just under the plastic collapse load; it is shown for comparison with M1 - M3. One can see that, compared to M5, the test specimens M1 - M3 had a lower rise in electric potential below the plastic collapse load.

Assuming an initial crack having standard dimensions, when assessing integrity, it appears to be safe to assume that a fracture will occur with a collapse load computed using the net stress concept based on the plastic flow stress for unaged material in a medium-sized pipe and for aged material having low ferrite content. A summary of the test results for test specimens M1 - M3 that have undergone plastic collapse is shown in Table 2.2-1. Compared to the unaged materials, the aged material had lower ductile crack growth starting loads and maximum loads, and the difference with the plastic collapse load became small.

Table 2.2-1 Test Results for Test Pieces M1 - M3

Medium-Sized Pipe Material	Low Ferrite Content 10.9%		High Ferrite Content 22.7%
	Non-Aged Material M1	Aged Material M2	Non-Aged Material M3
Initial Crack Depth a(mm)	14.0	14.7	14.5
Initial Crack Half Angle θ (rad)	0.433	0.433	0.433
Plastic Flow Stress σo (MPa)	274	303	358
Plastic Collapse Load L (kN)	470	516	612
Ductile Crack Start Load (kN)	569	553	738
Maximum Load (kN)	608	579	741

② Test Results for Test Specimens M4 and M5

With test specimens produced by thermally aging materials with a high ferrite content, ductile cracks grew under loads that were smaller than the plastic collapse load. As for the order of trials, using test specimen M5, we first confirmed that ductile cracks were produced under loads that were below the plastic collapse load, and then, using

test specimen M4, we applied loads up to the maximum load. Table 2.2-3 shows the relationship between the electric potential output and the load and load point displacement for both test specimens.

The test results for test specimen M5 are shown by the hollow points in the figure. Based on the tendencies of electric potential output, we were able to confirm that ductile cracks grew when the load was 665 kN, at which point we unloaded the specimen. The load point displacement at this point was 26.8 mm. The maximum load 665 kN was approx. 94% of the computed plastic collapse load of 704 kN for pipes having the initial crack dimension. The maximum withstand load for a pipe having the same specification, as obtained in the test for test specimen M4, was 684 kN, which was slightly below the computed plastic collapse load. After removing the load on test specimen M5, and after allowing the specimen to cool naturally, we induced fatigue surface fractures in the ligament section using repeated four-point bending loads, and

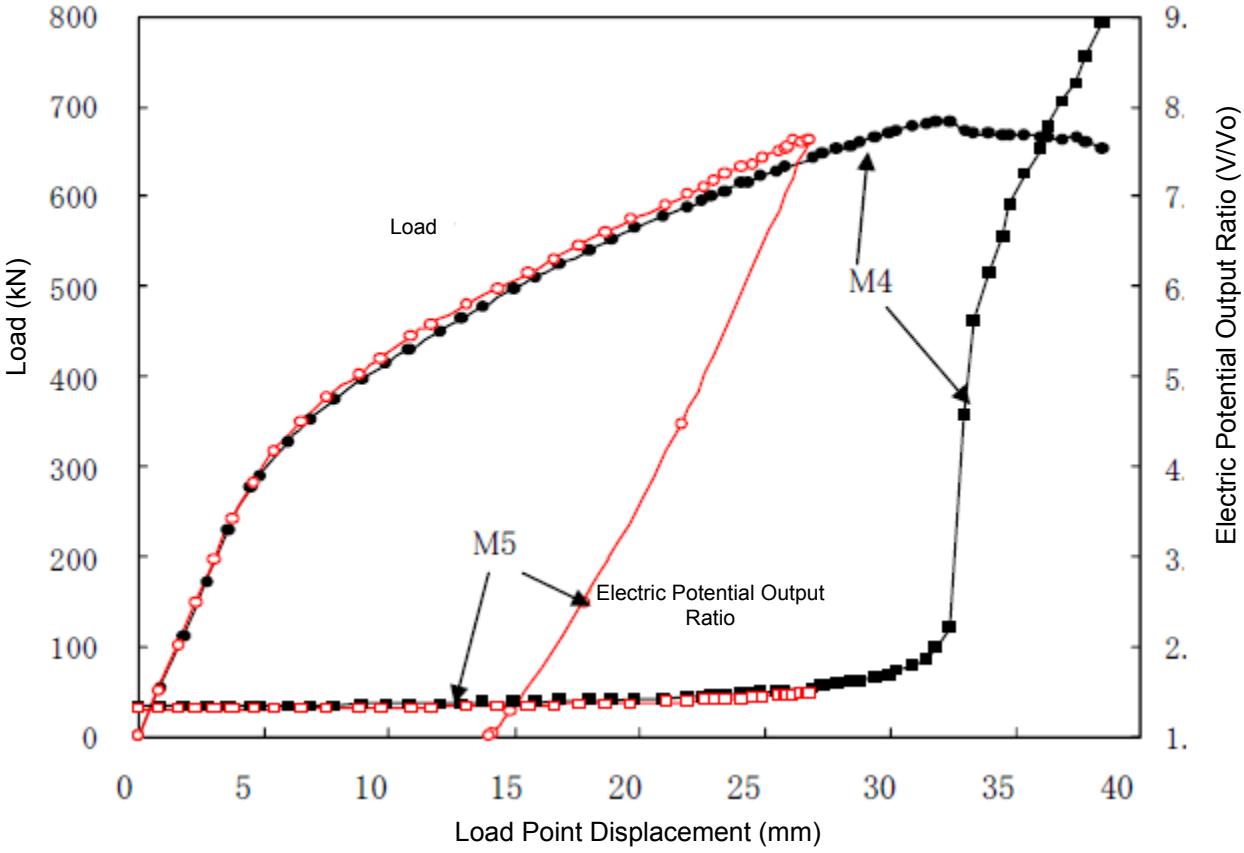

Figure 2.2-3 Test Results for Test Specimens M4 and M5

we exposed fracture surfaces. By measuring the fracture surfaces, we determined that the initial crack was a semi-elliptical surface crack having a depth of 14.07 mm and a

length of 72.5 mm. The ductile fracture surface propagated 1.71 mm in the plate thickness direction from the crack's deepest portion, and once the tests were concluded, it was 15.78 mm deep and 72.6 mm long. In addition, the initial crack for test specimen M4, for which the maximum load was measured, was 14.54 mm deep and 72.70 mm long. The ductile crack propagated from the fatigue fracture surface so as to pass through in the plate thickness direction. Once the test had been concluded, the inner surface revealed that through cracks approx. 210 mm long had been produced.

(2) Large-Sized Pipe Tests

We measured the growth behavior of ductile cracks using thermally aged test specimens having a low ferrite content (L1) and high ferrite content (L2) in which standard cracks were induced, as well as thermally aged test specimens having a high ferrite content (L3) in which cracks deeper than a standard crack were induced.

① Test Specimen L1 (Thermally Aged Pipe with a Ferrite Content of 11.4% in Which Standard Cracks Were Induced)

Figure 2.2-4 shows the relationship between the electric potential output and the load and load point displacement. Based on the tendencies for electric potential output, we determined that ductile crack growth occurred in the vicinity of the computed plastic collapse load, at which point the specimen load was removed. The maximum load was 609 kN, and the load point displacement was 176.00 mm. The maximum load 609kN was approx.90% of the plastic collapse load hypothesized for the initial crack. Fracture surface images are shown in Figure 2.2-5.

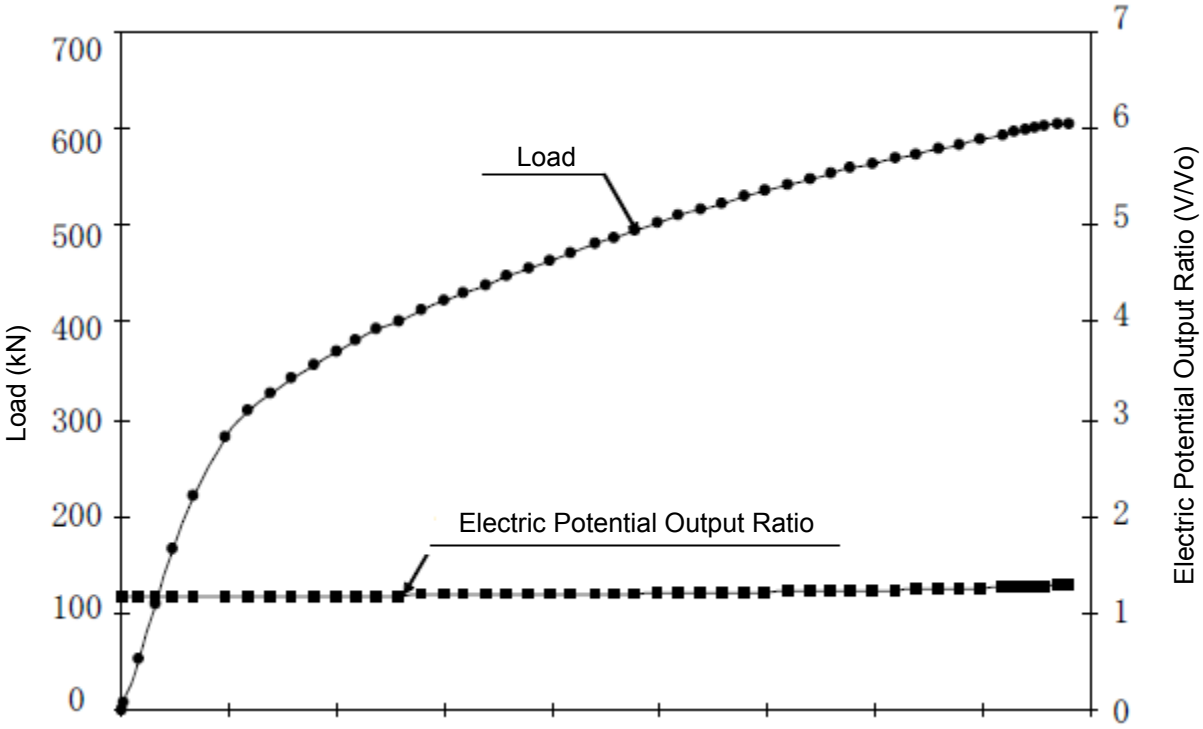

Figure 2.2-4 Load Point Displacement, Load, and Electric Potential Output Ratio for Test Specimen L1

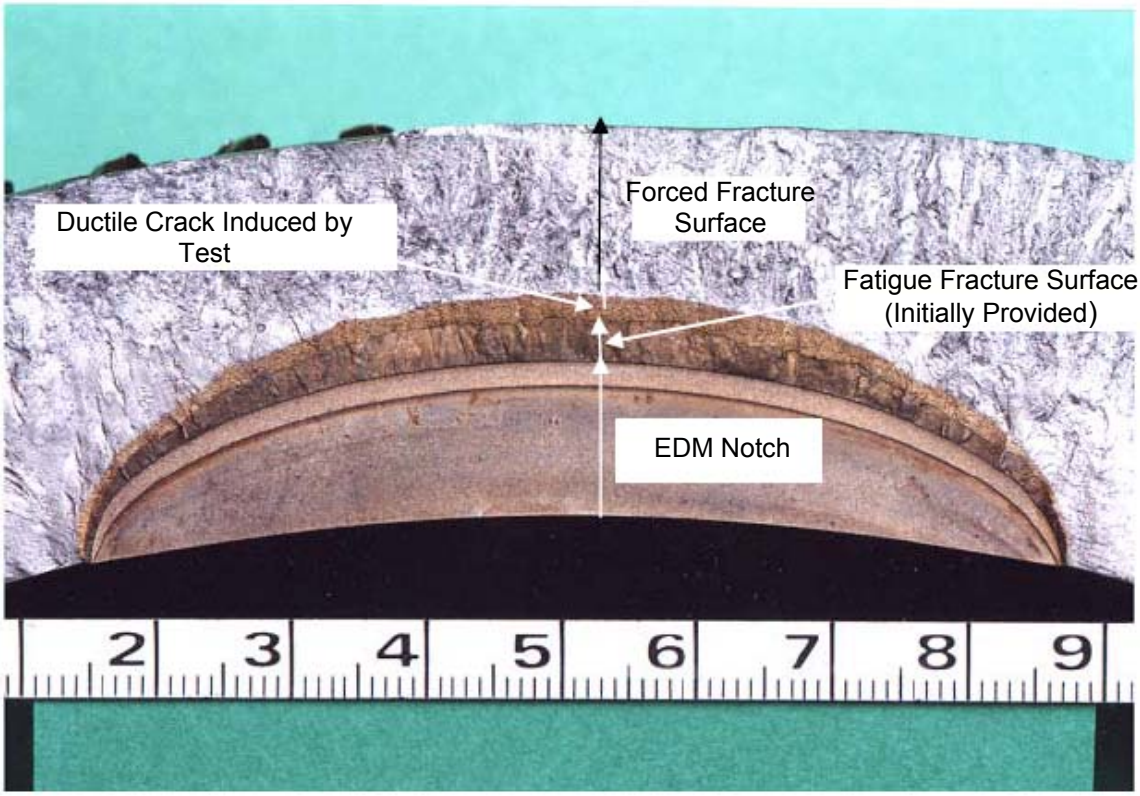

Figure 2.2-5 Fracture Surface Image for Test Specimen L1

Measurements of the fracture surface indicated that the initial crack was a semi-elliptical surface crack having a depth of 14.35 mm and a length of 72.7 mm. In the ductile fracture surface, the crack propagated 1.85 mm in the plate thickness direction at its deepest. After the test was completed, it was 16.20 mm deep and 73.13 mm long.

② Test Specimen L2 (Thermally Aged Pipe with a Ferrite Content of 23.7% in Which Standard Cracks Were Induced)

Figure 2.2-6 shows the relationship between the electric potential output and the load and load point displacement. Through observations of the tendencies in the electric potential output, at the point where we could see that the ductile crack had grown sufficiently, we stopped the load and unloaded the specimen. The maximum load was 690 kN, and the load point displacement at that time was 92.8 mm.

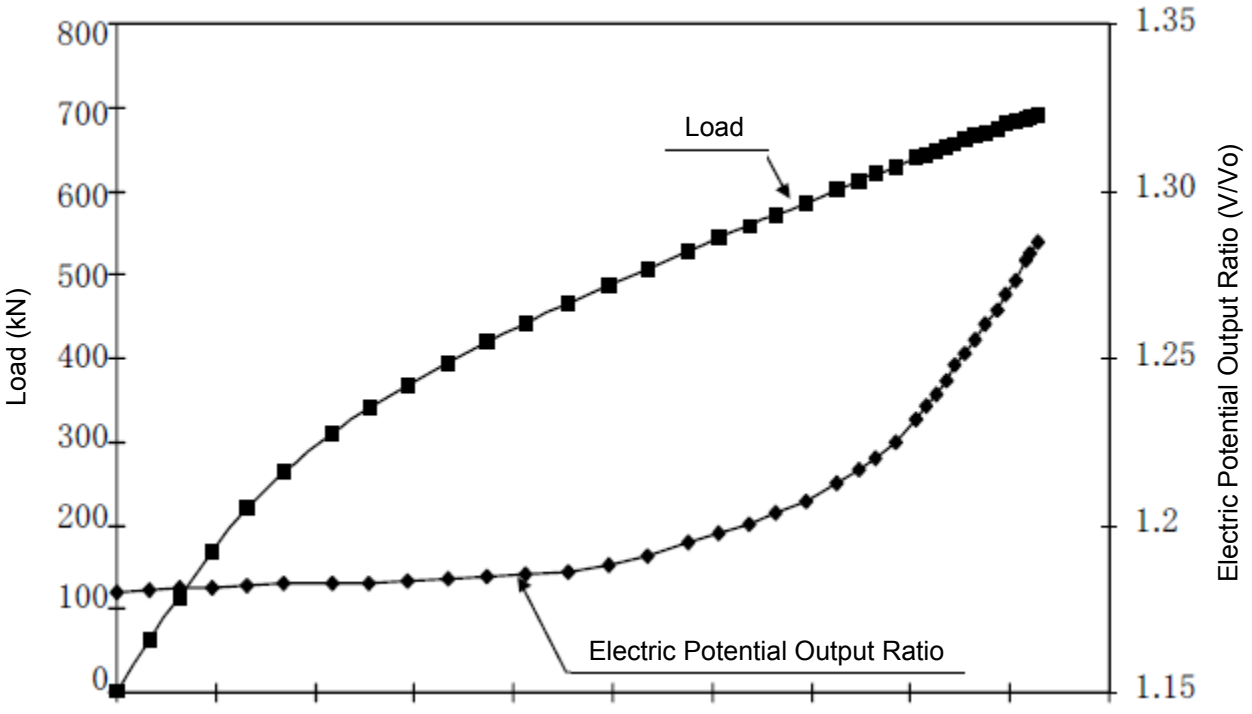

Figure 2.2-6 Electric Potential Ratio, Load, and Load Point Displacement of Test Specimen L2

Figure 2.2-7 Fracture Surface Photograph of Test Specimen L2

Moreover, the maximum load of 690 kN was approx. 85% of the plastic collapse load of 815 kN assumed for the initial crack. A photograph of the fracture surface is shown in Figure 2.2-7. The initial crack was a semi-elliptical surface crack having a depth of 14.95 mm and a length of 72.52 mm. A ductile crack propagated from the fatigue fracture surface in the plate thickness direction, and at the end of the test, the crack shape was 17.32 mm and 72.52 long. The ductile crack grew 2.37 mm in the depth direction in the ductile crack growth experiment.

③ Test Specimen L3 (Thermally Aged Pipe with a Ferrite Content of 23.7% in Which Deep Flaws Were Induced)

Figure 2.2-8 shows the relationship between the electric potential output and the load and load point displacement. The maximum load was 609 kN, and the load point displacement was 78.9 mm. The maximum load 609 kN was approx. 78% of the plastic collapse load 781 kN assumed for the initial crack.

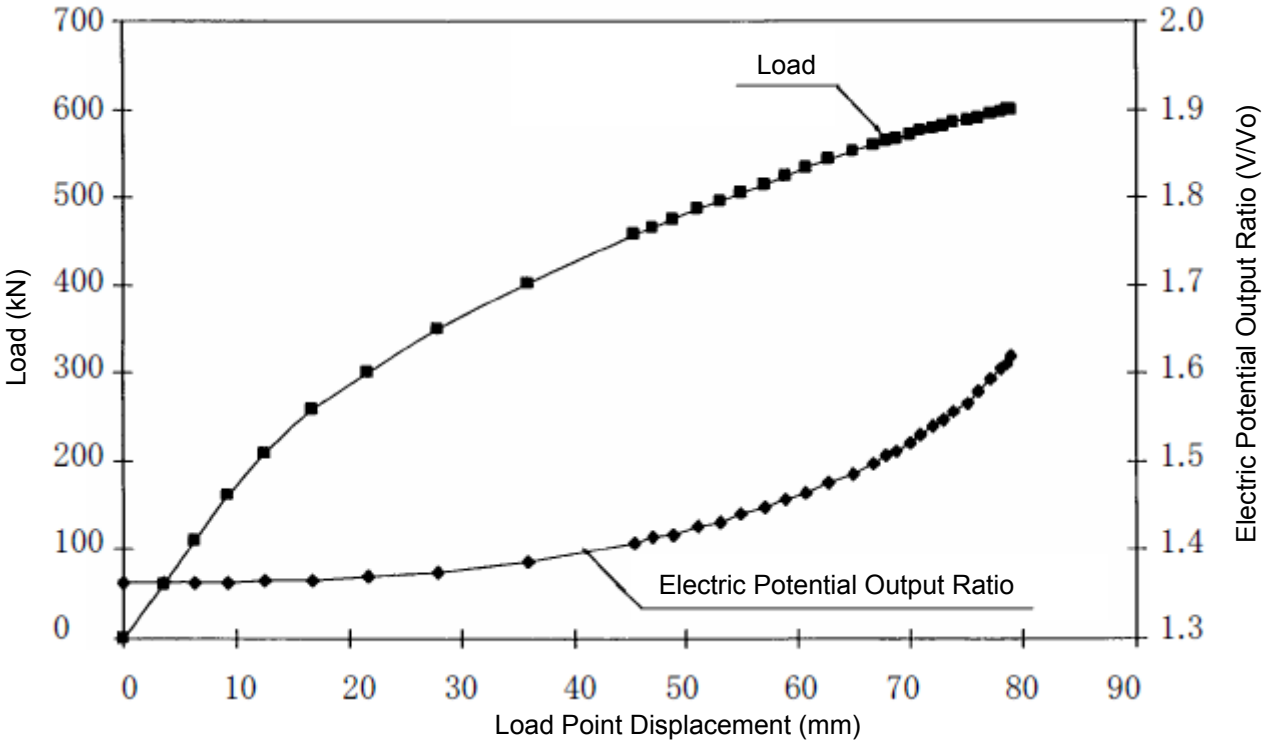

Figure 2.2-8 Electric Potential Output, Load, and Load Point Displacement of Test Specimen L3

Figure 2.2-9 Fracture Surface of Test Piece L3

Figure 2.2-9 shows a photograph of the fracture surface. The initial crack was a semi-elliptical surface crack having a depth of 18.95 mm and length of 92.63 mm. The crack shape at the conclusion of the test was 21.12 mm deep and 92.91 mm long. In the ductile crack growth experiment, the ductile crack grew 2.17 mm in the depth direction.

2.3 Test Specimen Analysis

(1) Modeling the Analysis

We verified the manual analytical evaluation method using the material test results for the material and the ductile crack growth test results obtained in the size-reduced test piece.

① Material Characteristics

The material characteristics were used as input for the true-stress - true strain characteristics of the material. Of the true-stress - true-strain characteristics obtained using multiple tensile test pieces manufactured from the material, we inputted the highest strength characteristic. In cases where we modeled the test piece as a whole containing connecting pipes, the true-stress - true-strain input in the connecting pipe section was the value as separately measured, which is given in the appendix.

② Modeling Range

We examined a test piece model that modeled a 1/4 sector of the entire test piece and a short pipe model that modeled a 1/4 sector having a length of approx. 2D on one side in the pipe's longitudinal direction from the center section to which a crack had been imparted.

(a) Test Piece Model

Modeling of the overall test piece is shown in Figure 2.3-1 taking, by way of example, the medium-sized pipe M5 test piece model. The analysis code that we used was ABAQUS, and the finite elements were a 20-node set of two-dimensional brick-shaped elements and 50-node set of triangular prism elements.

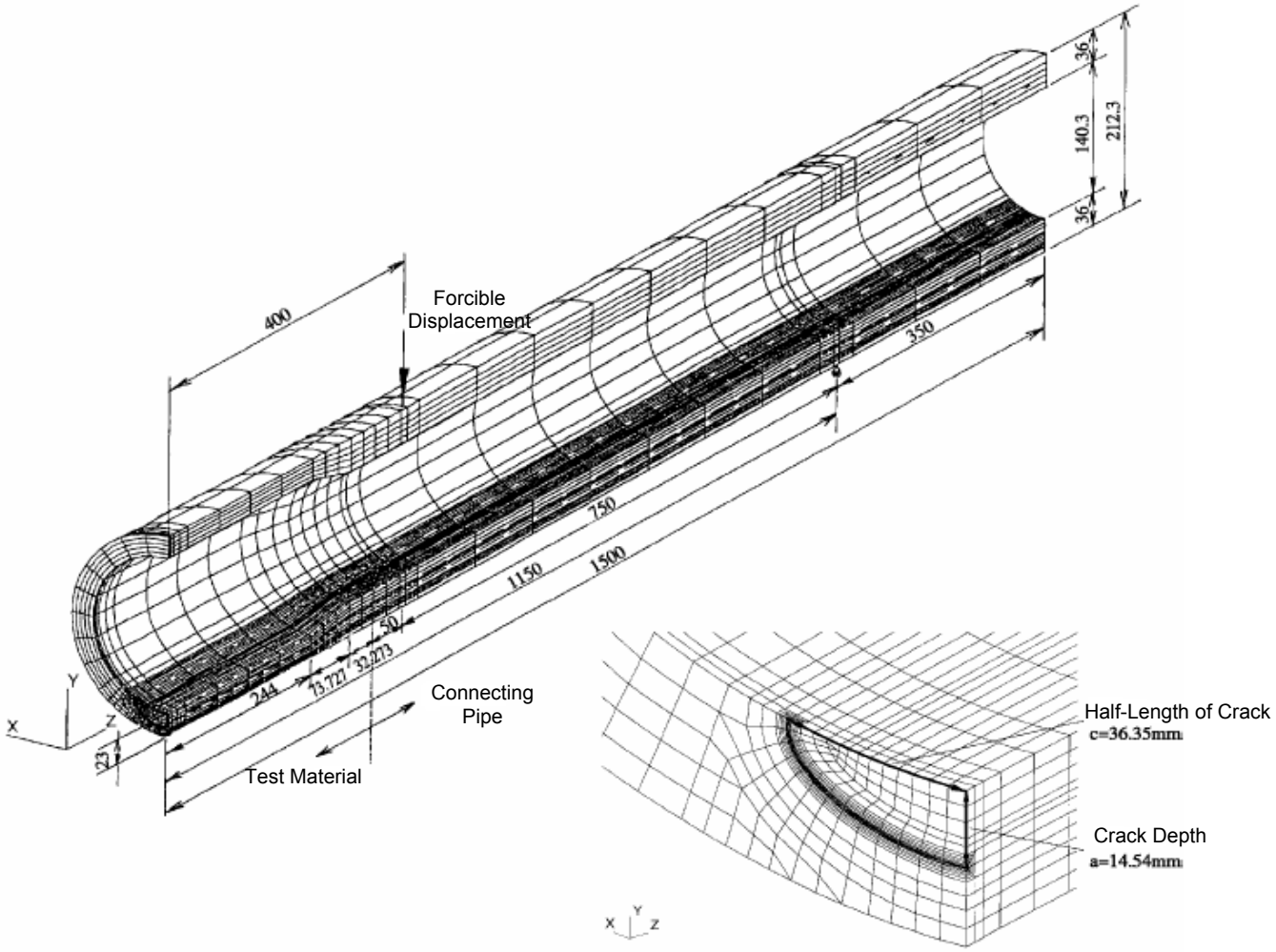

Figure 2.3-1 Test Specimen Analysis Overall Modeling (Using the Example of Test Specimen M5)

The restraint conditions were such that, taking into consideration symmetry, movement was constrained respectively in the X direction of the central surface, the Z direction other than crack surface of the section containing the crack, and Y direction of the test specimen end section. The test-time displacement at the time of the maximum load on the four-point bending load point was made to be forcible displacement input. Analysis of the J-integral value was based on the path integral method. In order to apply this modeling and analysis to predict the load displacement at the time of testing and confirm the validity of the results, we had it performed by a test practitioner.

(b) Short Pipe Model

In order to investigate the modeling method when applied to multiple numerical tests on actual-sized equipment, we performed our analysis based on the path integral

method using only the model for the central region of the test specimen, and compared this against the test results and test specimen analysis results. In this analysis, we kept the fracture toughness of the material covered up, and had a practitioner different from the one who implemented the test perform the analysis with a separate analytical code FINAS from that used for the test piece analysis. Figure 2.3-2 shows the mesh partition diagram for the short-pipe model. The finite elements were a 20-node section of two-dimensional brick elements. The constraint conditions were such that, taking symmetry into consideration, movement was constrained in each of the X direction of the central surface and in the Z direction, other than in the crack surface of the section containing the crack. The end surface to which no crack was applied was a rigid body element, and we applied a bending moment to the model while imparting a load in the Z direction to the rigid body element. The crack shape was modeled as a semi-elliptical surface crack having the deepest depth and surface length to which ductile cracks had grown.

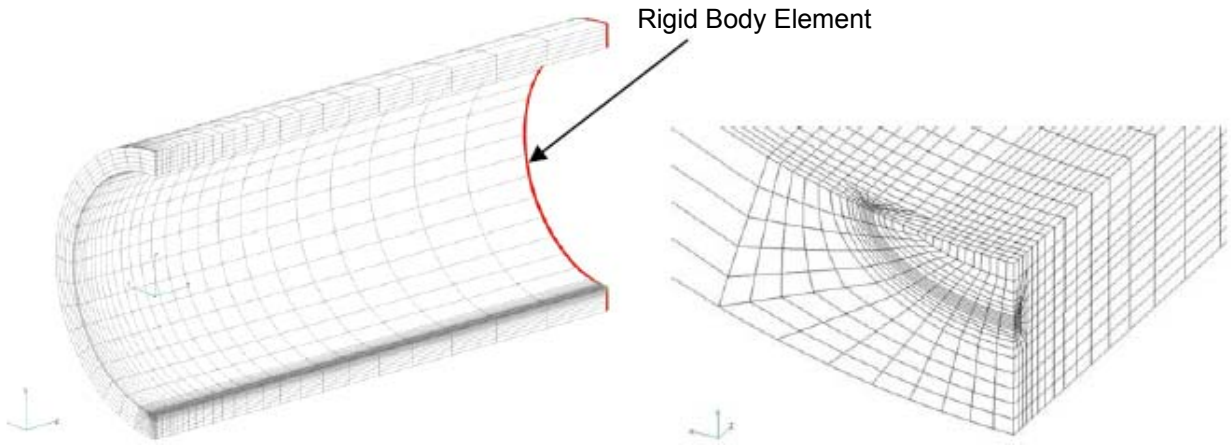

Figure 2.3-2 Short Pipe Model

In the test specimen analysis, regardless of whether using the test model or short pipe model, we obtained J_{app} using a hypothesized crack propagation method for multiple domains of integration in the vicinity of the crack tip. With the test mode, we set a plurality of regions in a range where 1/2 the side length of a rectangle centering on the crack tip is from 0.3 mm to 5 mm. When computed with a domain of integration from the crack tip to within 2 mm, one sees changes in J_{app}, but the value computed in a domain of integration broader than 2 mm was nearly stable. On the other hand, when performing an analysis using the short pipe mode based on FINAS, J_{app} was almost constant irrespective of the domain of integration, as shown in Figure 2.3-3. We defined the

average value of J_{app} as the average of the analytical values from the second domain of integration to the fourth domain of integration.

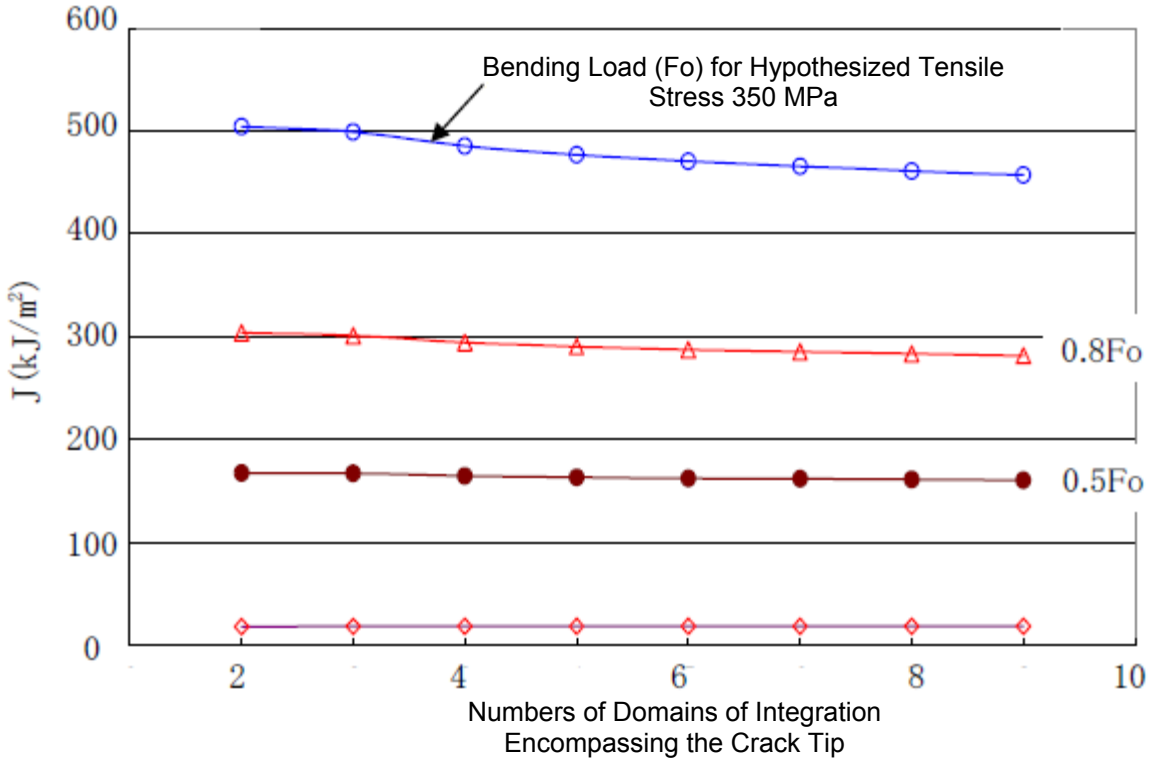

Figure 2.3-3 Sample Computation of J_{app} and Domain of Integration in the Short Pipe Model

(2) Specimen Analysis

① Medium-Sized Pipe with High Ferrite Content to Which Standard Cracks Were Imparted (Test Specimen M5)

Using the test specimen analytical model, when computing the J_{app} value for the deepest portion of the crack corresponding to the maximum bending load applied during the test, a value of 304 kPa•m was obtained. Figure 2.3-4 plots a comparison between the J-Δa curve obtained by the material test of the material against the J_{app} value obtained by computation. The J_{app} value slightly exceeded the upper limit of the data obtained from the 1TCT* test for three pieces of the material. Here, the 1TCT* test piece was a CT test piece having a standard dimension with W being 25.4 mm and the depth being 12.7 mm. Consequently, if one evaluates J_{app} using the domain of integration and this analytical model, by using the J-Δa curve obtained using the 1TCT* test piece for the average ductile crack growth evaluation, one can see that it is possible to make a conservative estimation of ductile crack growth behavior for the medium-sized pipe. The

estimate is felt to be safe because the degree of plastic restraint of the crack tip region of the medium-sized pipe test specimen is smaller than the 1TCT* test piece.

For reference, we obtained J_{app} in the case where a simple evaluation formula[14] for thin-walled pipes for which Rm/t is 10 was applied to test specimen M5. Because a simple evaluation formula for inner surface semi-elliptical cracks in the circumferential direction had not been developed, for the inner surface crack, we targeted a crack having a fixed depth of 15.78 mm and a length of 72.6 mm. The computed J-integral value obtained when the maximum load was being applied to this crack during the test became a value that was more than three times this analytical result. It could be that applying a simple evaluation formula for thin-walled pipes to thin-walled pipes like those used as primary cooling pipes ends up being extremely safe.

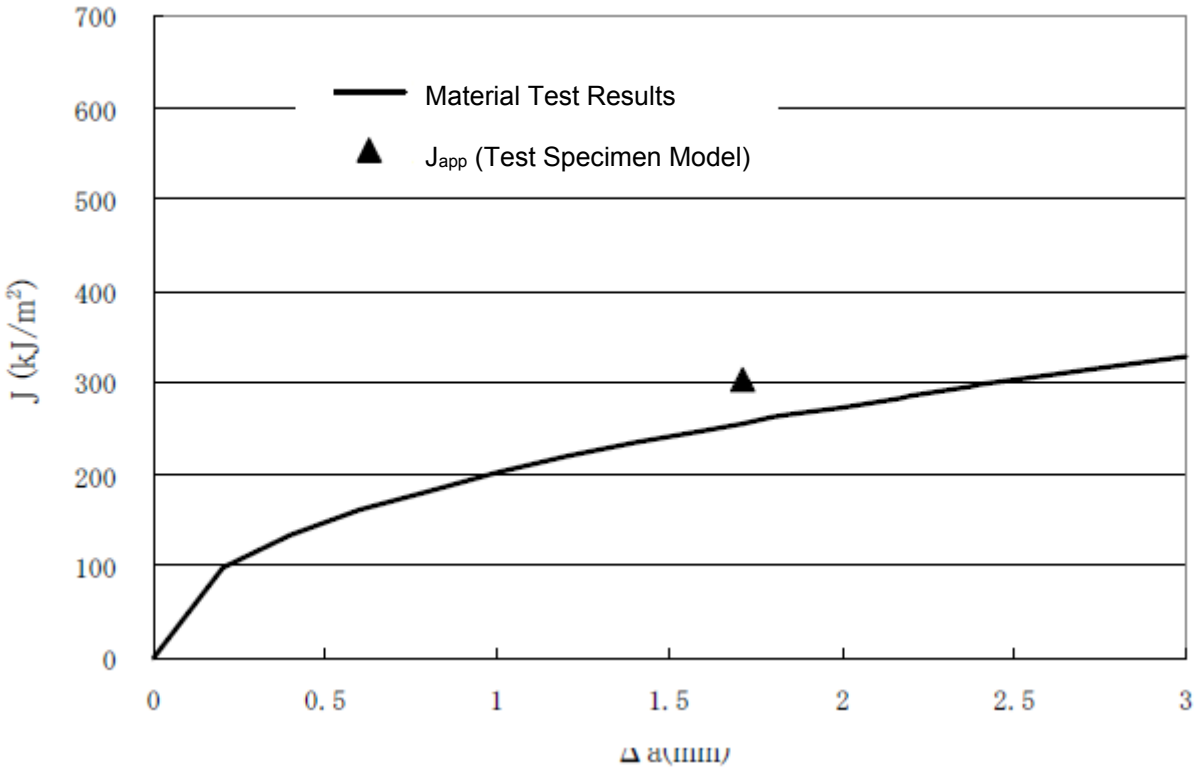

Figure 2.3-4 Test Specimen Analytical Results and Material Test Results for M5

For reference purposes, we computed J_{app} by applying the simple evaluation formula[14] for thin-walled pipes having an Rm/t of 10. The simple J-integral computation value when, during tests, a load was applied on an inner surface crack having a length of 72.6 mm and a fixed depth of 15.78 mm was a large value over three times greater

than this analytical result. One can see that when a single evaluation method for thin-walled pipes is applied to a thin-walled pipe with an Rm/t of approx. 4, the error is large.

② Large-Sized Pipe with Low Ferrite Content with Standard Cracks Applied (Test Specimen L1)

The value of J_{app} when the maximum bending load of 609 kN was applied to the large-sized test specimen L1 was 528 kPa•m. Figure 2.3-5 is a diagram that plots the values of J_{app} based on the central region model and the overall model over the Jmat-Δa curve. Just as in the case of the test specimen M5, J_{app} values showed a good match with the values obtained from the three 1TCT* test pieces. In all cases, J_{app} was slightly larger than the minimum value of J_{mat} obtained with the CT test pieces. Consequently, in cases where an analysis was performed based on the integral path and the constructed analytical model, by comparison with the lower limit value of the Jmat-Δa curve obtained with the 1TCT* test pieces from the large-sized pipe materials having a low ferrite content, it was possible to estimate ductile crack growth conservatively.

Just as in the case of the medium-sized pipe, we computed J_{app} using a simple evaluation formula used for thin-walled pipes. If one assesses the simple J-integral value when, during the test, a load was applied to an inner surface crack having a fixed depth of 16.2 mm and a length of 73.13 mm, it became a large value more than three times this analytical result. Rm/t for the large-sized pipe specimen was set to a typical value for actual equipment, and if one evaluates actual equipment with the existing simple evaluation formula, there is a possibility of generating a large error.

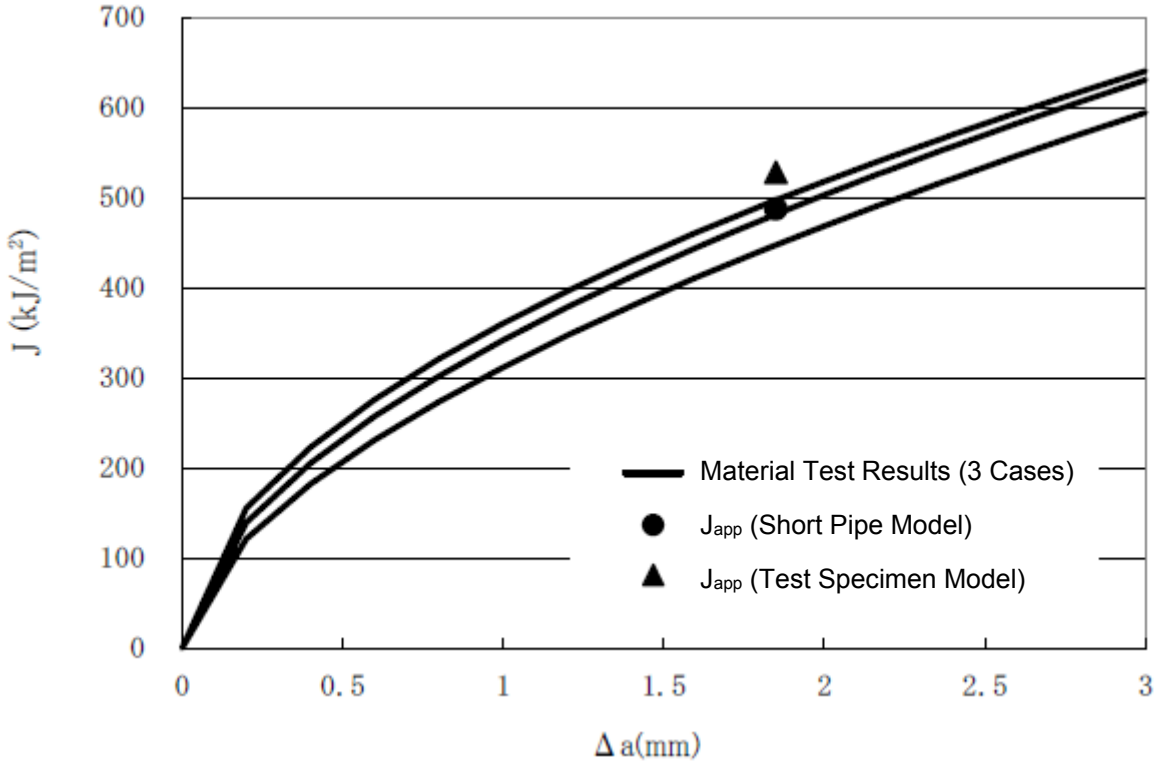

Figure 2.3-5 Test Specimen Analysis Results and Material Test Results for L1

③ Large-Sized Pipe with High Ferrite Content

Figure 2.3-6 shows the test specimen analytical results for test specimen L2 to which standard defects were applied and test specimen L3 to which deeper defects were applied. The J_{app} values computed using the test model and short pipe model both closely matched the value of J_{mat} measured using the CT* test piece.

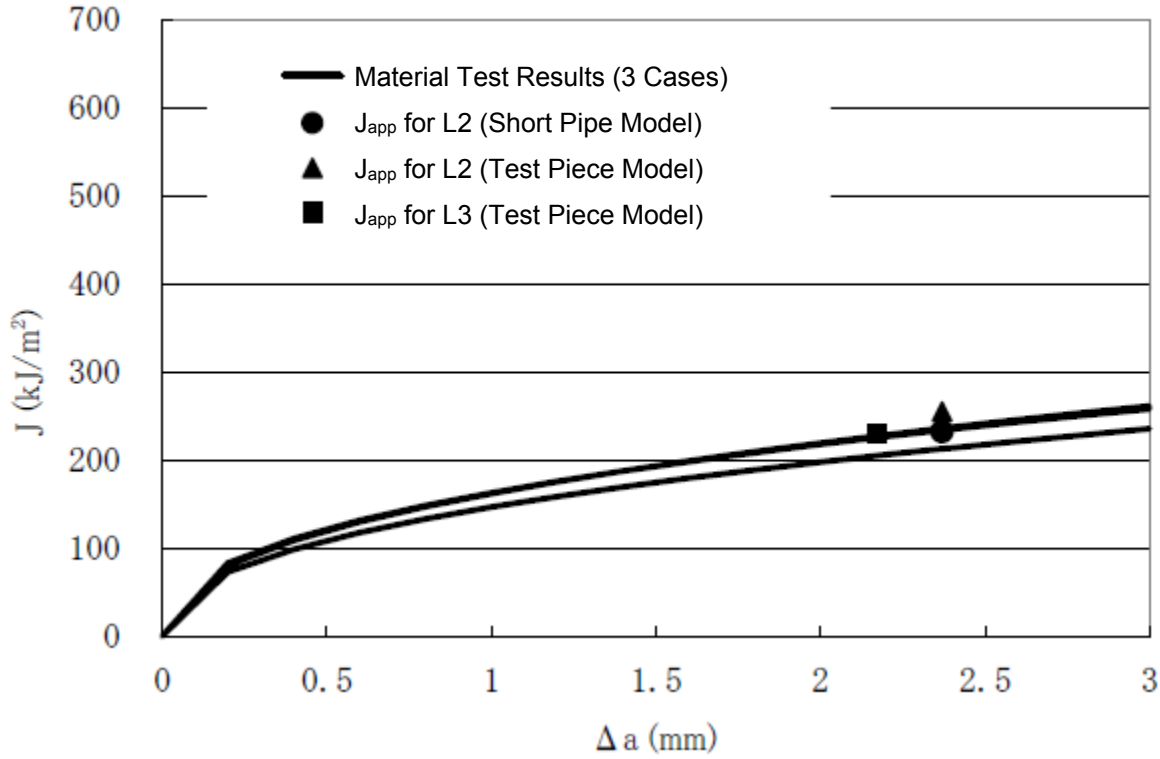

Figure 2.3-6 Analytical Results for Large-Scale Pipe Test Specimen with High Ferrite Content

Based on the above test specimen analytical results, we were able to confirm that there was a close match between the results of the test specimen analysis, the results of the pipe test, and the results of the material test. In addition, although there were few evaluation points, the large-scale pipe test specimen exhibited better consistency on both sides. In order to study the precision in the case where a life-sized pipe was modeled in the same way as the pipe test specimens, we compared the degree of plastic constraint for the test piece, test specimen, and life-size model. The greater the degree of plastic constraint on the crack tip region, the more damage there tended to be. In a given stress field within a body expressed by the multi-axial stress q, if the average value of the three orthogonal stress components (hydrostatic pressure stress) is defined as σ_h and the equivalent Von Mises stress is defined as σ_{eq},, then the degree of plastic constraint is given by Eq. 2.3.3-3.

$$q = \sigma_h / \sigma_{eq} \qquad (2.3.3\text{-}3)$$

We analyzed the degree of plastic restraint for CT test pieces, pipes having a typical size for actual equipment, and each of the test specimens to which standard defects were applied. Examples of the analytical results are shown in Figure 2.3-7. In this

analysis, in order to view the change in multiple degrees of freedom in the vicinity of the crack in detail, the element breakdown in the vicinity of the crack is more finely divided. In addition, in order to determine the effects of the reduction in dimensions, we unified the analytical conditions as shown below.

- The true-stress - true-strain relationship underwent unified analysis with thermal aging performed at 325°C for the large-scale pipe having a high ferrite content
- The load was applied in such a way that J_{app} became 90 kN/m, which matches the J_{Ic} when the large-sized pipe having a high ferrite content underwent thermal aging at a temperature of 325°C. We sequentially applied bending loads under the following conditions: a test load applied to the CT test piece, a pure bending load on a pipe specimen shape, and an axial force load typical for actual equipment on a life-sized pipe (an internal pressure of 15.4 MPa and axial forces of 9.52 MN originating from its own weight, heat expansion loads, and earthquakes).

As can be seen from the figure, multiple degree-of-freedom intensity in the vicinity of the crack tip was in the order of 1TCT, 1CT* (thickness only 1/2), actual equipment pipe, large-sized pipe, and medium-sized pipe. In a range of 1.0 - 1.3 mm or greater from the crack tip, ITCT* and

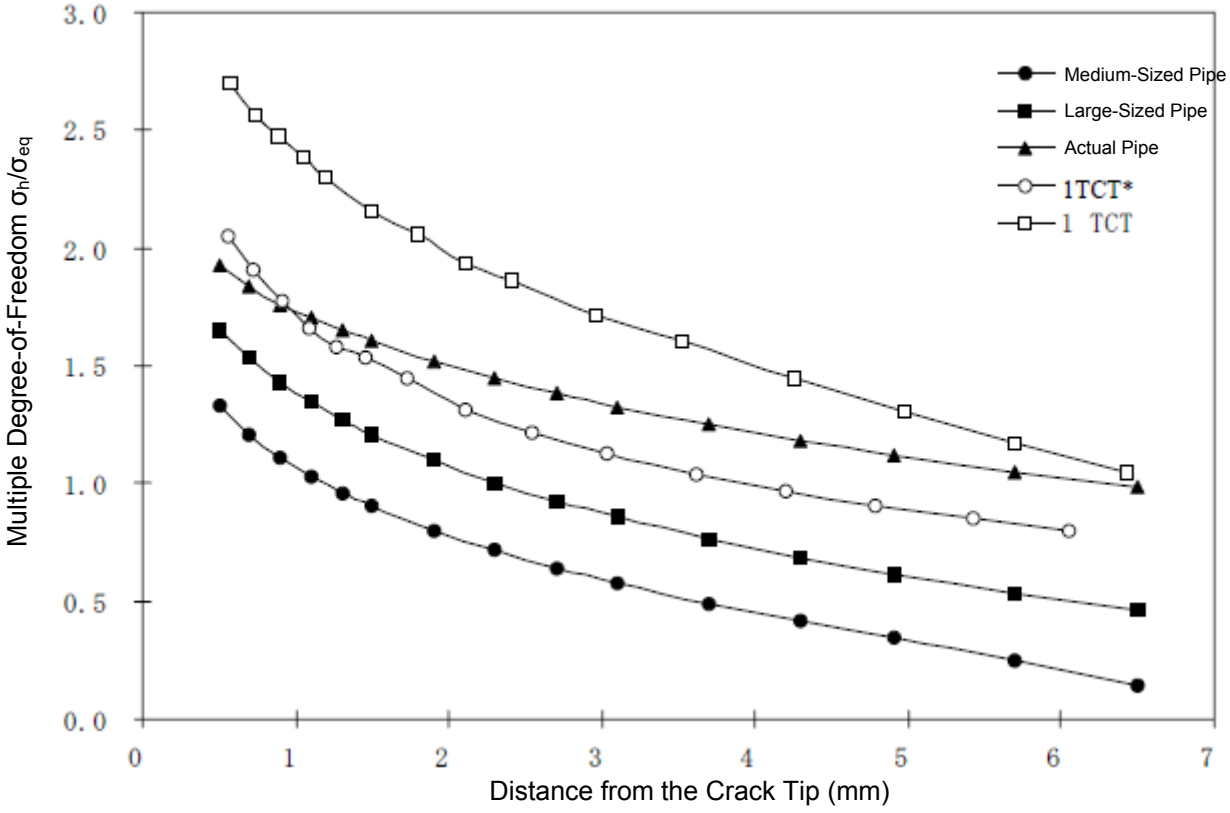

Figure 2.3-7 Comparison of the Degree of Plastic Constraint

the life-sized pipe are reversed, but very near the crack tip, the multiple degrees of freedom of 1TCT* is larger. Based on these results, with regards to the life-sized pipe, large-sized pipe, and medium-sized pipe, using the J-Δa curve obtained with the CT test piece was conservative, and compared to the large-sized and mid-sized pipes, the life-sized pipe had multiple degrees of freedom close to that of the CT test piece, which we felt could be appropriately assessed.

(3) Investigation of the Fracture Analysis Curve

Within the maintenance standards, there is a two-parameter evaluation method for defects in austenite metal tubes detected during in-service investigations. A general purpose fracture evaluation curve has also been determined. In the range over which the two-parameter method is applied, there are no limits on the ferrite content. Only the defect evaluation method can be applied to cast stainless steel having a substantially high ferrite content. The two-parameter method is a simple evaluation method that analyzes fractures using two parameters Kr and Sr for fracture stress and plastic collapse stress based on linear fracture mechanics computations as in the case of thermally aged cast stainless steel pipe having a high ferrite content for fracture under large-scale yield conditions between brittle fracture and plastic collapse. Here, using the test results and actual-sized model analysis results, we assessed its applicability to thermally embrittled cast stainless steel for general purpose fracture evaluation curves prescribed by the maintenance standards.

① Regarding the General Purpose Fracture Evaluation Curve

In the maintenance standards, a general purpose fracture evaluation curve subjected to applicable limits to austenitic stainless steel is given by the following equation.

$$Kr = [f(Sr)+0.1578+0.278Sr^2/(0.7396+Sr^2)]^{-0.6}$$

$$f(Sr)=0.8242\ (1+8.0541Sr^{4.07}) \qquad Sr \leqq 1.3$$

$$0.8242\ (87.55-82.6271/Sr) \qquad Sr>1.3$$

In cases where this equation cannot be used, it has been determined that one must establish a fracture evaluation curve that meets the material characteristics. However, in the maintenance standards, thermally aged primary cooling pipes also satisfy the limits of applicability of this formula. The general purpose fracture evaluation curve prescribed in the maintenance standards is the same as the curve prescribed in ASME Sec. XI

Appendix H. In ASME, initially, the general purpose fracture evaluation curve was created for use with ferrite steel pipes. Because various fracture evaluation curves taking the type of load and the crack length as parameters were created under conditions where the pipe radius/thickness was 10, the crack depth/thickness was 0.5, and the crack center angle was 45° to 360°, the lower limit line corresponding to when the center angle was 90° was defined as the general purpose fracture evaluation line. For the evaluation of the J-integral value for creating a fracture evaluation curve, a Ramberg-Osgood type stress-strain characteristic was used, and a lower-limit line that passed through the minimal yield point of the ASME standards was used. When a general-purpose fracture evaluation curve for use with austenitic steel pipe was created later, in addition to the same kind of investigation as in the case of carbon steel, rather than using the Ramberg-Osgood formula, a law was adopted where strain in the low-stress region must be large and the strain-stress relationship had to be 0.2% or greater. For this reason, the plastic component of the J-integral Jp became large, and the fracture evaluation curve became steep. The lower limit line of the fracture evaluation curve produced in this manner was made to serve as the general-purpose fracture evaluation curve for use with austenitic steel pipes. It has been confirmed that the general purpose fracture evaluation curve could safely estimate the test results for the Degraded Piping Program (NUREG/CR-4082) that was conducted in the 1980s. In the case of thermally aged cast stainless steel, as described in Section 2.1, tests confirmed that the 0.2% proof stress increased, manufacturing hardness decreased, and the stress-strain characteristic was expressed well using the Ramberg-Osgood parameters. Even the L1 specimen test, for which thermal embrittlement was not that severe, was well expressed using the Ramberg-Osgood parameters, and the crack propagation force obtained as a result of the test specimen analysis closely matched the fracture toughness values.

For the reasons described above, although it is safe to apply the general purpose fracture evaluation curve for use with austenitic steel pipes to thermally aged cast stainless steel, it is not likely to extend so far as to appropriately assess fracture behavior.

② Evaluation of Test Results

Figure 2.3-9 plots the test results for test specimens M5 and L1 - L3 for which ductile crack had grown 1.7 - 2.4 mm and the general purpose fracture evaluation curve of the maintenance standards. The test points were evaluated using the following formula,

which is stated in Appendix E-10 of the maintenance standards. However, the safety factor (SF) was set to 1.

$$Kr' = (Je/J)^{0.5}$$

Je: $(1-\nu^2)\ K^2/E'$

J: J_{app} that was obtained in test analysis

$$Sr' = (\pi/4)Pb(SF)/(\sigma y \Gamma m)$$

Pb: largest moment during test/cross section coefficient

σy: 0.2% proof stress

$$\Gamma m : \{Ro^2 - Rc^2 + (1-\theta/\pi)(Rc^2 - Ri^2)\}/(Ro^2 - Ri^2)$$

Ro: Outer diameter

Rc: Inner diameter + crack depth

Ri: Inner diameter

The test point was the point where the ductile crack in thermally aged material had grown slightly, and it was greatly distanced to the upper right from the fracture evaluation curve of the maintenance standards. It is safe to use the general purpose fracture evaluation curve with austenitic stainless steel for the evaluation of thermally aged primary cooling pipes. When taking the safety factor of the maintenance standards into account, it is clear that it becomes extremely conservative.

We believe that this fact signifies that it is rarely possible to confirm integrity by simply applying the general purpose fracture evaluation curve to thermally embrittled primary cooling pipes. In order to conduct more realistic evaluations, there is another method in which one sets the fracture evaluation curve in consideration of individual stress-strain characteristics. However, in order to study measures for pipes where there is not a large assessment margin while grasping the stress limit and crack detection performance needed, it is practical to adopt a method whereby one directly compares J_{mat} with the crack propagation force obtained taking those [factors] as parameters.

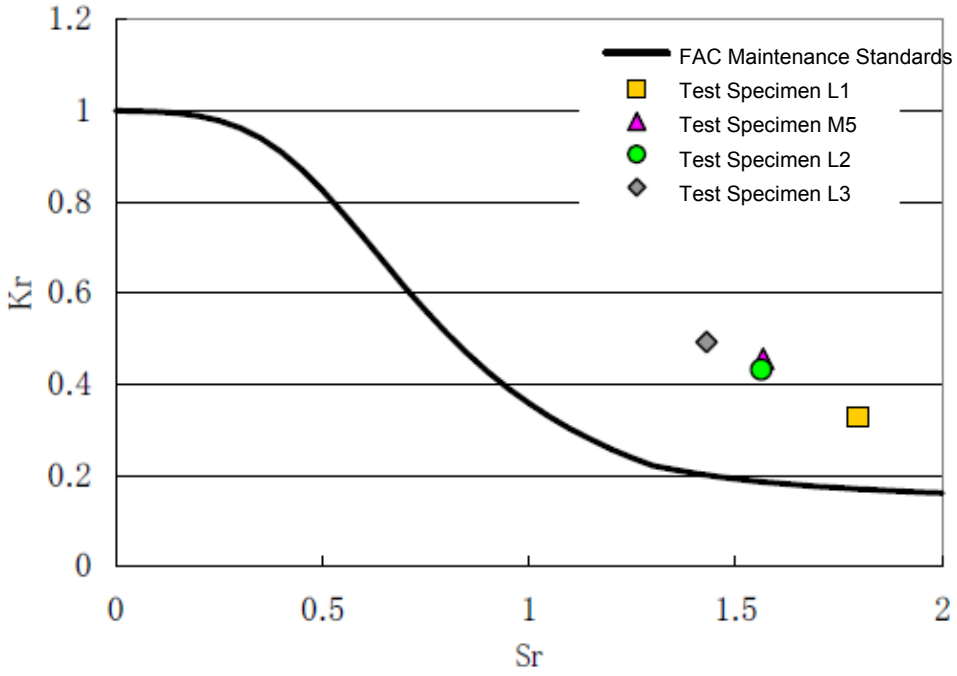

Figure 2.3-9 Investigation of the General Purpose Fracture Evaluation Curve

2.4 Actual Equipment Analysis

We analyzed the actual equipment size based on a modeling method verified based on a test specimen analysis, and constructed a database for J_{app} that could serve as a basis for integrity assessments of real equipment.

2.4.1 Analysis Principles

(1) Material Properties

In test specimen analysis, the true-stress - true-strain characteristic used in analysis and the J-Δa characteristic used in evaluation are well-known. However, when analyzing actual equipment, one must be able to predict both of these values.

① J_{mat}-Δa Characteristic

For the J_{mat}-Δa characteristic, we adopted a lower limit value taking into consideration two times the standard deviation for the optimal value obtained by the predictive formula of Reference Document 3. A simple evaluation chart of the lower limit value of the predicted characteristic is shown in Appendix 1. For a lower limit value for the low fracture toughness value during long-term operation that is not dependent on the aging temperature, one can compute J_{Ic} and J_6 using Eq. 2.4-1.

$$J_{IC}(kJ/m^2)=10^{2.79241-0.05297\times FN}$$
$$J_6(kJ/m^2)=10^{3.37187-0.04904\times FN} \qquad (2.4-1)$$

The J_{mat}-Δa characteristic is computed based on the shape of C_1 $(\Delta a)^{C2}$ that passes through J_{Ic}, J_6, and the origin. Here, the Δa of J_{Ic} point is $J_{Ic}/(2\sigma_f)$ + 0.2 mm. σ_f is obtained using the method described in the next section based on a predictive formula for true-stress - true-strain.

② Stress-Strain Characteristic

The true-stress - true-strain characteristic is obtained taking Ramberg-Osgood parameters based on the method of Reference Document 3 as predictive values. Because lower limit values of the prediction values for fracture toughness are used as the judgment criterion for the assessment, the true-stress - true-strain characteristic corresponding to the fracture toughness is thought to correspond to the most hardened upper limit. Here, using the optimal value of the safe-side true-stress - true-strain characteristic, we evaluated the crack propagation force.

For descriptive purposes, we analyzed the crack propagation force using the optimal line of the true-stress - true-strain characteristic following long-term thermal aging for ferrite contents of 20%, 15%, and—for reference purposes—10%. As can be seen from Figure 2.1-2, comparing the optimal value predicted based on Reference Document 3 to the actual measurement values of this study, we obtained safe crack propagation forces for materials having a high ferrite content. In cases of a low ferrite content, under the same conditions, the crack propagation force was assessed too low when the stress was low; but under high stress conditions, which was what was important from the standpoint of evaluation, it ended up being safe. For this reason, with a ferrite content of 10 mm, we evaluated crack propagation forces in cases where the crack tip region reached a von Mises stress on the order of 3Sm. J_{app} obtained from the stress - stain characteristic for each ferrite content could be applied to materials having large quantities of ferrite. Table 2.4-1 and Figure 2.4-1 show the true-stress - true-strain predicted characteristic used in the calculations. The true-stress - true-strain characteristic depends not just on the ferrite content but also on C and Mo. We selected a representative chemical composition shown in Table 2.4-1 and obtained the Ramberg-Osgood parameters. The analysis temperature was 325°C, and the longitudinal modulus of elasticity was 174,000 MPa.

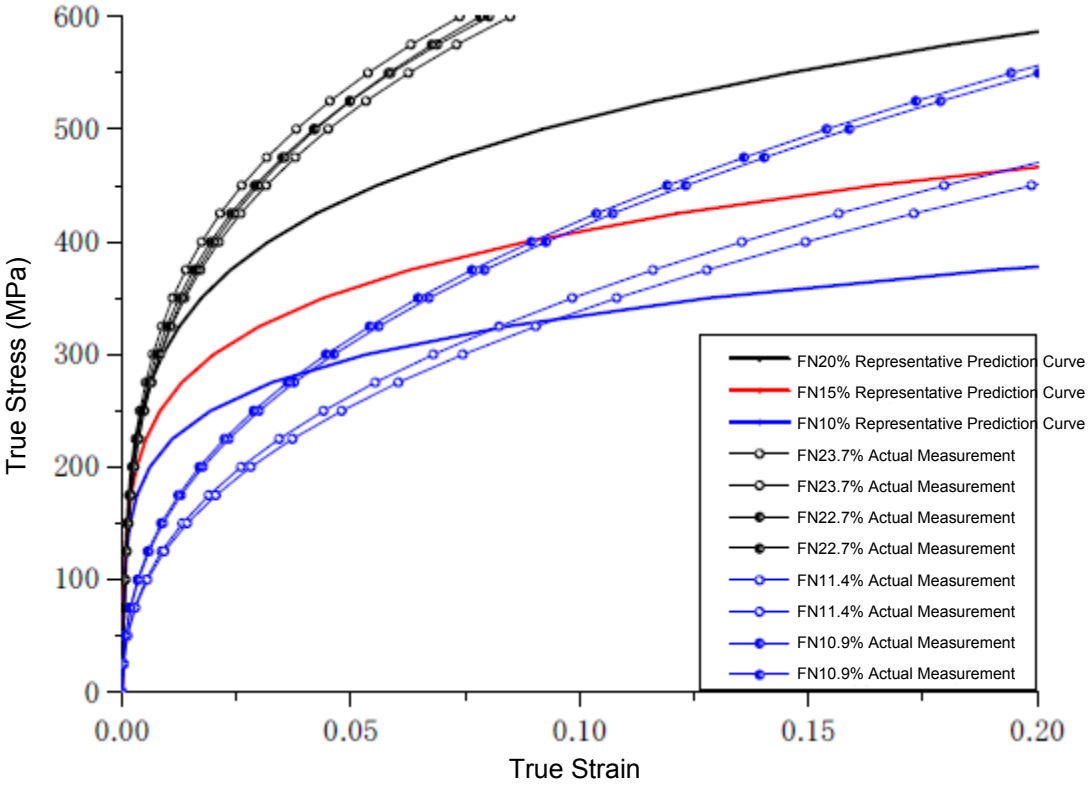

Figure 2.4-1 True-Stress - True-Strain for Analysis Use

Table 2.4-1 True-Stress - True-Strain Characteristic Predicted After Long-Term Thermal Aging

		Unit	FN = 20%	FN = 15%	FN = 10%
Component	C	mass-%	0.05	0.05	0.05
	Mo	mass-%	2.23	2.23	2.30
σo		MPa	228.6	199.7	171.7
α			1.51	1.95	2.8
n			4.67	4.87	5.09

(2) Analysis Target

① Pipes Targeted for Analysis

For analysis, we targeted elbows and the straight pipe sections of hot legs and cold legs. The pipe cross-section shape (outer diameter and wall thickness) were set in such a way as to cover that of actual equipment. Because the crossover leg experiences lower stress compared to these pipes and is not felt to have to endure such intense thermal shock loads, it was not targeted for analysis. Cast nozzles also undergo thermal shock loads, but because their diameter/wall thickness ratio is extremely large and the influence of flatness is low, they were not targeted for analysis.

Semi-elliptical cracks formed in the circumferential and longitudinal directions along the pipe's inner surface. The detectability of cracks in cast stainless steel pipes during in-service inspections was tested through practical nuclear power generation facility inspection technology developmental work in 2004. A summary of that study is shown in Appendix 4. Test specimens were created in which semi-elliptical cracks were provided on the inner surface in the circumferential direction at the weld-girth thermally influenced regions of centrifugally spun cast pipe and static cast pipe with an outer diameter of 850 mm and a plate thickness of 75.8 mm. These dimensions were equivalent to what is found on actual equipment. Detectability was tested from the outer surface using oblique angle ultrasonic inspection with vertical and longitudinal waves. The imparted fatigue cracks had a depth of 5.1 - 14.9 mm and an aspect ratio of 1/6.7. Three teams of inspectors conducted inspections, and their conclusions reported the following: "Most of the target defects were detected at DAC 20% - DAC 50%. Moreover, with regards to false positives in defect recognition, a certain number of cases were discovered in inspections from the centrifugal cast side, but in judgments based also on inspection results from the static cast side, none of the teams experienced false positive defect

recognition." Moreover, they succeeded in detecting cracks that were smaller than the standard crack depth of 14.5 mm, which was set as being 20% of the plate thickness of the representative size of pipe specified for the experiment. The crack size assumed to exist prior to fatigue crack propagation needs to be set appropriately taking into consideration Appendix 4 and the actual conditions of the inspection, but the assumption is that a depth of 1/5th the plate thickness should be sufficiently safe. For the crack depth, we targeted a range of 7.5 - 20 mm in consideration of the defect detectability outlined in Attachment 3. The crack length on the pipe inner surface was set to five times the depth of the defect.

(3) Stress (Assumed Elastic Stress)

① Total Stress

When subjected to a bending load, a pipe that is free of defects will have a hypothetical elastic stress of $4\sigma_f/\pi$ when undergoing plastic collapse. If one sets σ_f to the average value of the tensile strength and the design yield point to 325°C, that value will be 350 MPa. To arrive at the total stress in the axial direction, one must take into consideration the membrane stress, bending stress due to the axial bending moment, and thermal shock stress. We set as our analysis target a range where the sum total of these stresses was as high as 3Sm. This value is the same as that for 3Sm at 325°C.

According to the "Design and Construction Standards" of the Power Generation Nuclear Equipment Standards, the evaluation of the primary and secondary stresses in pipes is a simple evaluation method employing stress coefficients. There are times when that value exceeds 3Sm, and a simple elasto-plastic analysis is performed. However, in the analysis of crack propagation forces, stress in the region assumed to have cracks is obtained by a detailed analysis of the member forces in that region, and generally does not reach Sm.

Thermal shock may be produced on a pipe's inner surfaces due to design-exceeding modifications such as malfunctions in safe injection. Because, in the above standards, stress in the plate thickness direction due to the excessive temperature distribution is not considered to contribute to deformation in the beam of the pipe, the provisions only consider fatigue assessments. However, when assessing crack propagation forces in embrittled materials, one must also consider the thermal shock stress. For the total stress, we performed an analysis up to 3Sm, taking into consideration the contribution from thermal shock stress.

② Membrane Stress

Axial membrane stress due to internal pressure of the cross-sections having cracks in the circumferential direction is typically greater than 0.3Sm. If the total stress is the same, because the side where the ratio of membrane stress to total stress is large means pipe flatness is low, J_{app} has a tendency to diminish. For this reason, for the analysis condition, we set the membrane stress to a low value. For the magnitude of membrane stress, we took 0 as the standard condition, and for purposes of comparison analyzed the case of 0.3Sm.

2.4.2 Crack Propagation Forces in Straight Pipes

Figures 2.4-2 and 2.4.3 show analytical results for pipes having a typical thickness in a large-diameter hot leg having relatively high crack propagation forces on identically sized cracks. These were analyzed using the average relationship of true-stress - true-strain following long-term heat aging on materials having ferrite contents of 15% and 20%. Each figure indicates that it is safe when applied to materials having relatively high ferrite content. That said, because there is much variability in the true-stress - true-strain relationship, it is important to provide an appropriate margin. In relatively thin-walled pipes, the crack propagation forces tend to be higher. In cases where J_{app}-Δa for actual equipment is set from the figures taking the crack depth as a parameter, one takes the following points into consideration.

① In cases where the crack depth is the same, if the diameter is small, J_{app} will be larger.

② In cases where the crack depth is the same if Rm/t is large, J_{app} will be larger.

Appendix shows J_{app} for hot legs and cold legs in cases where Rm/t differs.

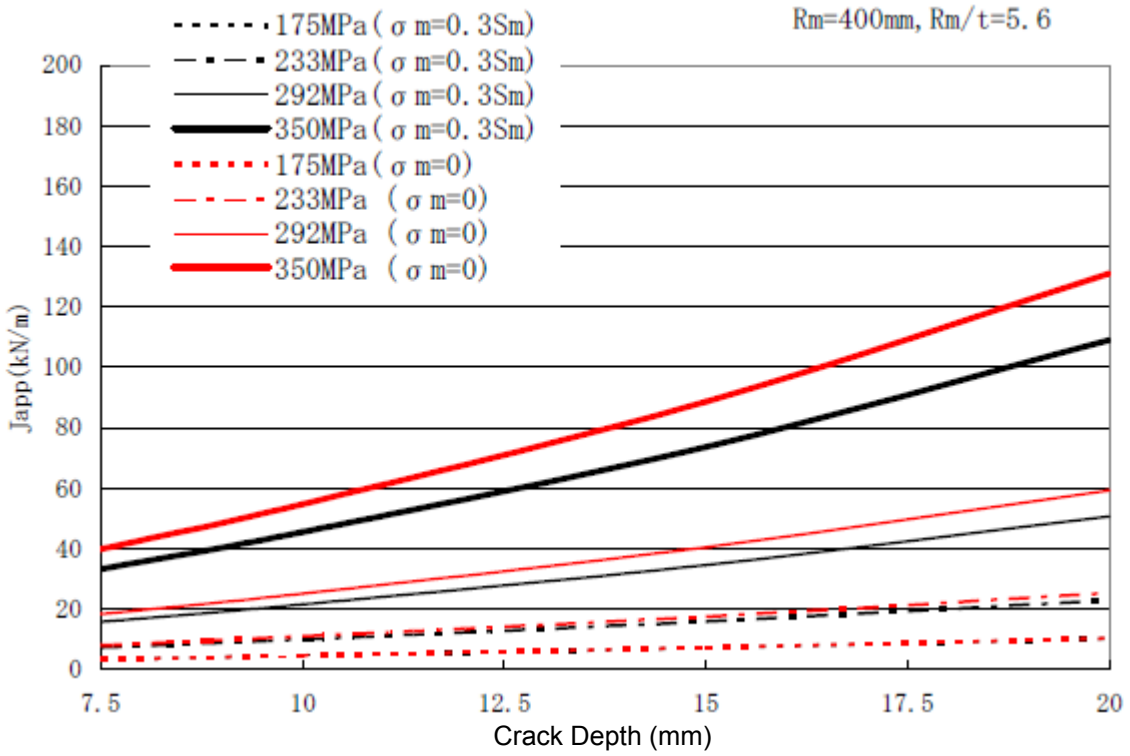

Figure 2.4-2 FN = 20% Hot Leg Representative Thickness

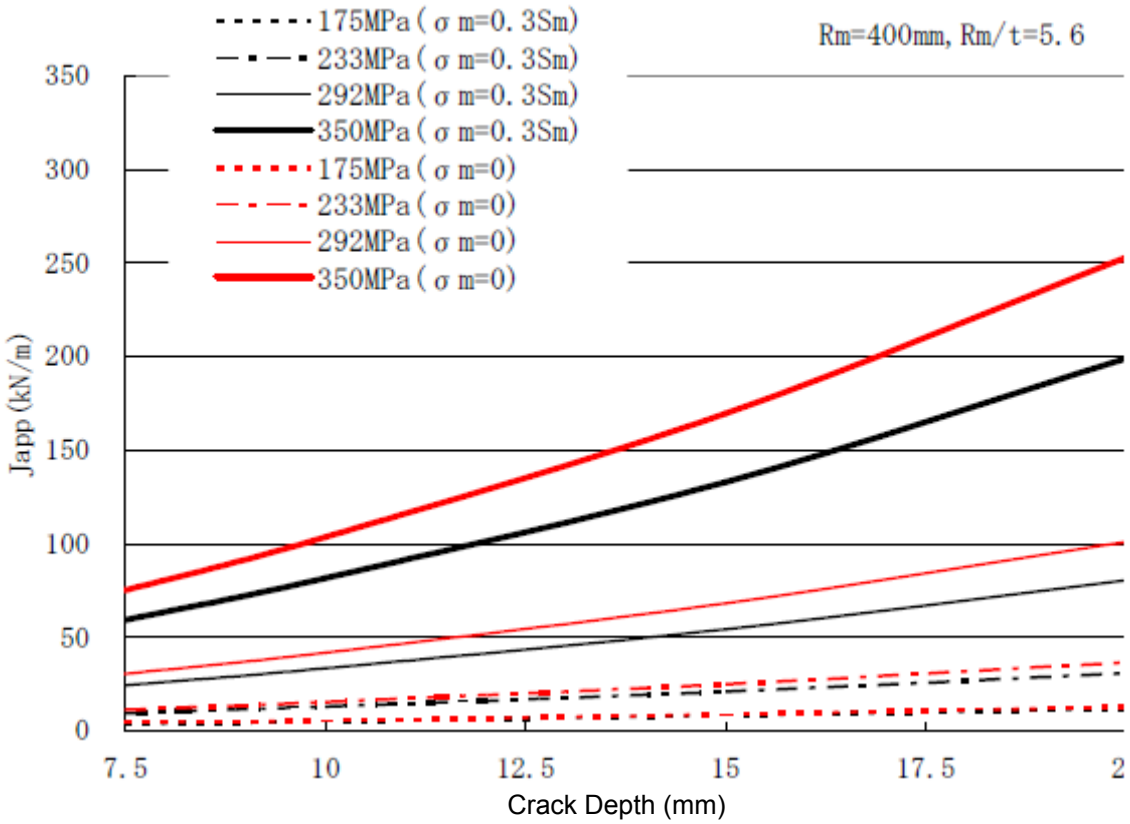

Figure 2.4-2 FN = 15% Hot Leg Representative Thickness

2.4.3 Crack Propagation Forces in Elbows

(1) Setting Representative Dimensions

At predetermined sections of primary cooling pipes, 50° elbows are placed in the hot leg, 40° and 90° elbows are placed in the crossover leg, and 35° elbows are placed in the cold leg. The stress produced on elbows by the same member force increases with the flatness and tendency to deform of the elbow. The flatness and tendency to deform are evaluated using the elbow pipe coefficient and bending angle. The pipe coefficient h is defined by tR/r^2. t is the depth, R is the radius of curvature of the elbow's center line, and r is the average radius of the elbow. The smaller the pipe coefficient h, the easier it is for the elbow to deform, and the greater the stress compared to a straight pipe. Assuming that the pipe coefficients are the same, the greater the bending angle, the smaller the restraint on the cross section shape due to the connecting pipe, and the easier it is for it to flatten. Table 2.4-2 shows the pipe coefficients, bending angles, and stress levels of pipes that are representative of actual equipment. In Table 2.4-2, a hot leg elbow having a high stress level and small pipe coefficient was made the representative elbow. For the representative dimensions, we set a plate thickness of 84.75 mm, an average radius of 433.83 mm, and a radius of curvature for the elbow center line of 1,208.5 mm. We compared the values of J_{app} for this elbow and that of a pipe having the same cross section specification.

Table 2.4-2 Elbow Specifications

Part	Pipe Coefficient	Bending Angle	Stress Level (Relative Comparison)
Hot Leg	0.54	50°	High
Crossover Leg	0.50	40°	Low
	0.56	90°	Low
Cold Leg	> 0.60	≤ 35°	Low

(2) Analytical Model

① Assumed Crack Position

In order to obtain a high stress point causing the assumed crack position, we performed an elastic analysis. We employed a 1/4 sector model for the 50° elbow. The boundary conditions and loads of the model are shown in Figure 2.4-8. The analysis code was ABAQUS. For the load, we loaded a dominant planar bending moment on

actual equipment, together with initial pressure. The value of the bending moment was determined taking into consideration the maximum load level for actual equipment.

As for the distribution of axial stress on the inner and outer surfaces of the pipe, changes in the bending angle direction of the elbow were small, but in the direction of the circumferential angle, the changes were complex. In addition, applying a reverse bending moment resulted in a relatively higher axial stress compared to the application of a forward bending moment. Figure 2.4-9 shows the axial stress distribution in the direction of the circumferential angle of the central cross section of the elbow. The circumferential angle of the back of the elbow is 0°, and that of its "belly" is 180°. The center of cracks in the circumferential direction was set so that the axial direction stress on the inner surface was a maximum and the axial direction stress of the center of the pipe plate thickness was a maximum.

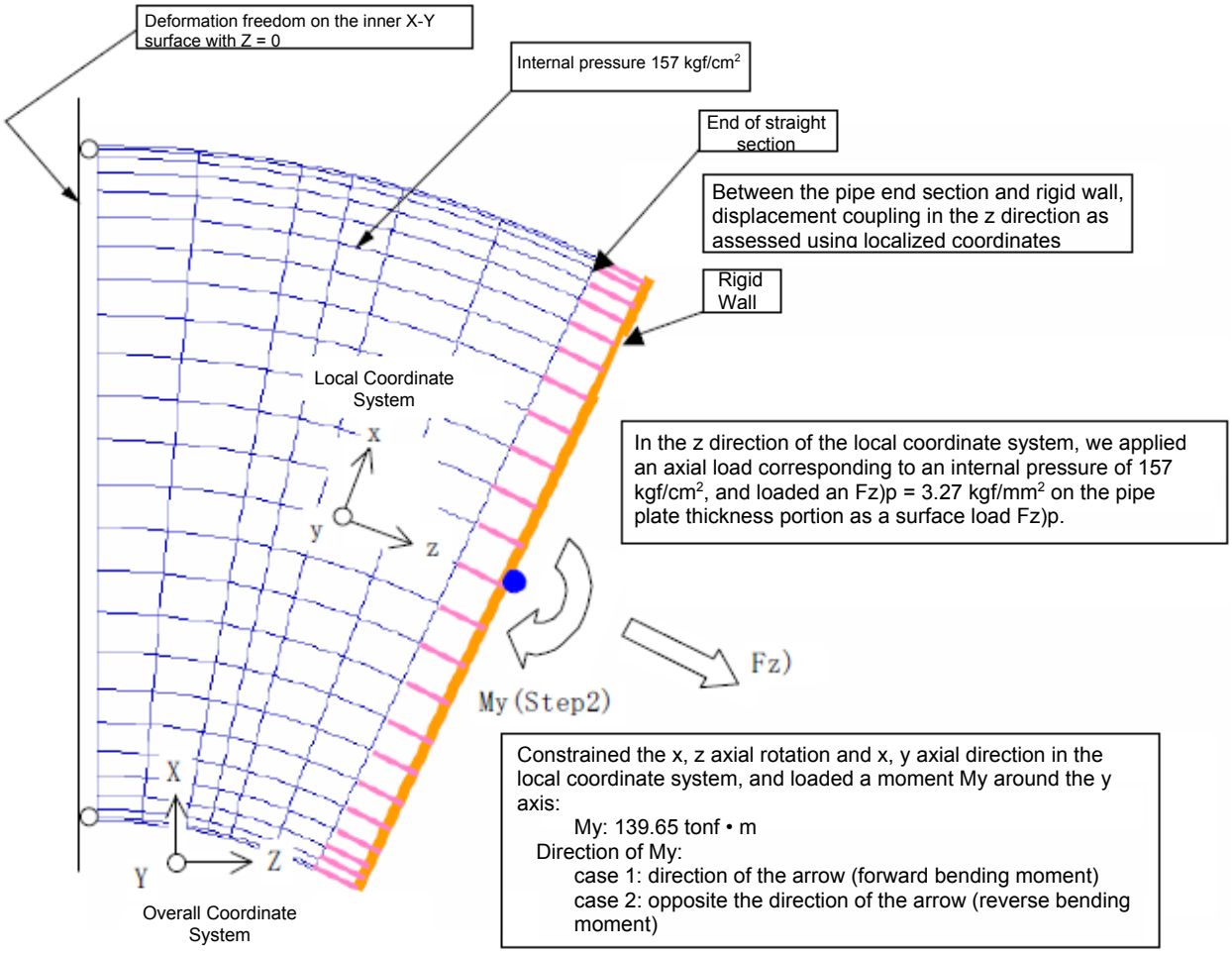

Figure 2.4-8 Elbow Analytical Model and Boundary Conditions

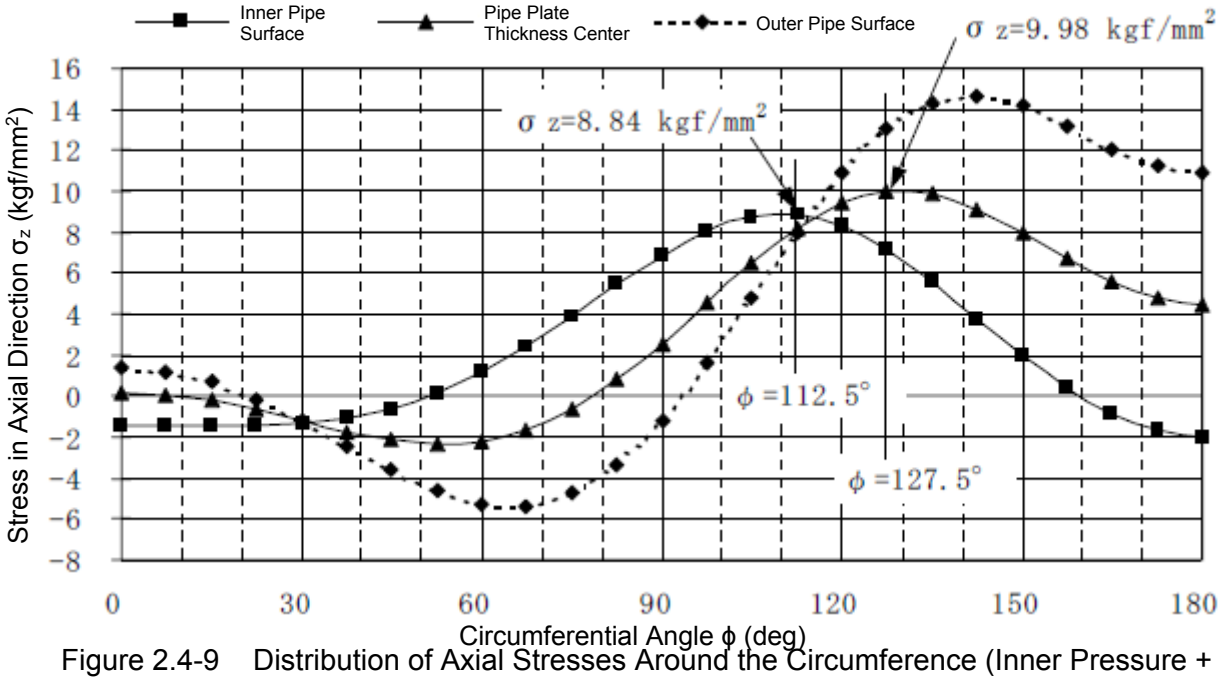

Figure 2.4-9 Distribution of Axial Stresses Around the Circumference (Inner Pressure + Reverse Bending Moment)

② Analytical Model

The assumed crack was set to be a semi-circular crack in the circumferential direction on the inner surface having an aspect ratio of 0.2 and a depth of 14.5 mm and 10 mm. The analytical mode was the same as the stress evaluation mode, but because

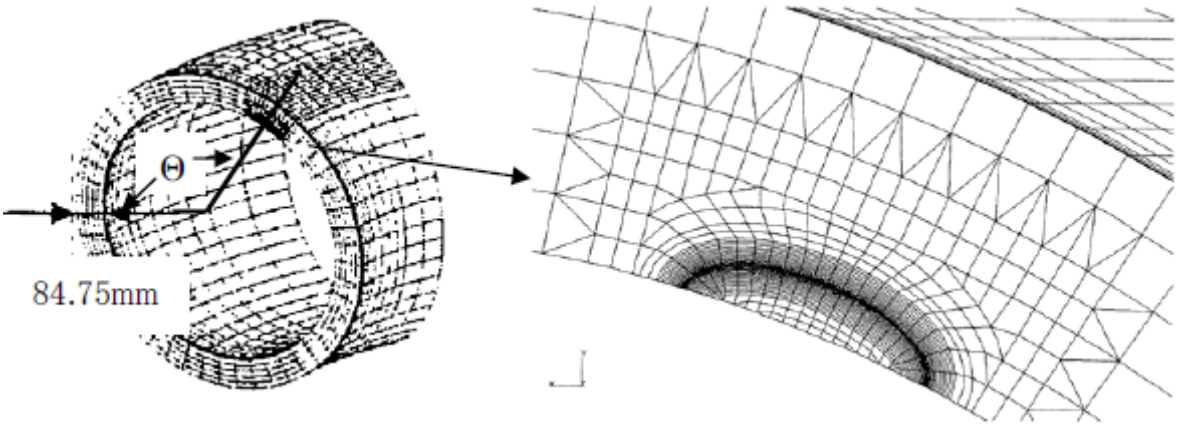

Figure 2.4-10 Analytical Model

of asymmetry in the circumferential direction we decided on a 360° cross-section model. For the stress-strain characteristic, we targeted characteristics where the ferrite content of Table 2.4-1 was 20% and 50%. For the load, we considered a case where a load

corresponding to where the assumed elastic stress of a straight pipe was 3Sm was applied up until the bending moment unit reached 3Sm; and a case where a reverse bending moment was added to an internal pressure of 17.2 MPa and the nominal tensile stress in the axial direction of a straight pipe reached 0.3Sm.

(3) Analysis Results

When performing comparisons on crack position, compared to the case where axial stress in the central cross section is maximum, the J-integral value is greater for the position where the axial stress on the inner surface reaches a maximum. For this reason, the results for all positions where the axial stress on the inner surface reached a maximum are shown below.

Figure 2.4-11 shows an overlay of the relationship of nominal stress rendered dimensionless in the form of $J_{elbow}/J_{straight\ pipe}$ for a standard defect and a crack that is shallower than that. As described above based on this figure, the behavior of $J_{elbow}/J_{straight\ pipe}$ is the same regardless of whether it is a standard defect or a crack that is shallower than that. If one looks at it in terms of absolute values, overall, the shallow crack is higher up, but the difference between the two is very small.

By using this figure, for example, instead of implementing a detailed J-integral solution column for elbows, one obtains the J-integral value for a straight pipe, and by substituting the corresponding nominal stress, one then obtains $J_{elbow}/J_{straight\ pipe}$. By multiplying this value with the J-integral value for straight pipes, one can predict the J-integral value for an elbow.

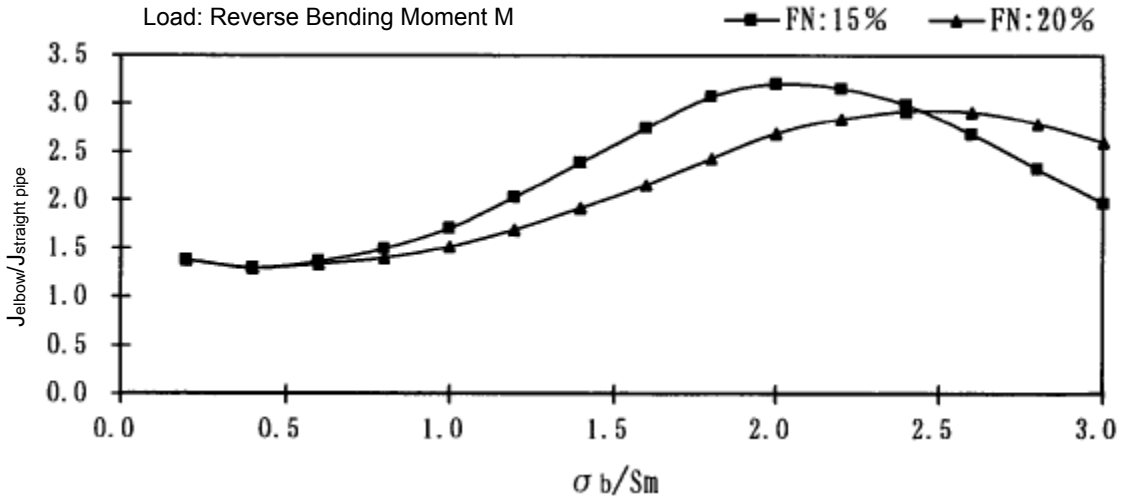

Figure 2.4-11 (1/4) Crack Depth 14.5 mm • Reverse Bending Moment Load

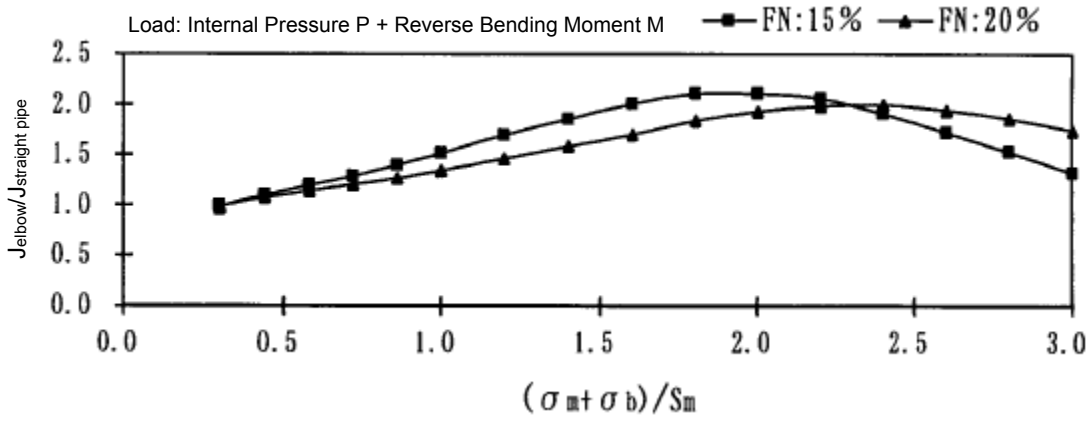

Figure 2.4-11 (2/4) Crack Depth 14.5 mm, Internal Pressure of 17.2 MPa + Reverse Bending Moment

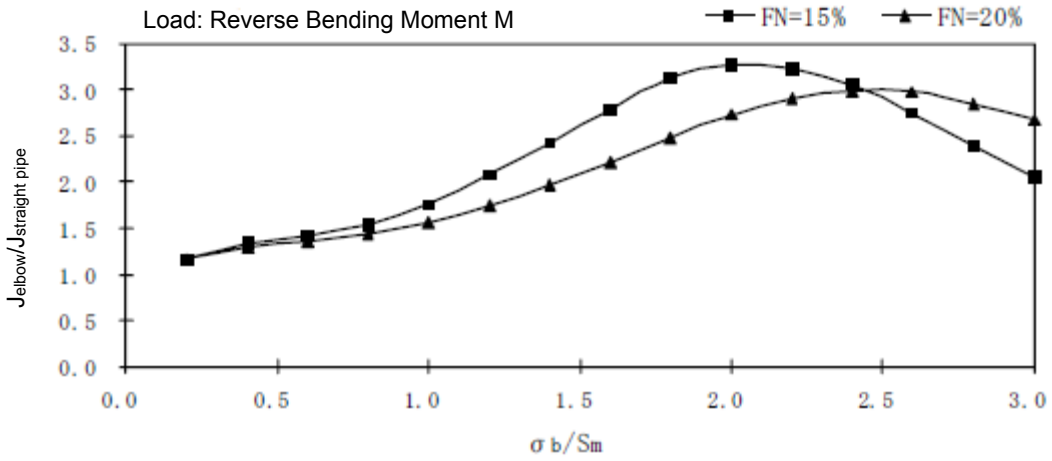

Figure 2.4-11 (3/4) Crack Depth 10 mm, Length 50 mm, Reverse Bending Moment

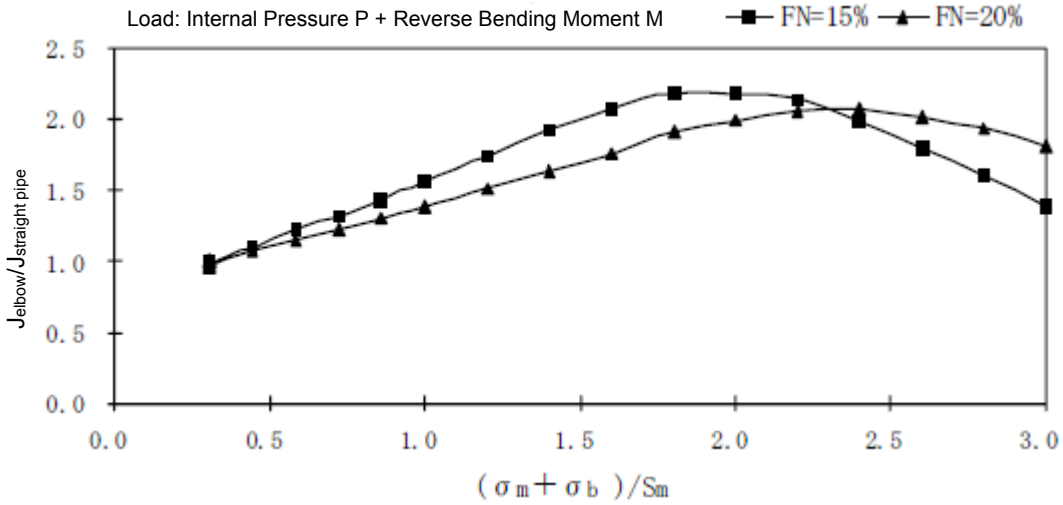

Figure 2.4-11 (4/4) Crack Depth 10 mm, Internal Pressure of 17.2 MPa + Reverse Bending Moment

3. Conclusion

3.1 Summary of Tests and Analytical Study

Based on the pipe fracture tests, cast stainless steel pipes that are not very thermally embrittled undergo plastic collapse, but in cases where the ferrite content is high and long-term thermal aging has transpired, we confirmed that at loads below the plastic collapse load, after a ductile crack has grown, it undergoes unstable ductile fracture. This kind of elasto-plastic fracture behavior was evaluated using elasto-plastic fracture mechanics. Because actual equipment has special thin-walled pipes, when using a simple evaluation method for thin-walled pipe use, the crack propagation force J_{app} in the elasto-plastic fracture mechanics are estimated much too high, and when modeling is performed on thick-walled flat plates, its estimates are too high. As a result, when performing integrity assessments on actual equipment, one must perform a detailed assessment of J_{app}. The results of our assessment of ductile crack growth in pipe fracture tests indicate that fracture behavior is precisely estimated when using the fracture toughness J_{mat} measured using test piece 1TCT and J_{app} based on the stress-strain characteristic measured using the tensile test piece.

In order to assess the integrity of actual equipment that has been thermally embrittled, it is necessary to evaluate J_{mat} and J_{app}. However, because it is not possible to conduct actual measurements of the material's properties, one must end up evaluating them using a predictive formula. Document 3 shows a predictive formula for the Ramberg-Osgood parameters, as well as a predictive formula for J_{mat} based on test data from Japan and abroad on thermally embrittled cast stainless steel. In this study, we measured the material characteristics of cast stainless steel that had actually been thermally aged, and confirmed that our results were not inconsistent with predictive assessments based on Document 3. With these predictive formulas, we were able to obtain a lower limit value taking into consideration doubling of the standard deviation and the optimal and predicted values. Discrepancies in both the optimal value and lower limit value were large, and in the example of Table 2.1-3, the lower limit value was on the order of 1/3 the optimal value. For the value of J_{mat} for use in assessing actual equipment, we adopted a predicted lower limit value that was on the safe side. Representative values thereof are shown in Appendix 1. On the other hand, for the stress-strain characteristic needed to analyze J_{app}, we employed predicted optimal values for the Ramberg-Osgood parameters, typical examples of which are shown in Appendix 2. Moreover, one might think that what must be compared against the lower limit J_{mat} is a J_{app} that corresponds to the upper limit stress-strain characteristic, but here, on the

safe or conservative side, we decided to compare the value of J_{app} obtained using optimal characteristics.

We analyzed J_{app} for actual equipment pipes using optimal values for the predicted stress-strain characteristic for material having ferrite contents of 10%, 15%, and 20% that had been thermally aged 60 years at 325°C. Crack dimensions consisted of semi-elliptical inner surface cracks in the circumferential direction having an aspect ratio of 0.2 and a depth greater than and less than the defect detectability during the currently employed in-serve inspection methods. For the load, we considered loads below the plastic collapse load based on the standard strength of a pipe having no defects. We also prepared a chart that permits the ready evaluation of J_{app} for a straight pipe based on the load, crack size, ferrite content, and pipe cross-section. In addition, we also obtained an overdesign factor based on straight pipes for the J_{app} produced within elbows, taking into consideration the case where a defect is supposed to exist in an elbow.

3.2 Overview of Integrity Assessment

We prepared data that was necessary for using elasto-plastic fracture mechanics to assess the fracture behavior of actual equipment that has undergone thermal embrittlement, as was needed for integrity assessments. The maintenance standards prescribe a number of practical pipe fracture assessment methods—including plastic collapse and elasto-plastic fracture mechanics evaluations (a method based on Z coefficients), as well as the two-parameter method. A procedure for selecting among the fracture evaluation methods is also determined. That said, here, based on the data prepared in this study, we do not prescribe a range within which plastic collapse transpires, and have not added our data to the fracture evaluation curve or Z coefficient. The reason for this is that the purpose and range of applicability are limited, general applicability and simplicity are not important here, and there are times where the assessment margin is narrow. Consequently, we decided that an approach whereby one makes assessments directly based on fundamental data is more suitable for studies on focus inspections or on the size of cracks that need to be detected. Here, we studied a procedure for evaluating direct integrity by comparing J_{mat} and J_{app}. Moreover, as discussed in Chapter 2, because we have confirmed that a general purpose fracture curved based on the two-parameter method of the maintenance standards provides an exceptionally wide assessment margin for thermally embrittled materials, there should be no problem in using that approach to obtain assessments that are on the safe side.

(1) Regions Evaluated

For the parts targeted for evaluation, we selected high stress regions or regions in which embrittlement was significant from within the base material of primary cooling pipes. We defined regions having significant embrittlement as being regions with a high ferrite content as computed by the method of ASTM A800 based on the chemical composition of a pipe targeted for evaluation under the same aging temperature. For the high stress region, in addition to regions having a high Sn as based on literature certified in the industry, we decided on regions for which large thermal shock are significant due to malfunctions during safe injection.

(2) Assumed Cracks

For the cracks assumed to exist at the time of evaluation, we adopted semi-elliptical cracks running in the circumferential direction on interior surfaces whose aspect ratio was prescribed as 0.2 taking into consideration the crack size that is detected during in-service inspections as well as the detectability of such cracks. The crack size assumed at the time of evaluations was determined taking into consideration fatigue crack propagation due to stress cycles up to the time of the evaluation applied to the crack presumed to exist at the present time. The crack size presumed to exist at the present time must be set appropriately with reference to Appendix 4 as well as the conditions under which the inspection is implemented, but setting a depth of 1/5th the plate thickness for cracks not discovered during the inspection is assumed to be sufficiently safe.

For the fatigue crack propagation assessment, we evaluated propagation due to S_0 earthquakes (with an amplitude of 1/3 an S_1 earthquake) as well as transients of service states A and B up to the time of the evaluation. The in-air fatigue crack propagation characteristic for thermally aged cast stainless steel has been reported as being slower than for non-aged material in regions where ΔK is 30 Mpa$\sqrt{m}$ or less.[15] The reason for this is said to be that with materials that have not been thermally aged, whereas cracks penetrate the α and γ phases, with thermally aged materials, cracks tend to bend when passing through the hardened α phase, and so propagation becomes slower. This mechanism is thought to also take place in the presence of water. For these reasons, we determined that for our crack propagation rule we could adopt the crack propagation rules for austenitic stainless steel in water as prescribed by the maintenance standards.

(3) Load Conditions

With regards to load conditions, we took into consideration the loads that are generated by ground motion, thermal expansion, weight, and internal pressure during

the various operating states. For the transient states, we focused on those transient states where J_{app} is maximized among the bundle of service conditions.

Service states A and B:	Loads of operating conditions I and II
Service state C:	Operating condition II, or S1 ground motion plus the load at time of output operation
Service state D:	Operating condition IV, or S2 ground motion plus the load at time of output operation

With regards to the displacement-controlled load in the evaluation of unstable ductile fracture one can perform evaluations as needed using elasto-plastic analysis. In addition, to evaluate the appearance and growth of cracks, in addition to the above-described loads, one may also consider the stresses produced by thermal shock loads.

(4) Crack Propagation Forces

Crack propagation forces were obtained by means of an elasto-plastic analysis employing the appropriate true-stress - true-strain characteristic. In cases where there was no characteristic that had been actually measured, the true-stress - true-strain characteristic was determined referencing the method shown in Appendix 2 or in Reference Document 3 and taking into consideration the chemical composition or the like of the actual equipment.

Section 2.4.2 or Appendix 6 shows J_{app} for cracks in the circumferential direction of primary cooling pipes having typical chemical compositions and cross-section shapes. When evaluating elbow regions, we considered the analysis results from section 2.4.3 and, as a maximum, adopted 3.26 times the J_{app} of Appendix 6. The result of these computations is an analytical result based on the predicted stress-strain characteristic in the case of thermal aging at 325°C, and can be used to evaluate regions where the thermal aging temperature is 325°C or less.

(5) Fracture Toughness

Fracture toughness after thermal aging was predicted in accordance with Reference Document 3. The optimal value and lower limit value for the fracture toughness base value in accordance with the temperature of thermal aging are shown in Appendix 1. The fracture toughness used for judgments was the lower limit value of the predicted fracture toughness.

(6) Methodology for Integrity Assessments

a) Prevention of unstable ductile fracture

For unstable ductile fracture, a structure is considered sound provided that there is a safety factor (SF) in accordance with the service conditions. That is, it should satisfy the following equation.

$$J_{app}\ (a_o + \Delta a) \leqq J_R(\Delta a) / (SF)$$

a_o	Assumed crack depth
SF = 3	Service states A, B, C
SF = 1	Service state D

Here, Δa is the maximum value that satisfies the following equation, but it must not exceed 6 mm.

$$\partial J_{app}\ (a_o + \Delta a) / \partial a \leqq \partial J_R(\Delta a) / \partial a$$

b) Preventing the growth of large cracks (service states A, B, and C)

In the case of service states A, B, and C, one must confirm the fact that large crack growth is not produced. Under the conditions computed in Appendix 1-1, because J_6 is 3 times or greater J_{Ic}, in regions where thermal shock loads are not produced, in cases where unstable ductile fracture is not produced under the above-stated conditions, J_{app} will not exceed J_{Ic}, and so the crack will not grow. When predicting fracture toughness under conditions differing from those of Appendix 1-1, one must separately confirm that especially large crack growth is not produced. In addition, for regions where it is necessary to consider thermal shock, one must separately confirm the fact that the following equation is also satisfied.

$$J_{app}\ (a_o + \Delta a) \leqq J_R(\Delta a = 2.5\text{mm})$$

References

1) K. Chopra, "Long-Term Embrittlement of Cast Duplex Stainless Steels in LWR Systems" NUREG/CR-4744, 1992
2) O. K. Chopra, "Estimation of Fracture toughness of Cast Stainless Steels during Thermal Aging in LWR Systems—Revision 1" NUREG/CR-4513 Rev. 1 1994
3) S. Kawaguchi et al. "Prediction Method of Tensile Properties and Fracture toughness of Thermally Aged Cast Duplex Stainless Steel Piping" ASME PVP 2005
4) "Fracture Toughness Verification Test Method for Equipment to be Used in Nuclear Power Plants." JEAC-4206 (2004), Japan Electric Association.
5) "Design and Construction Standards of the Standards for Nuclear Power Facilities for Power Generation Use", JSME S NC1-2001, Japan Society of Mechanical Engineers
6) "Report on the 2004 Inspection Technology Verification Activities for Nuclear Power Generation Facilities" (On the Confirmation of Defect Detectability and Sizing Precision in Ultrasonic Wave Inspection Tests [Summary Version]), April 2005, Japan Nuclear Energy Safety Organization
7) Design Standards for the Prevention of Pipe Fracture, JSME S ND1-2002, Japan Society of Mechanical Engineers
8) NUREG/CR-4082 "Degraded Piping Program: Phase II" Vol. 6, Sixth Program Report, Oct. 1986 - Sept. 1987, 1988
9) "Maintenance Stands of the Standards for Nuclear Power Facilities for Power Generation Use", JSME S NA1-2002, Japan Society of Mechanical Engineers
10) Standard Practice for Steel Casting, Austenitic Alloy, Estimating Ferrite Content Thereof, ASTM A800
11) Gysel. W. et. al. "Influence of Long-Time Aging of CF8 and CF8M Cast Steel at Temperatures Between 300 and 500°C on Impact Toughness and Structural Properties" ASTM STP 756, 1982
12) C. W. Marschall et. al, "Loading Rate Effects on Strength and Fracture Toughness of Pipe Steels Used in Task 1 of the IPIRG Program" NUREG/CR-6098, 1993
13) Tabata et. al. "Four-Point Bending Test of Aged Cast Duplex Stainless Steel," ICPVT-9 pp. 745-752
14) Ductile Fracture Handbook EPRI NP-6301 1989

15) Natsu Honda, "Evaluation of Mechanical Characteristics of Stainless Steel Under Simulated Aging," Proceedings of the Japan Society of Mechanical Engineers (A Edition) Vol. 59, No. 565, 1993

Acknowledgements

This paper is a summary of part of the research on embrittlement conducted from 1999 to 2005.

Up until September 2003, planning, manufacture, testing, and analysis were conducted under the guidance of the Nuclear Plant Machinery High-Level Safety Policy Committee of the Japan Power Engineering and Inspection Corporation (Foundation). From October 2003 onwards, the independent administrative agency, the Japan Nuclear Energy Safety Organization conducted analyses and testing while obtaining the advice of the Materials Evaluation Technology Investigation Committee of that same organization, and summarized the results. We wish to express our deep felt gratitude for the guidance of every one of the members of that investigation committee.

We also want to express our deep felt thanks to all of those who provided their helpful advice when we undertook various tests and analysis and summarized the report. Moreover, special mention must be given to the realization of difficult pipe tests and the publication of predictive formulas that reflected a wealth of provide material test data, and therefore express our gratitude to the persons involved in such activities.

Appendix 1 Decrease in Fracture Toughness as a Function of Material, Time, and Temperature

Simple Table (Based on Reference Document 3) for Predictive Evaluations of Fracture Toughness (JR-Δa characteristic) for Cast Stainless Steel Using the Chemical Composition, Thermal Aging Temperature, and Thermal Aging Time of the Material

Appended Figure 1-1 Predicted Fracture Toughness

										Min	Max	
C %	0.05	0.0495	0.049	0.048	0.0475	0.047	0.0465	0.046	0.0455		0.08	
Mn w%	0.850	0.845	0.840	0.830	0.825	0.820	0.815	0.810	0.805		1.5	
N w%	0.056	0.054	0.052	0.048	0.046	0.044	0.042	0.040	0.038			
Ni w%	9.90	9.85	9.80	9.70	9.65	9.60	9.55	9.50	9.45	9	12	
Cr w%	19.03	19.22	19.64	19.85	20.06	20.23	20.49	20.70	20.88	18	21	
Mo w%	2.30	2.30	2.30	2.30	2.30	2.30	2.30	2.30	2.30	2	3	
Si w%	0.799	0.820	0.899	0.972	1.018	1.069	1.122	1.179	1.235		1.5	
Nb w%	0.00	0.00	0.00	0.00	0.00	0.00	0.00	0.00	0.00			
P w%	0.03	0.03	0.03	0.03	0.03	0.03	0.03	0.03	0.03		0.04	
X	1.188	1.211	1.256	1.297	1.326	1.354	1.388	1.420	1.450			
FN %	10.00	11.00	13.00	15.00	16.50	18.00	20.00	22.00	24.00			
JIC												
A	583.32	516.51	404.58	317.22	263.96	219.81	172.28	134.86	105.65			
Amin	182.94	161.99	126.88	99.48	82.78	68.94	54.03	42.30	33.13			
B325	3746796	3707080	3667786	3590443	3552385	3514730	3477475	3440614	3404145			
tF325	1716.20	1874.08	2046.47	2440.30	2664.79	2909.93	3177.61	3469.92	3789.13			
(tF + C)325	3773.81	3685.28	3598.82	3431.94	3351.43	3272.80	3196.02	3121.04	3047.82			
J6												
A	1512.59	1351.69	1078.49	861.27	726.68	613.55	489.82	390.58	311.67			
Amin	761.59	680.58	543.02	433.65	365.88	308.92	246.62	196.66	156.93			
B325	1171359	1403331	2092281	2554759	3119464	3666823	4695372	5755088	6803619			
tF325	1261.40	1417.16	1592.15	2009.63	2257.78	2536.58	2849.80	3201.70	3597.05			
(tF + C)325	1581.15	1837.79	2562.67	3026.15	3573.45	4088.22	5022.52	5949.70	6839.18			
t(hrs)	420480	420480	420480	420480	420480	420480	420480	420480	420480	60 Years of Service at 420,480 Hrs		
T	325	325	325	325	325	325	325	325	325	Aging Temperature (°C)		
P(t,T)	4.657	4.657	4.657	4.657	4.657	4.657	4.657	4.657	4.657	Activation Energy = 100 kJ/mol		
σyo	160.31	164.91	174.92	184.12	191.46	198.77	208.75	218.79	228.79			
σfo	288.81	294.98	308.14	320.48	330.19	339.87	352.99	366.19	379.34			
σy	171.68	176.60	187.32	197.17	205.03	212.86	223.55	234.30	252.36	Optimal Predicted Value (Mpa)		
σf	334.04	341.18	356.40	370.67	381.91	393.09	408.28	423.54	469.66	Optimal Predicted Value (Mpa)		
n	5.09	5.06	4.98	4.91	4.85	4.80	4.72	4.65	4.57	Optimal Predicted Value		
α	2.88	2.81	2.66	2.53	2.42	2.32	2.17	2.03	2.37	Optimal Predicted Value		
JIC	10.00	11.00	13.00	15.00	16.50	18.00	20.00	22.00	24.00			
280	627.5	560.3	448.1	360.1	306.5	262.1	214.3	176.6	147.1	Optimal Predicted Value (kJ/m^2)		
280	227.1	205.8	170.4	142.3	125.3	111.2	96.0	84.0	74.6	Minimum Predicted Value (kJ/m^2)		
290	613.6	546.6	434.4	346.5	293.0	248.6	200.9	163.3	133.8	Optimal Predicted Value (kJ/m^2)		
290	213.3	192.0	156.7	128.8	111.9	97.8	82.6	70.7	61.3	Minimum Predicted Value (kJ/m^2)		
325	592.2	525.3	413.3	325.7	272.4	228.2	180.6	143.1	113.8	Optimal Predicted Value (kJ/m^2)		
325	191.8	170.8	135.6	108.0	91.2	77.3	62.3	50.5	41.2	Minimum Predicted Value (kJ/m^2)		
J6												
280	1526.7	1368.6	1103.5	891.7	763.8	657.0	545.1	457.9	390.8	Optimal Predicted Value (kJ/m^2)		
280	775.7	697.4	568.0	464.1	403.0	352.4	301.9	263.9	236.0	Minimum Predicted Value (kJ/m^2)		
290	1522.2	1363.2	1095.6	882.1	752.1	643.3	527.8	436.9	366.2	Optimal Predicted Value (kJ/m^2)		
290	771.2	692.1	560.1	454.5	391.3	338.7	284.6	243.0	211.5	Minimum Predicted Value (kJ/m^2)		
325	1515.4	1355.0	1083.5	867.3	734.1	622.2	500.9	404.2	327.7	Optimal Predicted Value (kJ/m^2)		
325	764.4	683.9	548.0	439.7	373.3	317.6	257.7	210.3	173.0	Minimum Predicted Value (kJ/m^2)		
C1	10.00	11.00	13.00	15.00	16.50	18.00	20.00	22.00	24.00			
280	640.3	606.2	534.0	462.3	412.6	367.3	315.3	271.6	237.9	Optimal Predicted Value (kJ/m^2)		
280	354.8	330.3	285.9	246.3	221.0	199.0	175.3	156.4	142.7	Minimum Predicted Value (kJ/m^2)		
290	633.0	598.4	525.3	452.8	402.3	356.2	302.9	257.6	222.2	Optimal Predicted Value (kJ/m^2)		
290	345.9	321.1	275.7	235.4	209.3	186.4	161.3	140.9	125.5	Minimum Predicted Value (kJ/m^2)		
325	621.8	586.5	511.9	438.1	386.4	339.2	283.6	236.0	197.7	Optimal Predicted Value (kJ/m^2)		
325	332.2	306.7	259.7	218.2	190.8	166.6	139.2	116.4	98.3	Minimum Predicted Value (kJ/m^2)		
C2												
280	0.4850	0.4545	0.4051	0.3666	0.3437	0.3245	0.3055	0.2915	0.2770	Optimal Predicted Value		
280	0.4366	0.4171	0.3832	0.3536	0.3352	0.3190	0.3034	0.2921	0.2808	Minimum Predicted Value		
290	0.4897	0.4595	0.4103	0.3722	0.3492	0.3299	0.3100	0.2948	0.2789	Optimal Predicted Value		
290	0.4474	0.4286	0.3957	0.3673	0.3493	0.3334	0.3169	0.3041	0.2910	Minimum Predicted Value		
325	0.4971	0.4673	0.4185	0.3811	0.3581	0.3387	0.3175	0.3003	0.2822	Optimal Predicted Value		
325	0.4651	0.4476	0.4168	0.3911	0.3746	0.3600	0.3436	0.3301	0.3156	Minimum Predicted Value		

Appended Figure 1-2 Jmat = $C1(\Delta a)^{C2}$ Lower Limit Line at 60 Years of Operation

Aging Temperature 280°C

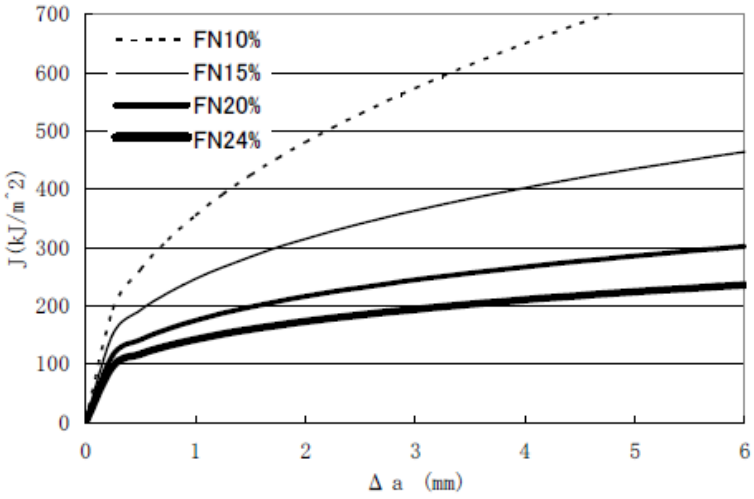

Aging Temperature 290°C

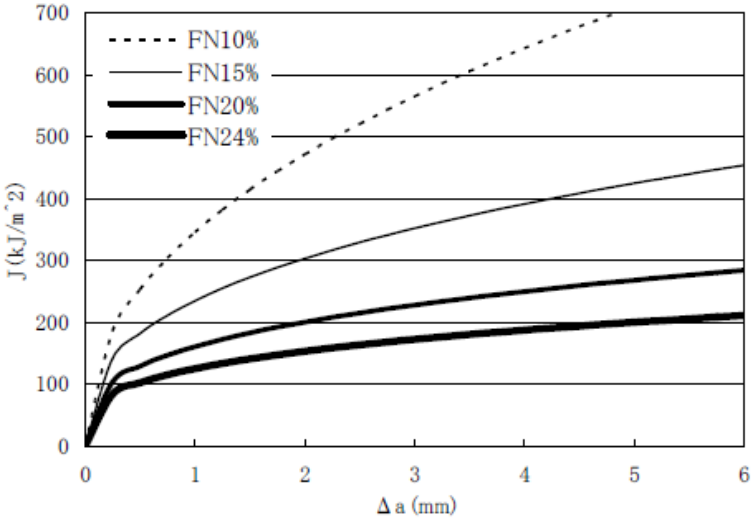

Aging Temperature 325°C

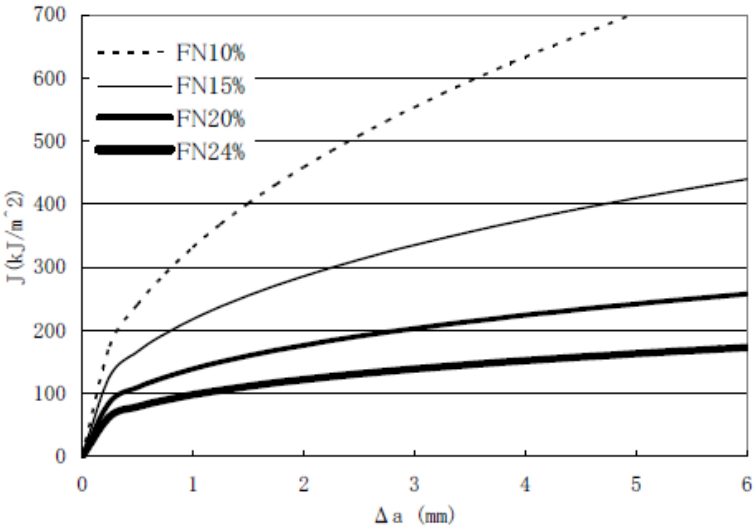

Appendix 2 Changes in Stress-Strain Characteristic as a Function of Material, Time, and Temperature

Simple Diagram for Predictive Evaluations Using the Chemical Aging Temperature, and Thermal Aging Time of Cast Stainless Steel (Based on Reference Material 3)

Appended Figure 2-1 Predictions of True-Stress - True-Strain Characteristic (Characteristic at 325°C After 60 Years of Service at 325°C)

										Min	Max	
C %	0.05	0.0495	0.049	0.048	0.0475	0.047	0.0465	0.046	0.0455		0.08	
Mn w%	0.850	0.845	0.840	0.830	0.825	0.820	0.815	0.810	0.805		1.5	
N w%	0.056	0.054	0.052	0.048	0.046	0.044	0.042	0.040	0.038			
Ni w%	9.90	9.85	9.80	9.70	9.65	9.60	9.55	9.50	9.45	9	12	
Cr w%	19.03	19.22	19.64	19.85	20.06	20.23	20.49	20.70	20.88	18	21	
Mo w%	2.30	2.30	2.30	2.30	2.30	2.30	2.30	2.30	2.30	2	3	
Si w%	0.799	0.820	0.899	0.972	1.018	1.069	1.122	1.179	1.235		1.5	
Nb w%	0.00	0.00	0.00	0.00	0.00	0.00	0.00	0.00	0.00			
P w%	0.03	0.03	0.03	0.03	0.03	0.03	0.03	0.03	0.03		0.04	
X	1.188	1.211	1.256	1.297	1.326	1.354	1.388	1.420	1.450			
FN %	10.00	11.00	13.00	15.00	16.50	18.00	20.00	22.00	24.00			
JIC												
A	583.32	516.51	404.58	317.22	263.96	219.81	172.28	134.86	105.65			
Amin	182.94	161.99	126.88	99.48	82.78	68.94	54.03	42.30	33.13			
B325	3746796	3707080	3667786	3590443	3552385	3514730	3477475	3440614	3404145			
tF325	1716.20	1874.08	2046.47	2440.30	2664.79	2909.93	3177.61	3469.92	3789.13			
(tF + C)325	3773.81	3685.28	3598.82	3431.94	3351.43	3272.80	3196.02	3121.04	3047.82			
J6												
A	1512.59	1351.69	1078.49	861.27	726.68	613.55	489.82	390.58	311.67			
Amin	761.59	680.58	543.02	433.65	365.88	308.92	246.62	196.66	156.93			
B325	1171359	1403331	2092281	2554759	3119464	3666823	4695372	5755088	6803619			
tF325	1261.40	1417.16	1592.15	2009.63	2257.78	2536.58	2849.80	3201.70	3597.05			
(tF + C)325	1581.15	1837.79	2562.67	3026.15	3573.45	4088.22	5022.52	5949.70	6839.18			
t(hrs)	420480	420480	420480	420480	420480	420480	420480	420480	420480	60 Years of Service at 420,480 Hrs		
T	325	325	325	325	325	325	325	325	325	Aging Temperature (°C)		
P(t,T)	4.657	4.657	4.657	4.657	4.657	4.657	4.657	4.657	4.657	Activation Energy = 100 kJ/mol		
σyo	160.31	164.91	174.92	184.12	191.46	198.77	208.75	218.79	228.79	Optimal Predicted Value (Mpa)		
σfo	288.81	294.98	308.14	320.48	330.19	339.87	352.99	366.19	379.34	Optimal Predicted Value (Mpa)		
σy	171.68	176.60	187.32	197.17	205.03	212.86	223.55	234.30	252.36	Optimal Predicted Value (Mpa)		
σf	334.04	341.18	356.40	370.67	381.91	393.09	408.28	423.54	469.66	Optimal Predicted Value (Mpa)		
n	5.09	5.06	4.98	4.91	4.85	4.80	4.72	4.65	4.57	Optimal Predicted Value		
α	2.88	2.81	2.66	2.53	2.42	2.32	2.17	2.03	2.37	Optimal Predicted Value		
σyo	141.4	146.0	156.0	165.2	172.6	179.9	189.8	199.9	209.9	Minimum Predicted Value (Mpa)		
σfo	274.4	280.5	293.7	306.0	315.7	325.4	338.5	351.7	364.9	Minimum Predicted Value (Mpa)		
σy	140.9	145.1	154.1	162.5	169.1	175.7	184.8	193.9	207.6	Minimum Predicted Value (Mpa)		
σf	300.3	306.6	320.2	333.0	343.0	352.9	366.5	380.1	434.1	Minimum Predicted Value (Mpa)		
n	6.20	6.16	6.08	6.01	5.96	5.90	5.83	5.75	5.54	Maximum Predicted Value		
α	3.53	3.46	3.29	3.13	3.01	2.88	2.72	2.55	1.89	Maximum Predicted Value		

Attached Figure 2-2 True-Stress True-Strain Characteristic Predictions
(60 Year Service Conditions at 325°C)

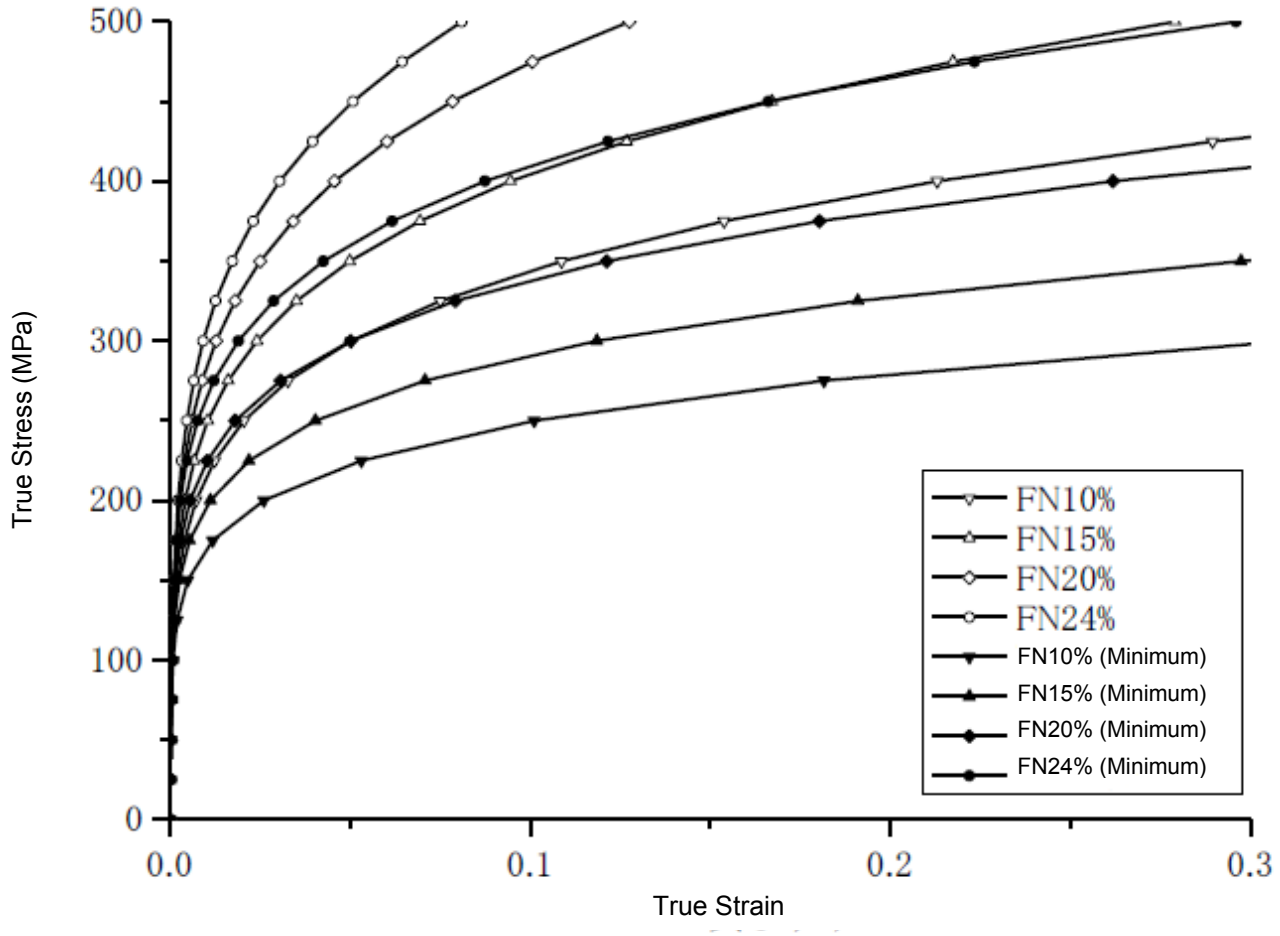

Appendix 3 Crack Detection Performance Data for Primary Cooling Pipes

Note: All charts and quotations are based on "Report on the Inspection Technology Verification Activities for Nuclear Power Generation Facilities" (On the Confirmation of Defect Detectability and Sizing Precision in Ultrasonic Wave Inspection Tests [Summary Version]) of the Japan Nuclear Energy Safety Organization, April 2005.

1. Test Conditions

Table 4.13.3.1 Detect Detectability Test Conditions in Cast Stainless Steel Test Specimens Provided with Fatigue Cracks (Shared)

Defect Detection	Regulation/Standard	Based on UT guidelines in draft of maintenance standards
	Test Method	Vertical method and standing wave oblique angle method based on normal probe
	Test Personnel	Those with two or three NDI qualifications, those with ISI experience, and those with ISI experience for stainless steel pipes
	Restrictions	Indicated only for the test range (private with respect to crack type, size, and detailed position or the like)

Table 4.13.3.2 Detect Detectability Test Conditions in Cast Stainless Steel Test Specimens Provided with Fatigue Cracks (Detailed)

Item		Conditions
Targeted Defect		Fatigue Cracks: 8 cracks (CP0F1-8), EDM slits: 8 slits(CP0E1-8)
Test Method	Test Technique	Manual inspections (three teams)
	Inspection Method	Vertical inspections Standing wave oblique angle inspection
Equipment and Materials Used	Ultrasonic Inspection Device	Pulse-reflection type analog display inspection device
	Test Probe	1Z25.4ND 1C40 × 30LAD45 (the probe selected during preliminary tests) 1C30 × 20LAD36 (employed when false echoes were detected)
	Contact Medium	Glycerin paste
	Comparison Test Piece	Comparison test piece provided with horizontal holds (JEAG4207 comparison test piece)
Others	Order of Tests *1	Inspections were first conducted from the centrifugally cast material side, and after determining whether anything was detected, inspections were conducted from the statically cast material side
	Training	Training was conducted prior to the tests using short strip-shaped test pieces having the same material quality and dimensions as EDM slits

(Notes) *1: The order of the tests was conducted taking into consideration the structure of the actual equipment. Because statically cast material consists of pipes, inspections from the statically cast material side would be restricted from the standpoint of shape.

2. Specimen Material and Shape

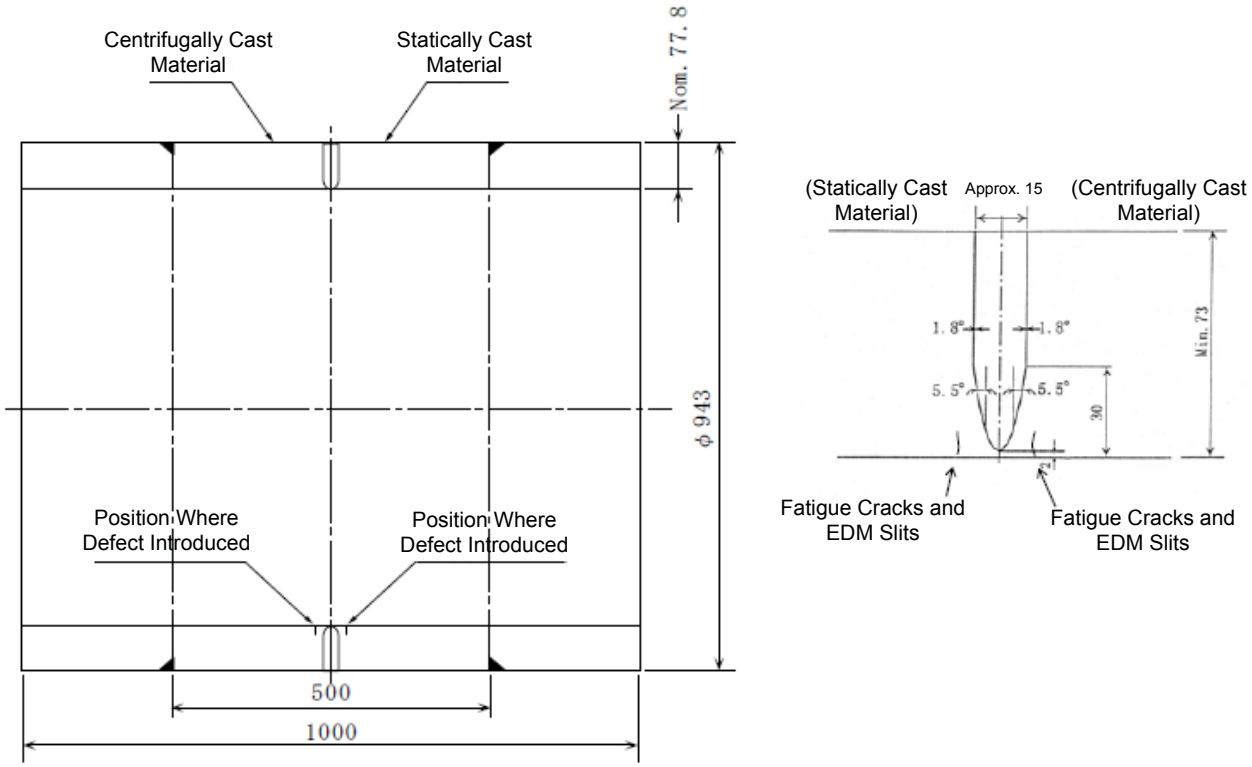

Statically Cast Material: 78S G5121-1991 SCS14A, Centrifugally Cast Material: JIS G5121-1991 SCS14A-CF

Figure 4.13.1.1 Sketch of Exterior of PWR Main Cooling Pipe Test Specimens with Fatigue Cracks Introduced

Table 4.13.3.3 Table of the Types of Defects Applied to Cast Stainless Steel Test Specimens in Which Fatigue Cracks Have Been Introduced

Test Specimen	Defect Category	Location Defect Applied	Defect No.	Defect Dimensions					Position Defect Applied	Classification	Notes (Characteristics of Defect Nature or the Like)
				Depth		Length	Aspect Ratio	Interval*1			
				a (mm)	a/t (%)	L (mm)	a/L	g (μm)			
PWR Main Cooling Pipes with Fatigue Cracks Applied	Fatigue Cracks	Statically Cast Material	CP0F1	6.2	8.0	40.6	0.15	10-20	Pipe interior surface, welded section, thermally affected section (bead centers were on the order of 7 mm)	Greater than defect dimensions for which evaluations not required	[Slight branching in locations in depth direction]
			CP0F2	9.2	11.8	61.2	0.15	20-30		Greater than defect dimensions for which evaluations not required	[Slight branching in locations in depth direction]
			CP0F3	11.9	15.3	82.6	0.14	20-30		Greater than defect dimensions for which evaluations not required	[Slight branching in locations in depth direction]
			CP0F4	14.4	18.5	106.0	0.14	10-20		Greater than defect dimensions for which evaluations not required	[Slight branching in locations in depth direction]
		Centrifugally Cast Material	CP0F5	6.6	8.5	40.7	0.16	10-15		Greater than defect dimensions for which evaluations not required	—
			CP0F6	8.9	11.4	65.4	0.14	10-20		Greater than defect dimensions for which evaluations not required	[Slight branching in locations in depth direction]
			CP0F7	13.3	17.1	110.7	0.12	10-20		Greater than defect dimensions for which evaluations not required	—
			CP0F8	15.2	19.5	99.8	0.15	20-30		Greater than defect dimensions for which evaluations not required	[Slight branching in locations in depth direction]
	EDM Slits	Statically Cast Material	CP0E1	4.6	5.9	31.0	0.15	≈ 200		Less than defect dimensions for which evaluations not required	
			CP0E2	6.1	7.8	41.0	0.15	≈ 200		Equal to defect dimensions for which evaluations not required	
			CP0E3	9.1	11.7	61.0	0.15	≈ 200		Greater than defect dimensions for which evaluations not required	
			CP0E4	12.1	15.6	81.0	0.15	≈ 200		Greater than defect dimensions for which evaluations not required	
		Centrifugally Cast Material	CP0E5	4.6	5.9	31.0	0.15	≈ 200		Less than defect dimensions for which evaluations not required	
			CP0E6	6.1	7.8	41.0	0.15	≈ 200		Equal to defect dimensions for which evaluations not required	
			CP0E7	9.1	11.7	61.0	0.15	≈ 200		Greater than defect dimensions for which evaluations not required	
			CP0E8	12.1	15.6	81.0	0.15	≈ 200		Greater than defect dimensions for which evaluations not required	

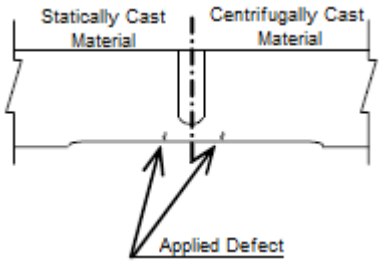

(Notes) *1 For fatigue cracks, the defect depth, length, and defect interval reflect cutting inspection results, and for EDM slits, they reflect records at the time of manufacture.

Table 4.13.3.4(1) Table of Defect Detectability Evaluation Parameters for Cast Stainless Steel Test Specimens in Which Fatigue Cracks Have Been Introduced (Fatigue Cracks)

Test specimen	Location Defect Applied	Defect No.	Defect Dimensions				Y Distance (mm)	Inspection Direction	Detection Rate (%)*2	Maximum Echo Height*3			Discrepancy in Maximum Echo Detection Position (X) (max - min) (mm)	Average Value of Specified Length with DAC20% (mm) *4	Reflection Source
			Depth	Length	Interval*1	Surface Area				Average Value		Variance			Average Value
			a (mm)	L (mm)	g (μm)	S (mm^2)				DAC%	dB	Max - Min .(dB)			
PWR Main Cooling Pipes with Fatigue Cracks Applied	Statically Cast Material	CP0F1	6.2	40.6	10 - 20	197.6	5.9	Centrifugally Cast Material	67 (100)	26.0	-11.7	0.0	14.0	20.6	0.8
								Statically Cast Material	100	30.0	-10.5	0.9	6.0		-1.2
		CP0F2	9.2	61.2	20 - 30	442.0	8.9	Centrifugally Cast Material	67 (100)	30.3	-10.4	0.9	35.0	43.1	8.5
								Statically Cast Material	100	24.3	-12.3	3.8	14.0		1.8
		CP0F3	11.9	82.6	20 - 30	771.6	9.2	Centrifugally Cast Material	67	32.3	-9.8	0.8	7.0	45.6	-0.7
								Statically Cast Material	67	33.0	-9.6	1.1	27.0		6.1
		CP0F4	14.4	106.0	10 - 20	1198.2	8.7	Centrifugally Cast Material	100	37.7	-8.5	2.6	3.0	68.5	-0.9
								Statically Cast Material	100	29.3	-10.7	2.1	74.0		21.8
	Centrifugally Cast Material	CP0F5	6.6	40.7	10 - 15	210.9	-5.2	Centrifugally Cast Material	100	27.3	-11.3	1.9	11.0	32.3	0.5
								Statically Cast Material	100	36.7	-8.7	2.4	8.0		0.5
		CP0F6	8.9	65.4	10 - 20	456.9	-3.5	Centrifugally Cast Material	100	36.0	-8.9	1.2	5.0	47.0	-0.9
								Statically Cast Material	100	36.7	-8.7	1.9	16.0		3.1
		CP0F7	13.3	110.7	10 - 20	1155.8	-6.7	Centrifugally Cast Material	100	26.0	-11.7	0.7	91.7	58.5	26.9
								Statically Cast Material	100	33.0	-9.6	4.3	86.0		26.9
		CP0F8	15.2	99.8	20 - 30	1190.8	-5.5	Centrifugally Cast Material	100	41.0	-7.7	6.7	4.0	54.0	1.0
								Statically Cast Material	100	42.7	-7.4	3.8	34.0		10.1

Notes

*1: Defect intervals indicate records at the time of manufacture.
*2: Indicates the detection rate based on judgments made only based on inspections from the centrifugally cast side. Numerical values in parentheses indicate detection rates based on two-sided inspections, meaning from the statically cast side and the centrifugally cast side. Moreover, detection rates show the case where the detection level is DAC20%.
*3: Computed based on two-sided inspection results. Includes values where echoes were detected.
*4: Overlapping values of length based on two-sided inspections.

Table 4.13.3.4(2) Table of Defect Detectability Evaluation Parameters for Cast Stainless Steel Test Specimens in Which Fatigue Cracks Have Been Introduced (EDM Slits)

Test specimen	Location Defect Applied	Defect No.	Defect Dimensions				Y Distance (mm)	Inspection Direction	Detection Rate (%)*2	Maximum Echo Height*3			Discrepancy in Maximum Echo Detection Position (X) (max - min) (mm)	Average Value of Specified Length with DAC20% (mm) *4	Reflection Source
			Depth	Length	Interval*1	Surface Area				Average Value		Variance			Average Value
			a (mm)	L (mm)	g (μm)	S (mm^2)				DAC%	dB	Max - Min .(dB)			
PWR Main Cooling Pipes with Fatigue Cracks Applied	Statically Cast Material	CP0F1	4.6	31.0	≈ 200	111.9	7	Centrifugally Cast Material	100	21.7	-13.3	1.2	17.0	23.4	1.6
								Statically Cast Material	100	32.0	-9.9	2.5	10.0		0.9
		CP0F2	6.1	41.0	≈ 200	196.3	7	Centrifugally Cast Material	100	36.3	-8.8	1.0	5.0	32.3	-0.9
								Statically Cast Material	100	28.3	-11.0	1.2	6.0		-1.3
		CP0F3	9.1	61.0	≈ 200	435.8	7	Centrifugally Cast Material	67 (100)	38.3	-8.3	2.0	29.0	43.1	7.6
								Statically Cast Material	100	30.3	-10.4	4.3	13.0		2.3
		CP0F4	12.1	81.0	≈ 200	769.4	7	Centrifugally Cast Material	100	33.3	-9.5	0.5	9.0	65.4	0.0
								Statically Cast Material	100	31.0	-10.2	1.4	43.0		11.4
	Centrifugally Cast Material	CP0F5	4.6	31.0	≈ 200	111.9	-7	Centrifugally Cast Material	100	21.3	-13.4	1.2	25.0	23.9	4.3
								Statically Cast Material	100	32.3	-9.8	1.6	2.0		-2.1
		CP0F6	6.1	41.0	≈ 200	196.3	-7	Centrifugally Cast Material	67	22.0	-13.2	0.8	11.0	18.9	-0.5
								Statically Cast Material	67	30.7	-10.3	2.0	6.0		-0.8
		CP0F7	9.1	61.0	≈ 200	435.8	-7	Centrifugally Cast Material	100	26.0	-11.7	2.6	29.0	51.8	6.6
								Statically Cast Material	100	56.7	-4.9	1.4	11.0		2.5
		CP0F8	12.1	81.0	≈ 200	769.4	-7	Centrifugally Cast Material	100	26.7	-11.5	1.3	8.0	65.7	-0.7
								Statically Cast Material	100	42.3	-7.5	6.0	60.0		19.5

Notes

*1: Defect intervals indicate records at the time of manufacture.
*2: Indicates the detection rate based on judgments made only based on inspections from the centrifugally cast side. Numerical values in parentheses indicate detection rates based on two-sided inspections, meaning from the statically cast side and the centrifugally cast side. Moreover, detection rates show the case where the detection level is DAC20%.
*3: Computed based on two-sided inspection results. Includes values where echoes were detected.
*4: Overlapping values of length based on two-sided inspections.

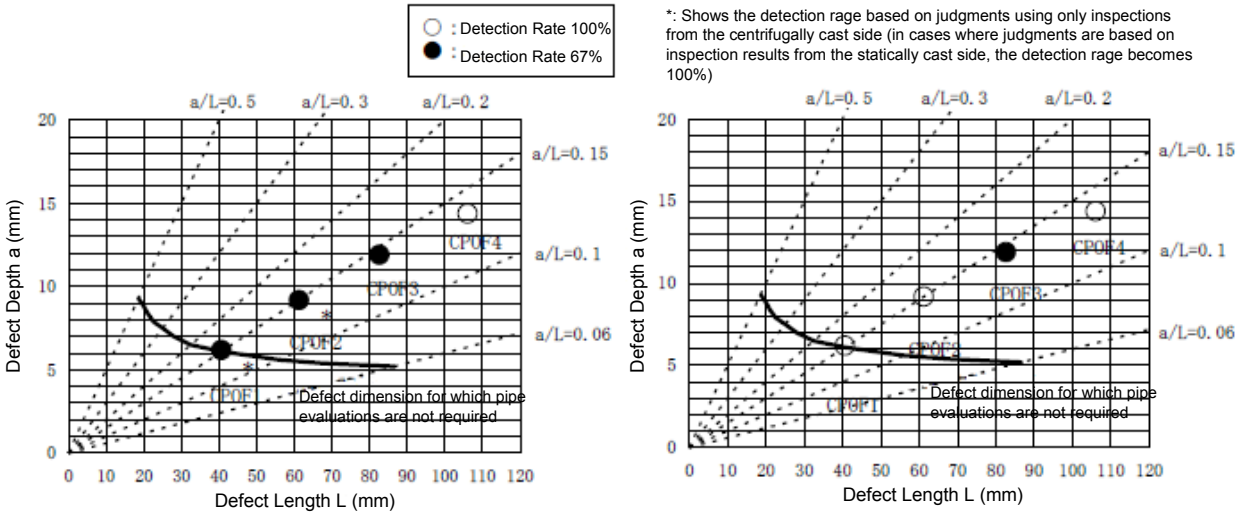

(a) Fatigue Cracks on Statically Cast Side

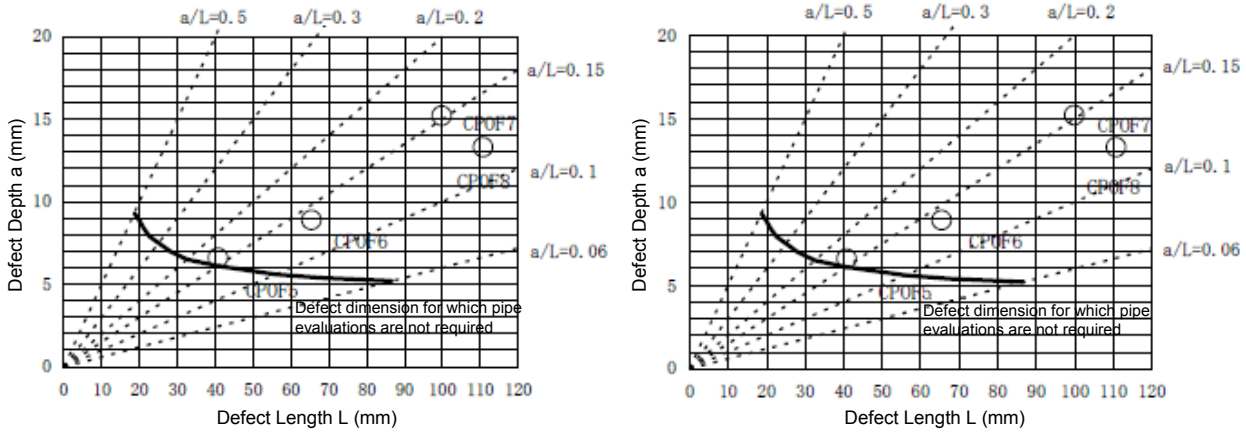

(b) Fatigue Cracks on Centrifugally Cast Side

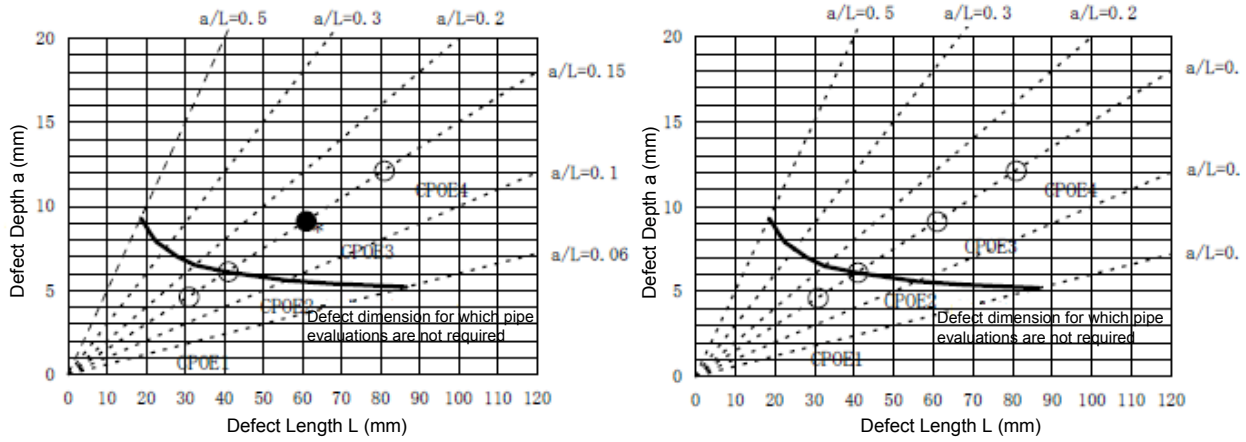

(c) EDM Slits on Statically Cast Side

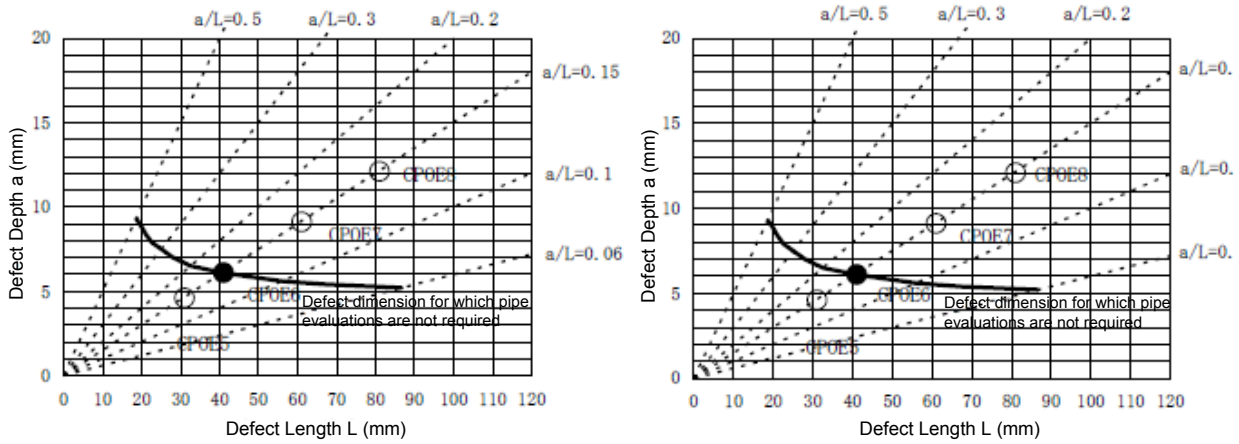

(d) EDM Slits on Centrifugally Cast Side

(1) One-Sided Inspection From Centrifugally Cast Side

(2) Two-Sided Inspection from Centrifugally Cast Side and Statically Cast Side

Figure 4.13.3.2 Defect Detection Rate of Cast Stainless Steel Test Specimens to Which Fatigue Cracks Have Been Introduced

Table 4.13.3.13 Summary of Defect Detectability of Cast Stainless Steel Test Specimens to Which Fatigue Cracks Have Been Introduced

Prerequisite Conditions	Contents
Evaluation Target Range (Defect Detectability Test)	The contents of detectability assessments for cast stainless steel test specimens to which fatigue cracks had been introduced were obtained from the fatigue cracks and EDM slits in the following ranges exhibited in PWR main cooling pipe test specimens. (1) Diameter x depth a. Diameter: ϕ943 mm b. Thickness: 75.5 mm (2) Materials a. Region corresponding to elbow: statically cast material (straight pipe), JIS G5121-1991 SCS14A b. Straight pipe section: centrifugally cast material, JIS G5121-1991 SCS14A-CF (3) Defect conditions a. Orientation: circumferential direction b. Range of dimensions in defect depth direction: 4.6 - 15.2 mm c. Range of dimensions in defect length direction: 31 - 110.7 mm d. Defect surface area (computed near the semi-ellipse): 111.9 - 1198.2 mm e. Aspect ratio: 0.12 - 0.16 d. Defect interval: 10 - 30 μm (fatigue crack), approx. 200 μm (EDM slits) e. Distance from weld center to defect opening region: 3.5 - 9.2 mm
Evaluation Items	Evaluation Results
Defect Detectability	(1) Defect level and defect detection rate When the defect level was DAC20%, the detection rate for defects exceeding the crack dimensions for which evaluations are not needed was approx. 96% for both fatigue cracks and EDM slits. (2) Defect dimensions and defect detection rate The smallest defect dimensions for which the defect detection rate was 100% were as follows: 13.3 mm for fatigue cracks when inspected from the centrifugally cast side and statically cast side; 12.1 mm for EDM slits when inspected from the centrifugally cast side, and 9.1 mm for EDM slits when inspected from the statically cast side. (3) Maximum echo height and defect dimension Due to the influence of columnar crystalline structures (the focusing of ultrasonic waves), we were not able to confirm a correlation between the maximum echo height and the defect dimension. (4) Maximum echo height and defect detection rate The echo height is at a low level below DAC50%, and we were not able to confirm a correlation between the maximum echo height and the defect detection rate.
Defect Detectability	(5) Variance in maximum echo height The maximum variance (maximum value - minimum value) in maximum echo height was 6.7 dB.

<<Continued on Next Page>>

Precision of Defect Detection Position	(1) Positional precision of maximum echo height in the X direction There was a large variance (maximum value - minimum value) in the position of maximum echo detection in the X direction, and with long defects in particular, in some regions, we were able to observe large variances exceeding transducer dimensions, and confirmed that the maximum echo detection position concentrates within the range where the defect is present. (2) Positional precision of reflection source For every defect, the average error and standard deviation of the position of reflection sources in the Y direction were sufficiently small values relative to the transducer dimension (40 mm). In addition, in inspections from the centrifugally cast material side and inspections from the statically cast material side, the reflection source position in the Y direction exhibited a tendency to be offset towards the centrifugally cast material side; and that tendency was particularly strong with fatigue cracks. (3) Positional precision of defect length detection In long defects, there were times where the defect indication for a single defect appeared to be split, but the rate of overlap of defect indications for the range of existing defects was low.
Defect Error Recognition	There were no false positives for defect detection.

Appendix 4 Photos of Pipe Tests

Installation of Large-Sized Pipe Test Specimen into Testing Device

State with Large-Sized Pipe Test Specimen Installed

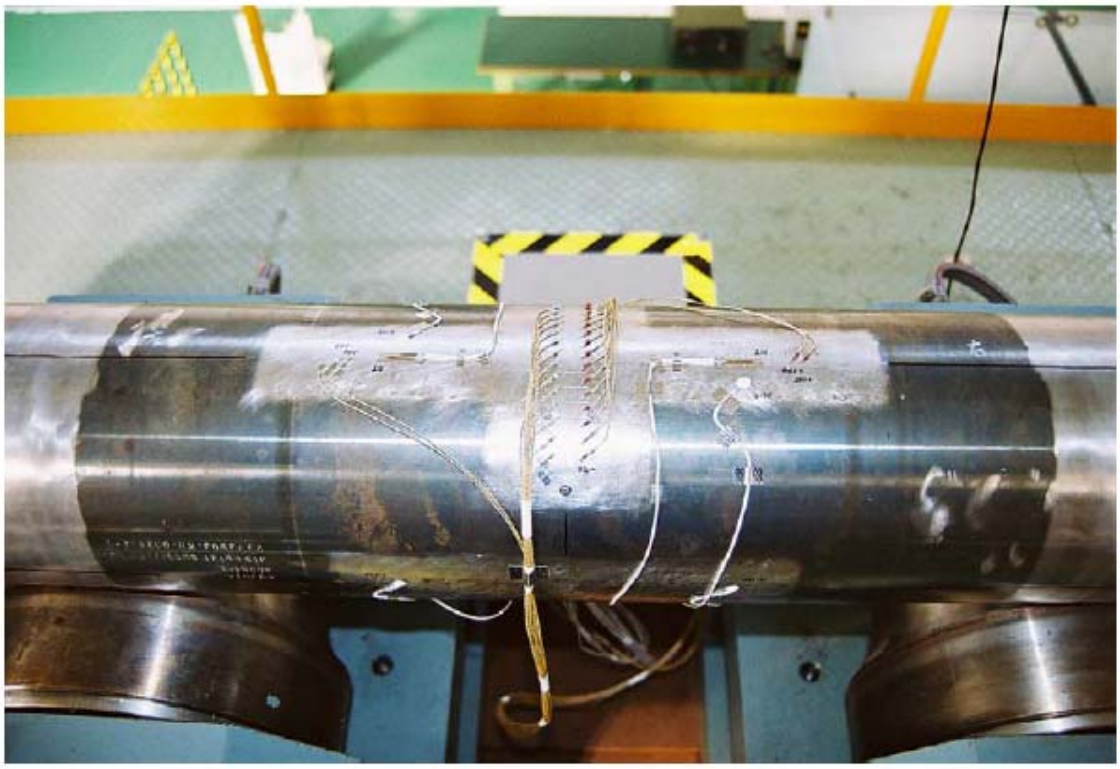

Mounting of Sensor onto Medium-Sized Pipe Test Specimen

Testing of Medium-Sized Pipe Test Specimen (Internal Heater Applying Heat)

Post-Test Crack States for Large-Sized Pipe Test Specimen

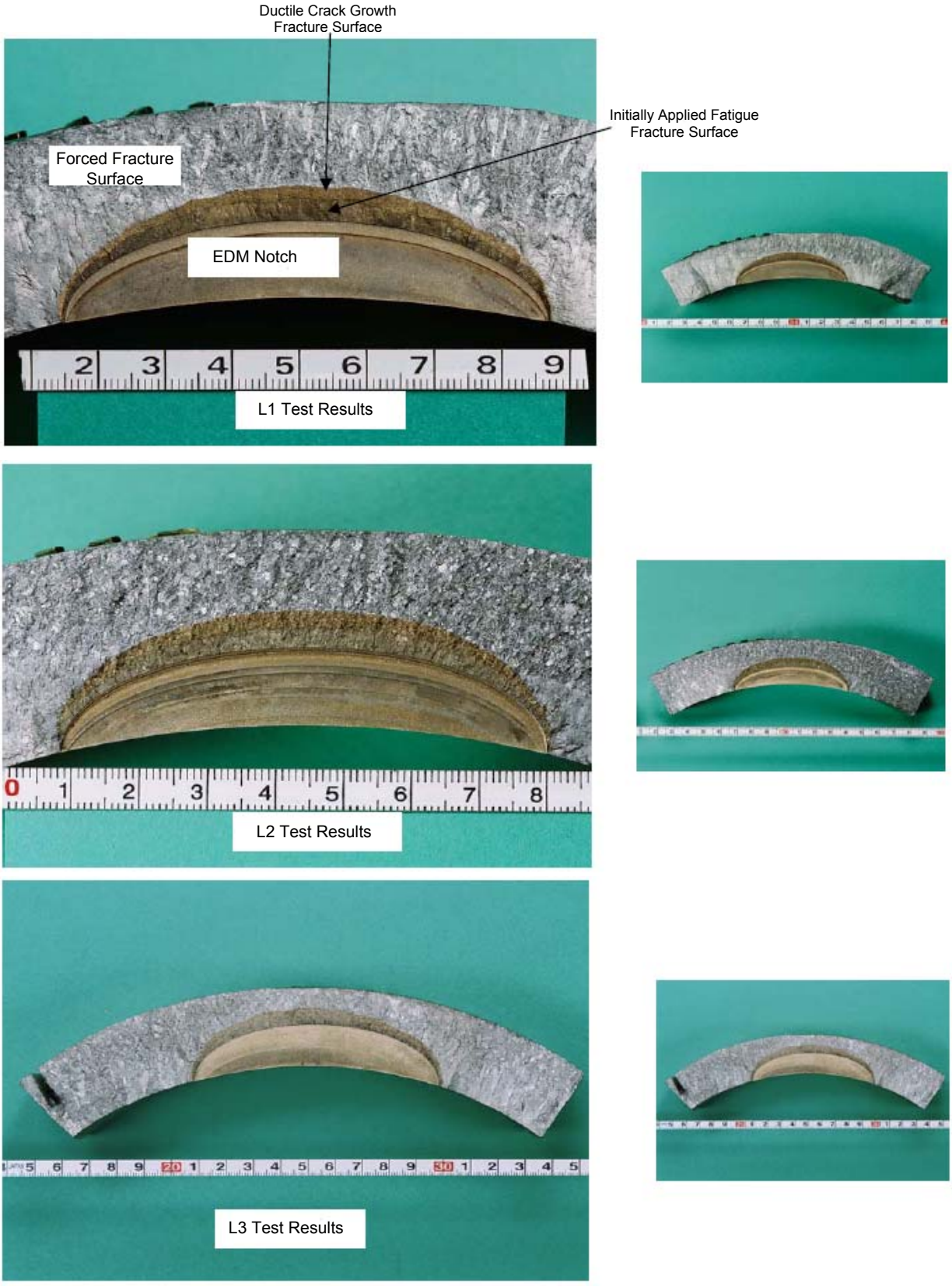

Post-Test Crack States for Medium-Sized Pipe Test Specimen


M4 Test
Specimen

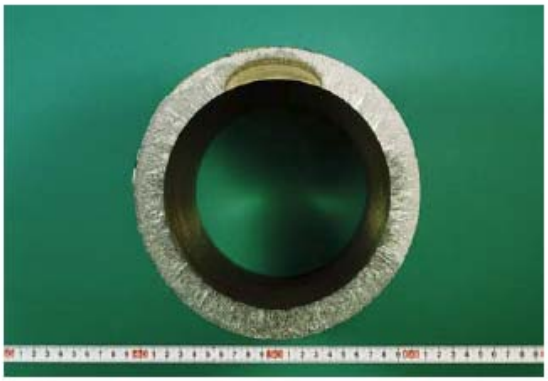


M5 Test
Specimen
2
3
4
5
6
7
8
9

Appendix 5 Pipe Test Data

Table Summarizing Pipe Tests

	Symbol	Unit	M1	M2	M3	M4	M5	L1	L2	L3
Test Type			Max. Load	Max. Load	Max. Load	Max. Load	Crack Growth	Crack Growth	Crack Growth	Crack Growth
Thermal Aging (450° C × 3300 hours)			No	Yes	No	Yes	Yes	Yes	Yes	Yes
Pipe Outer Diameter	Do	m	0.21230	0.21230	0.21230	0.21230	0.21230	0.35300	0.35300	0.35300
Pipe Thickness	t	m	0.02300	0.02300	0.02300	0.02300	0.02300	0.02910	0.02910	0.02910
Pipe Average Radius	Rm	m	0.09465	0.09465	0.09465	0.09465	0.09465	0.16195	0.16195	0.16195
Pipe Outer Diameter	Ri	m	0.08315	0.08315	0.08315	0.08315	0.08315	0.14740	0.14740	0.14740
Cross Section Coefficient	Z	m^4	0.00059	0.00059	0.00059	0.00059	0.00059	0.00222	0.00222	0.00222
Ferrite Content	FN	%	10.9	10.9	22.7	22.7	22.7	11.4	23.7	23.7
Initial Crack Depth	ao	m	0.01400	0.01470	0.01450	0.01454	0.01407	0.01435	0.01495	0.01895
Initial Crack Surface Length	lo	m	0.07201	0.07201	0.07201	0.07270	0.07250	0.07266	0.07252	0.09263
Initial Crack Half Angle	Θo	Rad	0.4330	0.4330	0.4330	0.4372	0.4360	0.2465	0.2460	0.3142
Test Conditions										
Temperature	T	℃	325.0	325.0	325.0	325.0	325.0	325.0	325.0	325.0
0.2% Proof Stress (Actual Measured Value)	σy	MPa	141.0	144.0	200.0	207.0	207.0	160.0	210.0	210.0
Tensile Strength (Actual Measured Value)	σu	MPa	392.0	460.0	496.0	604.0	604.0	494.0	585.0	585.0
Flow Stress (Actual Measured Value)	σo	MPa	266.5	302.0	348.0	405.5	405.5	327.0	397.5	397.5
0.2 Proof Stress (Prescribed Value)	cσy	MPa	129.0	129.0	129.0	129.0	129.0	129.0	129.0	129.0
Tensile Strength (Prescribed Value)	cσu	MPa	420.0	420.0	420.0	420.0	420.0	420.0	420.0	420.0
Flow Stress (Prescribed Value)	cσo	MPa	274.5	274.5	274.5	274.5	274.5	274.5	274.5	274.5
Four-Point Bending Moment Arm	La	m	0.750	0.750	0.750	0.750	0.750	2.575	2.575	2.575
Test Results										
Maximum Applied Load	LD	kN	608.0	579.0	741.0	608.0	684.0	609.0	690.0	610.0
General Load at Which Crack Growth Began	LC	kN	569.0	553.0	738.0	569.0				
Moment = LD/2 X La	M	kN· m	228.0	217.1	277.9	228.0	256.5	784.1	888.4	785.4
Maximum Test Stress = M/Z/1000	S	MPa	389.3	370.7	474.4	389.3	437.9	353.5	400.6	354.1
Crack Depth (ao in the Case of Plastic Collapse)	a	m	0.01400	0.01470	0.01450	0.01454	0.01578	0.01620	0.01732	0.02112
Magnitude of Increase in Crack Depth	Δa	m					0.00171	0.00185	0.00237	0.00217
Crack Length (lo in the Case of Plastic Collapse)	l	m	0.07201	0.07201	0.07201	0.07270	0.07260	0.07313	0.07252	0.09291
Magnitude of Increase in Crack Length	Δl	m					0.00010	0.00047	0.00000	0.00028
Crack Half Angle	Θ	Rad	0.43300	0.43300	0.43300	0.43716	0.43656	0.24807	0.24600	0.31516
β=0.5(π−aΘ/t)	β	Rad	1.43901	1.43242	1.43431	1.43261	1.42104	1.50175	1.49759	1.45643
F=2(2sinβ−a·sinΘ/t)/π	F		1.09960	1.09034	1.09300	1.09072	1.07431	1.18319	1.17756	1.12170
Plastic Flow Stress (Actual Measured Value Basis)	Fσo	MPa	293.0	329.3	380.4	442.3	435.6	386.9	468.1	445.9
Plastic Flow Stress (Prescribed Value Basis)	Fcσo	MPa	301.8	299.3	300.0	299.4	294.9	324.8	323.2	307.9
Plastic Collapse Stress (Actual Measured Value Basis)	Rσo	MPa	373.1	419.3	484.3	563.1	554.7	492.6	596.0	567.7
Plastic Collapse Stress (Prescribed Value Basis)	Rcσo	MPa	384.3	381.1	382.0	381.2	375.5	413.5	411.6	392.0
S/Rσo			1.043	0.884	0.980	0.691	0.790	0.718	0.672	0.624
S/Rcσo			1.013	0.973	1.242	1.021	1.166	0.855	0.973	0.903

Appendix 6 Life-Sized Straight Pipe Analysis Data

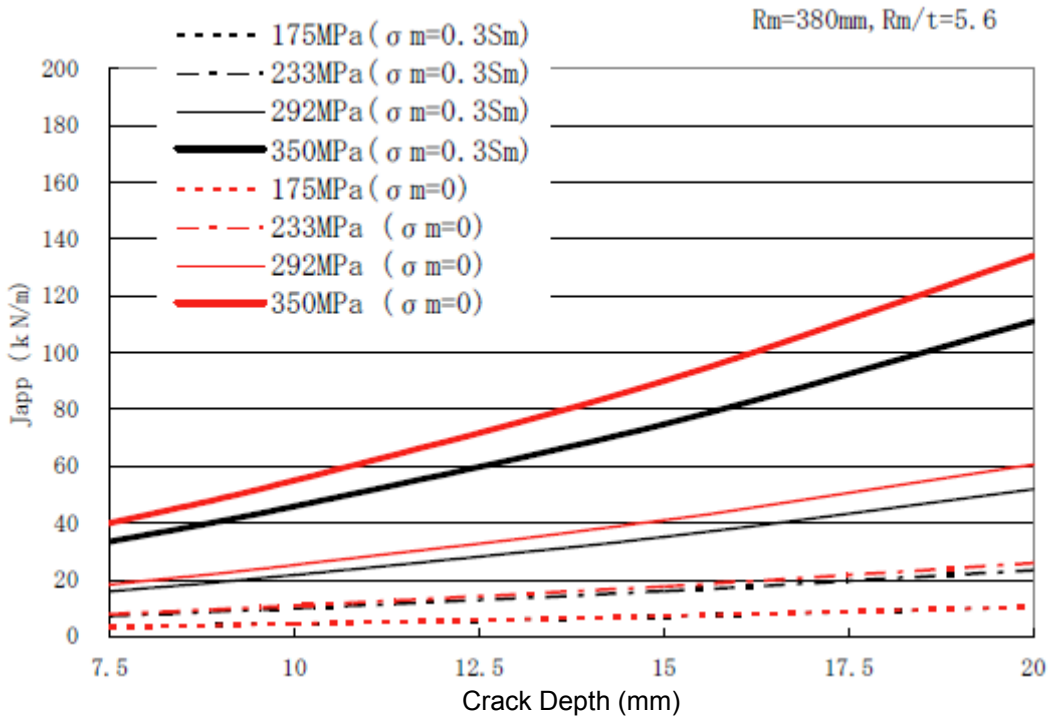

Predicted σ - ε for FN20% Cold-Leg Wall Thickness No. 1

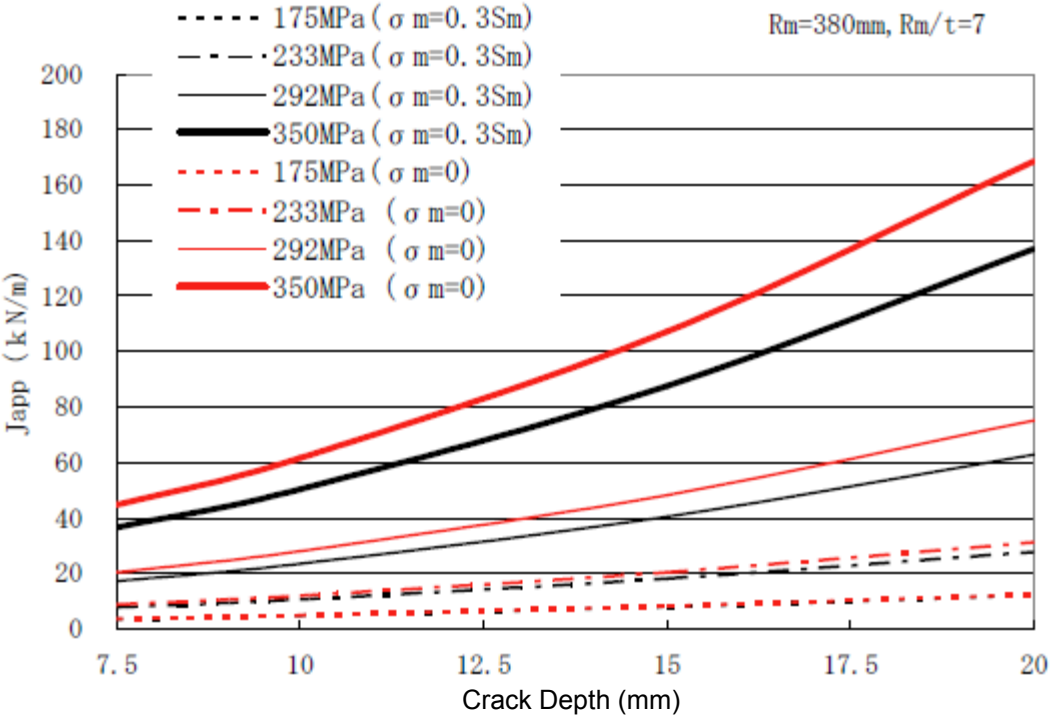

Predicted σ - ε for FN20% Cold-Leg Wall Thickness No. 2

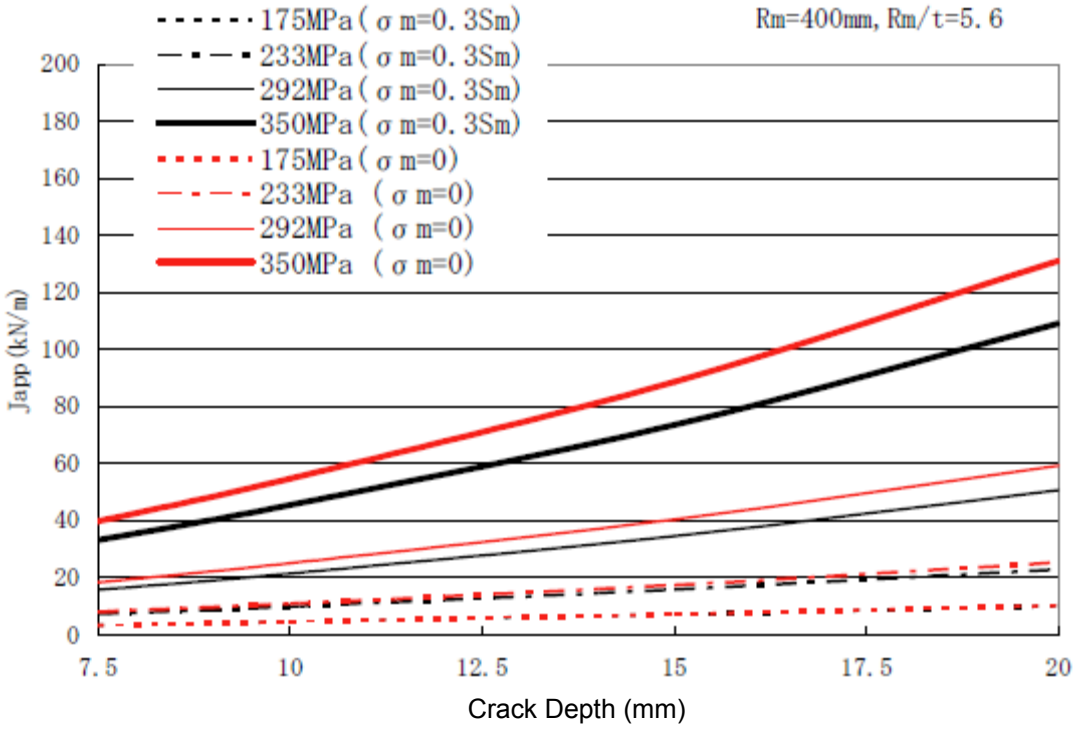

Predicted σ - ε for FN20% Hot-Leg Wall Thickness No. 1

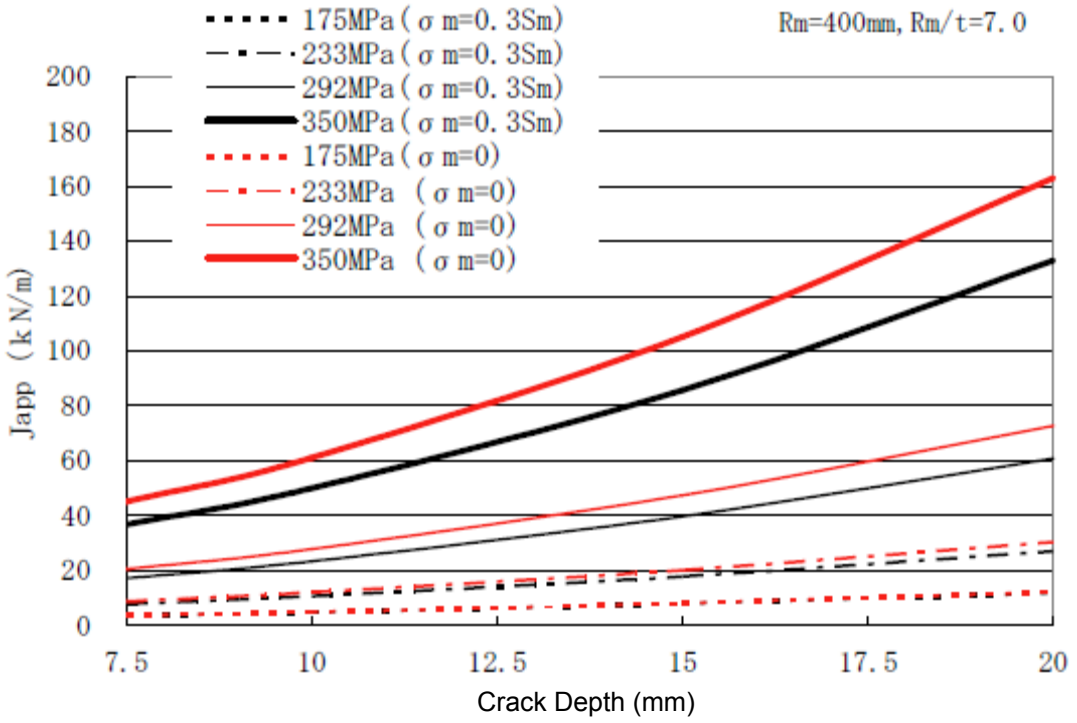

Predicted σ - ε for FN20% Hot-Leg Wall Thickness No. 2

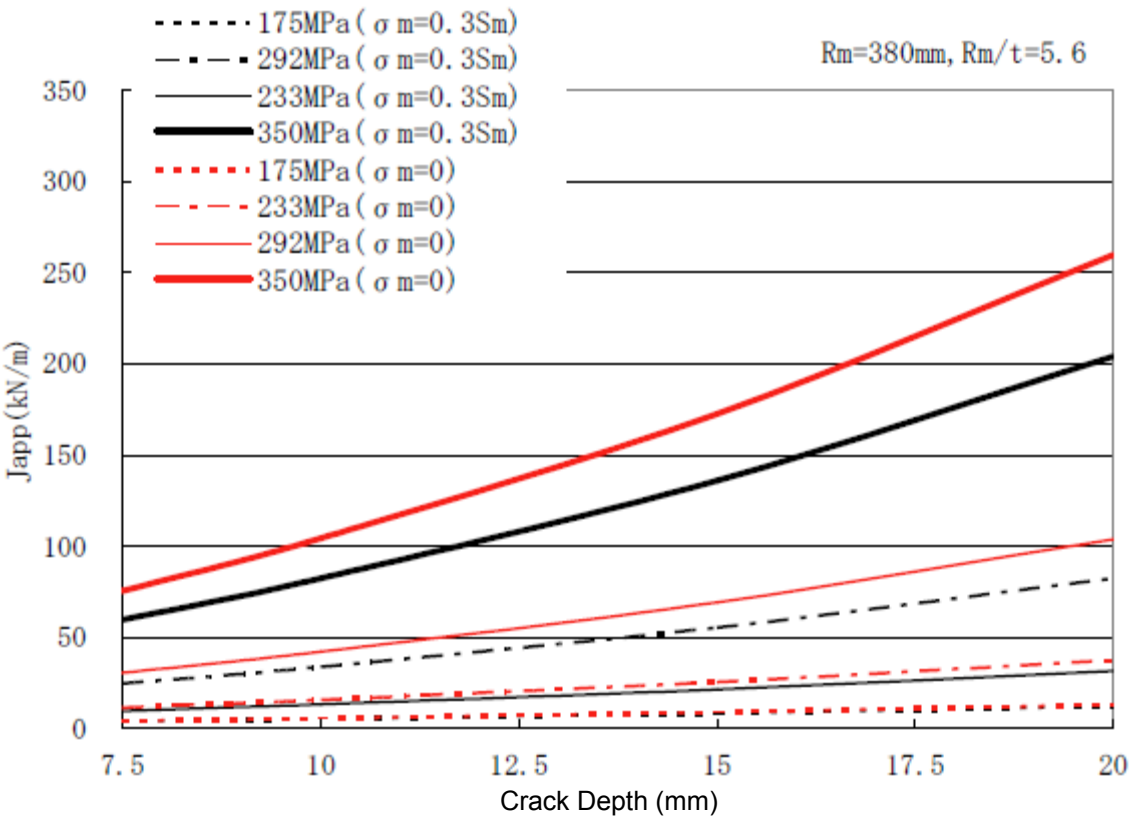

Predicted σ - ε for FN15% Cold-Leg Wall Thickness No. 1

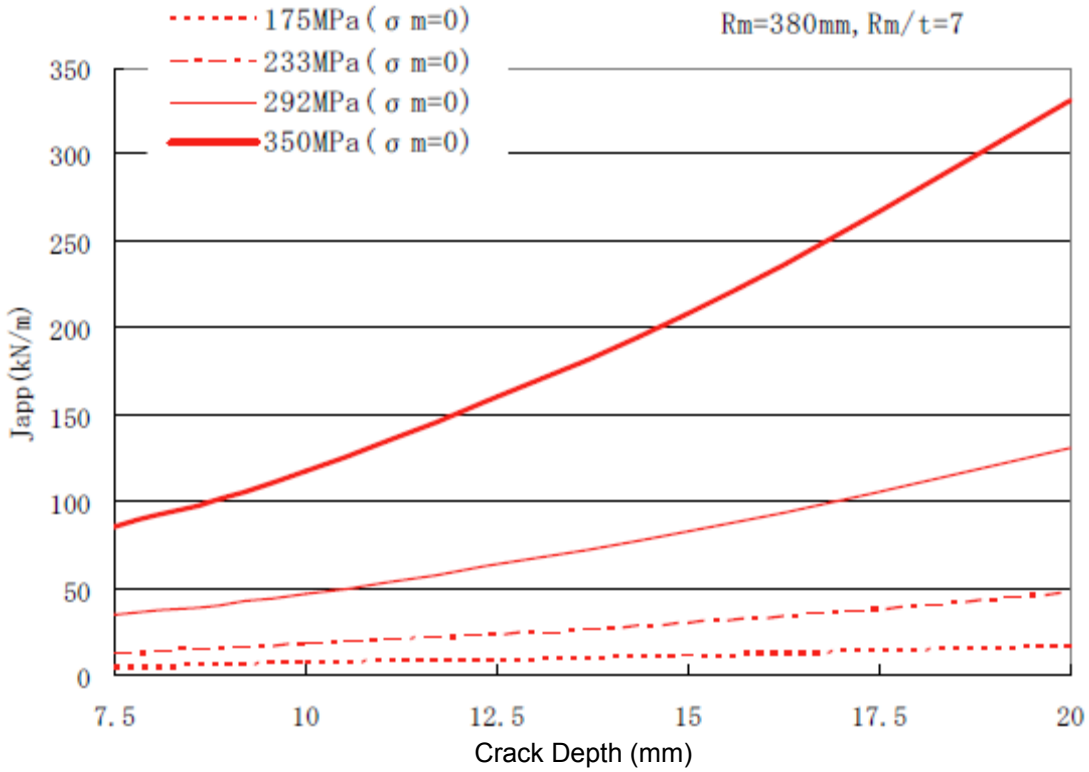

Predicted σ - ε for FN15% Cold-Leg Wall Thickness No. 2

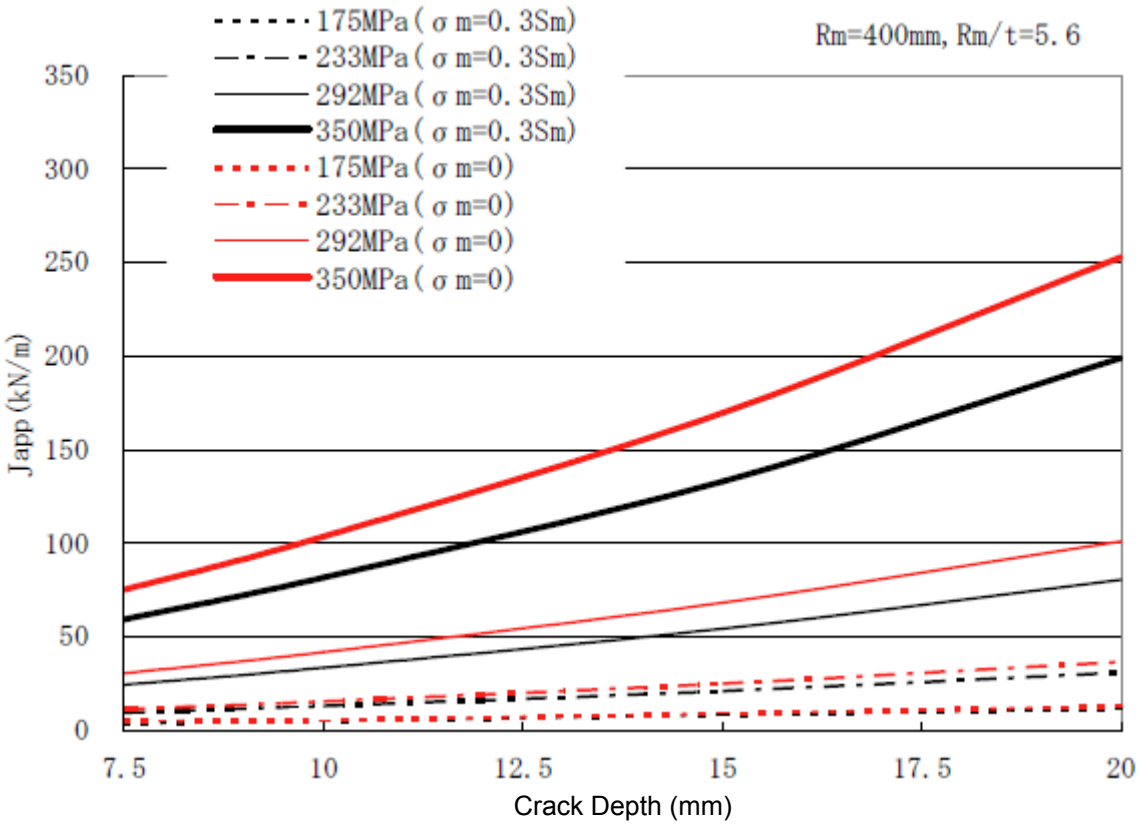

Predicted σ - ε for FN15% Hot-Leg Wall Thickness No. 1

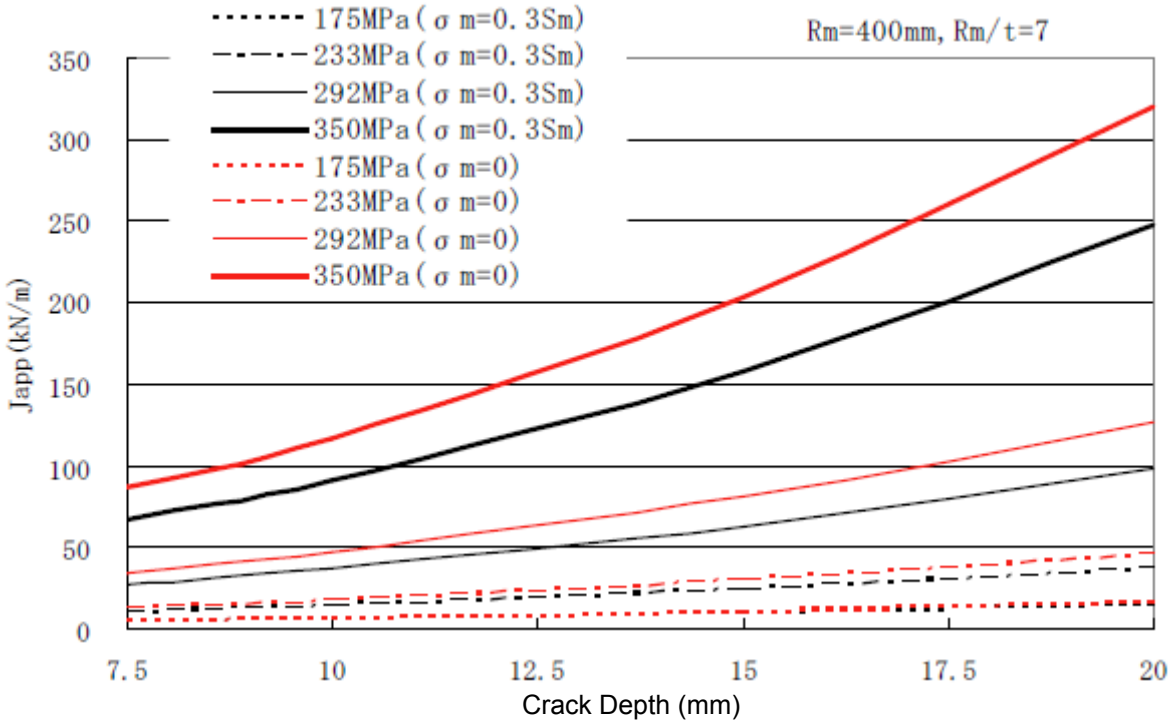

Predicted σ - ε for FN15% Hot-Leg Wall Thickness No. 2

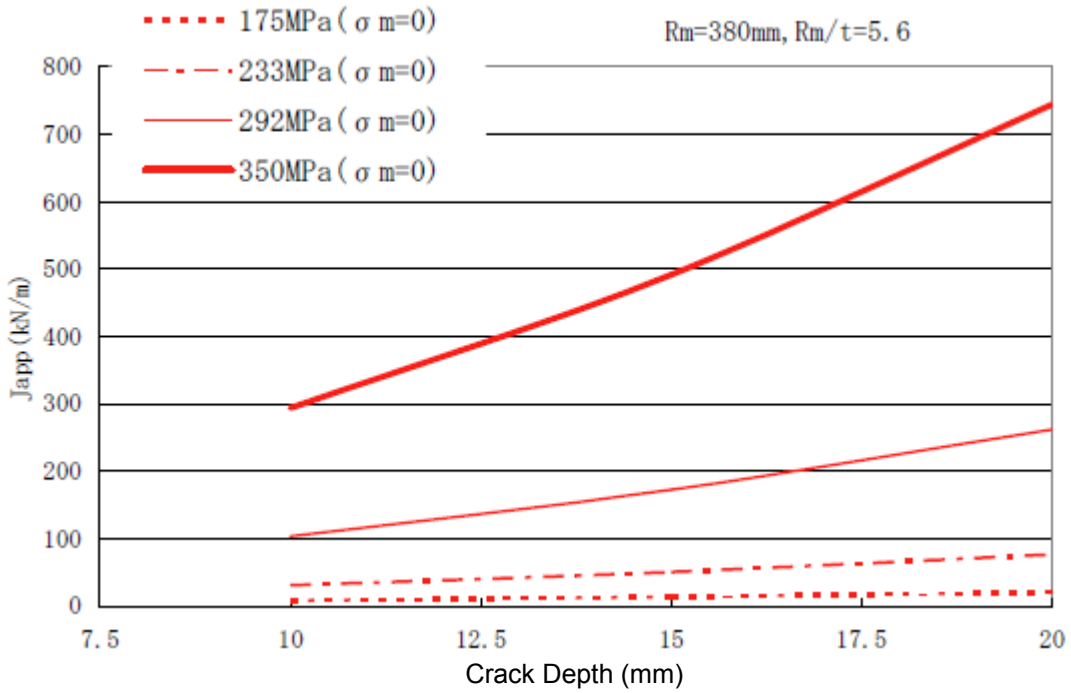

Predicted σ - ε for FN10% Cold-Leg Wall Thickness No. 1

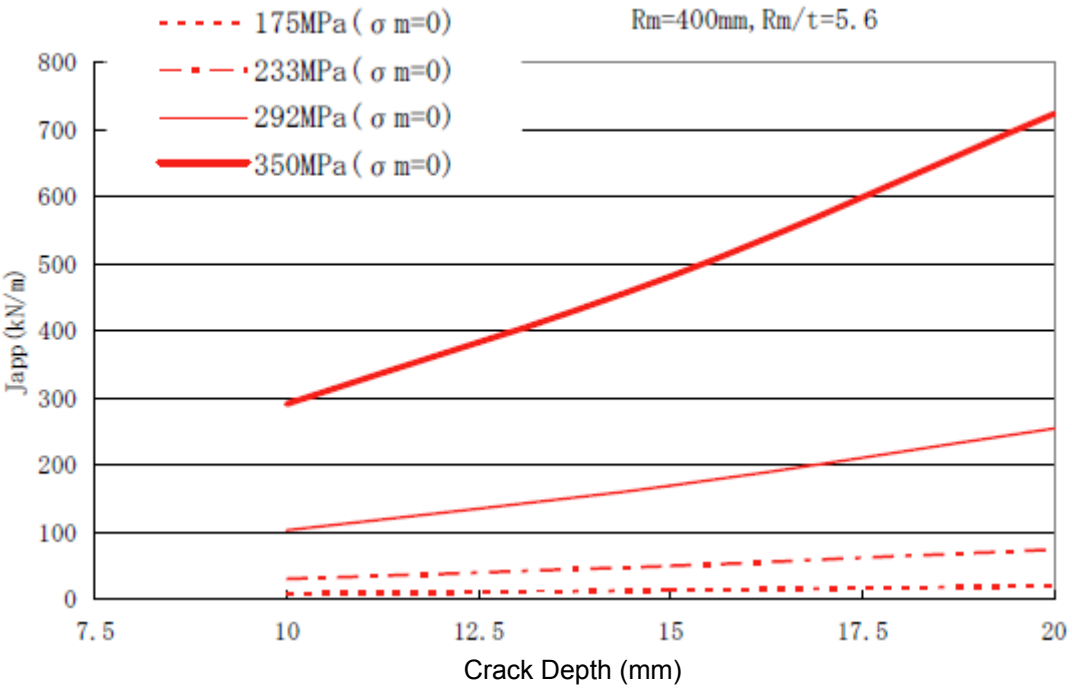

Predicted σ - ε for FN10% Hot-Leg Wall Thickness No. 1

JNES

An Independent Administrative Agency

Japan Nuclear Energy Safety Organization
Regulations and Standards Department

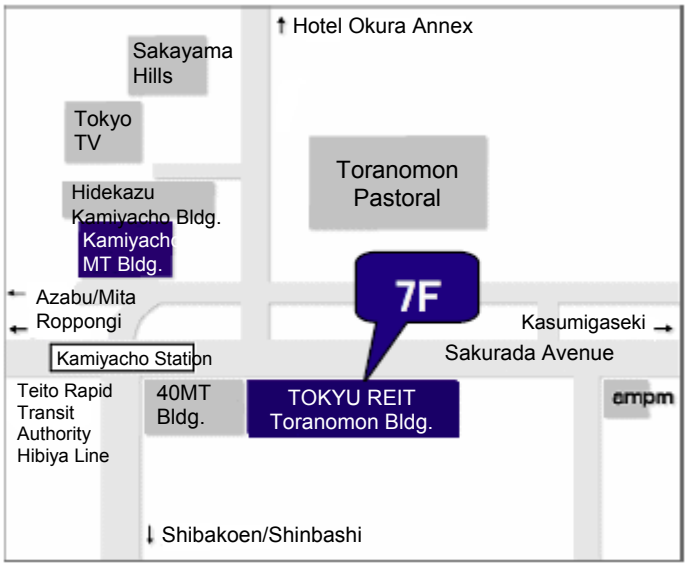

Postal Code 105-0001
TOKYU REIT Toranomon Building 7F, 3-17-1 Toranomon, Minato-ku, Tokyo

Standards Dept. Representative: 03-4511-1700
Standards Dept. Representative: 03-4511-1898